

# Self-Assembled Structures of Amphiphilic Ionic Block Copolymers: Theory, Self-Consistent Field Modeling and Experiment

Oleg V. Borisov, Ekaterina B. Zhulina, Frans A.M. Leermakers,  
and Axel H.E. Müller

**Abstract** We present an overview of statistical thermodynamic theories that describe the self-assembly of amphiphilic ionic/hydrophobic diblock copolymers in dilute solution. Block copolymers with both strongly and weakly dissociating (pH-sensitive) ionic blocks are considered. We focus mostly on structural and morphological transitions that occur in self-assembled aggregates as a response to varied environmental conditions (ionic strength and pH in the solution). Analytical theory is complemented by a numerical self-consistent field approach. Theoretical predictions are compared to selected experimental data on micellization of ionic/hydrophobic diblock copolymers in aqueous solutions.

---

O.V. Borisov (✉)

Institut Pluridisciplinaire de Recherche sur, l'Environnement et les Matériaux,  
UMR 5254 CNRS/UPPA, Pau, France  
and

Institute of Macromolecular Compounds of the Russian Academy of Sciences,  
199004 St. Petersburg, Russia  
e-mail: [oleg.borisov@univ-pau.fr](mailto:oleg.borisov@univ-pau.fr)

E.B. Zhulina

Institute of Macromolecular Compounds of the Russian Academy of Sciences,  
199004 St. Petersburg, Russia  
e-mail: [kzhulina@hotmail.com](mailto:kzhulina@hotmail.com)

F.A.M. Leermakers

Laboratory of Physical Chemistry and Colloid Science, Wageningen University Dreyenplein 6,  
6703 HB Wageningen, The Netherlands  
e-mail: [frans.leermakers@wur.nl](mailto:frans.leermakers@wur.nl)

A.H.E. Müller

Makromolekulare Chemie II and Bayreuther Zentrum für Kolloide und Grenzflächen,  
Universität Bayreuth, 95440 Bayreuth, Germany  
e-mail: [axel.mueller@uni-bayreuth.de](mailto:axel.mueller@uni-bayreuth.de)

**Keywords** Amphiphilic block copolymers · Micelles · Polyelectrolytes · Polymorphism · Self-assembly

## Contents

1	Introduction .....	58
2	Thermodynamic Principles of Micellization .....	61
2.1	Critical Micelle Concentration and Aggregation Number .....	61
2.2	Block Copolymer Micelles .....	65
3	Scaling Theory of Non-ionic Block Copolymer Micelles .....	69
3.1	Spherical Non-ionic Micelles .....	69
3.2	Polymorphism of Aggregates of Non-ionic Block Copolymers .....	72
4	Scaling Theory of Micelles with Polyelectrolyte Corona .....	78
4.1	Starlike Micelles with Quenched Polyelectrolyte Corona .....	78
4.2	Crew-Cut Micelles with Quenched Polyelectrolyte Corona .....	80
5	Mean-Field Theory of Block Copolymer Micelles: Boxlike Model .....	81
5.1	Non-ionic Block Copolymer Micelles .....	83
6	Mean-Field Theory of Block Copolymer Micelles with Quenched Polyelectrolyte Corona .....	84
6.1	Starlike Micelles with Quenched Polyelectrolyte Corona .....	85
6.2	Crew-Cut Micelles with Quenched Polyelectrolyte Corona .....	86
7	Mean-Field Theory of Block Copolymer Micelles with Annealing Polyelectrolyte Corona .....	87
7.1	Structural Transitions in Starlike Micelles with Annealing PE Corona .....	89
7.2	Crew-Cut Micelles with Annealing Polyelectrolyte Corona .....	94
8	Micelles with Quenched and Annealing Polyelectrolyte Corona: Nonlocal Mean-Field Approach .....	100
9	Self-Consistent Field Modeling of Micelle Formation .....	101
9.1	Spherical Micelles: Implementation of Numerical SF-SCF Method .....	102
9.2	Neutral Micelles of Amphiphilic Block Copolymers .....	104
9.3	Micelles with Quenched Polyelectrolyte Corona .....	107
9.4	Micelles with Annealing Polyelectrolyte Corona .....	110
10	Polymorphism of Self-Assembled Aggregates of Block Copolymers with Quenched Polyelectrolyte Blocks .....	113
10.1	Salt-Free Solution .....	114
10.2	Salt-Dominated Solution .....	115
11	Re-entrant Morphological Transitions in Aggregates of Block Copolymers with Annealing Polyelectrolyte Block .....	118
12	Experiment Versus Theory .....	121
	References .....	126

## 1 Introduction

The assembly of amphiphilic (macro)molecules in aqueous environments is a generic mechanism of self-organization on multiple length scales that is amply exploited by nature. The spontaneous formation of self-assembled structures of phospholipids and biomacromolecules, exemplified by living cells, is the outcome

of a delicate balance between attractive and repulsive forces, among which hydrophobic attraction, hydrogen bonding, metal-coordination forces, and steric or electrostatic repulsion play dominant roles.

In the realm of technology, the self-assembly of synthetic amphiphilic molecules is also widely exploited. Many water-based industrial formulations include small amphiphilic molecules (surfactants) and polymeric amphiphiles, which self- and co-assemble with other molecules and colloidal (nano)particles.

In the past decade, significant progress has been made in terms of understanding the self-assembly of amphiphilic diblock copolymers in selective solvents [1–9]. In aqueous solutions, the assembly is driven by hydrophobic attraction between associating blocks and is counterbalanced by electrostatic and/or steric repulsions between ionic or neutral water-soluble blocks. As a result, diverse nanostructures emerge. Among them, spherical core–corona micelles, formed by copolymers with a relatively long solvophilic block, have been extensively studied. Similarly to low molecular weight amphiphiles (surfactants), block copolymers with more bulky (longer) solvophobic blocks may self-assemble in cylindrical wormlike micelles, bilayer vesicles (“polymersomes”), lamellar mesophases, etc.

Self-assembled nanoaggregates of amphiphilic block copolymers attract strong research interest due to the large number of emerging and potential applications. These include smart nanocontainers for encapsulation, delivery and controlled release of biologically active molecules in nanomedicine, food and personal care products, and agrochemistry. Uptake of heavy metal ions, radionuclides, and toxic organic compounds is being explored for water treatment and environment monitoring purposes. Polymeric nanostructures of different and controlled morphologies could serve as molecular templates for nanoelectronic devices.

Necessary requirements for many applications include: (1) precise control over the size (on nanometer length scale) and morphology of the assembled aggregates, and (2) pronounced stimuli-responsive properties. The latter imply that these structures can change their size, aggregation number, etc. in a significant way when the physical and/or chemical properties of the surroundings (temperature, pH, ionic strength, etc.) are varied smoothly, or that the structures recognize weak specific stimuli such as trace concentrations of biologically active or toxic molecules. Both requirements can be met by nanoaggregates that emerge as a result of the assembly of amphiphilic block copolymers with tailored molecular architecture. The latter implies properly chosen molecular weight of the blocks and the correct balance of intramolecular hydrophilic and hydrophobic interactions or, more specifically, an appropriate composition of the macromolecule in terms of non-ionic, ionic and pH-sensitive, and hydrophobic (thermosensitive) components.

Self-assembly of block copolymers that are made of poly(ethylene oxide), PEO, as the hydrophilic non-ionic block, has been extensively explored. The research interest in PEO-containing block copolymers was motivated, to a great extent, by potential biomedical applications, which rely on the finding that PEO moieties are biocompatible. Because amphiphilic block copolymers of PEO and poly(propylene oxide) PPO (pluronics) are produced on an industrial scale, research on these non-ionic polymeric surfactants resulted in many technological applications. Both PPO and PEO are thermoresponsive, having a low solution critical temperature (LSCT),

so nanostructures formed from pluronics also demonstrate thermoresponsive features. Unfortunately, they do not show a pronounced response to salt or pH changes in the solution.

Structures formed by amphiphilic block copolymers composed of a hydrophilic block with ionic and, in particular, pH-sensitive (weak polyelectrolyte) segments, linked to a hydrophobic block, are more responsive. This is because the strength of repulsive Coulomb interactions between the polyelectrolyte (PE) segments can be efficiently tuned by variations in pH or/and ionic strength in the aqueous solution, while their thermoresponsive nature can be maintained if the hydrophobic block is well chosen.

The responsive features of micelles with a PE corona, e.g., the ability of micelles to change their size, aggregation number and morphology, as a response to variations in ionic strength and pH, were demonstrated and studied experimentally. However, association of the hydrophobic blocks in water often results in a dense core wherein structural rearrangements are hindered by high energy barriers (the cores are found in a glassy state). In this state, the dynamic equilibrium between copolymers in the micelle and freely dispersed in solution (unimers) does not exist, and these micelles must be characterized as out-of-equilibrium “frozen” aggregates. Under preparation conditions, either the temperature is very high or mixtures of water and a common (organic) co-solvent are used. In these mixed solvents or at high temperatures, the dynamic equilibrium between unimers and aggregates is attained and the responsive features can be exploited.

The response of frozen micelles to varied ionic strength and pH is thus limited to conformational changes in the hydrated PE corona domains, and is similar to that discussed for PE stars in [10].

One of the possible solutions for design of truly responsive (“dynamic”) micelles is to use copolymers with “soft” hydrophobic blocks. For example, at the stage of copolymer synthesis, one can incorporate a small fraction of pH-sensitive comonomer units in the hydrophobic moiety. This opens up the possibility of turning on some repulsive contributions in a net attractive domain, leading to a softer core. Alternatively, one can opt for copolymers that are made of a PE block that is linked to a thermosensitive block [11]. This gives the possibility of triggering the formation and dissociation of micelles by variations in the temperature [12].

In spite of significant experimental efforts made in the last decade, it remains difficult to provide an unambiguous proof of the dynamic (equilibrium) nature of polymeric micelles. A review of selected experimental results on the stimuli-responsive behavior of PE micelles is presented at the end of this chapter.

A number of theoretical studies have been devoted to analysis of the self-assembly of amphiphilic ionic/hydrophobic diblock copolymers [13–24]. Most of these studies considered copolymers with strongly dissociating (also referred to as “quenched”) PE blocks [13–18, 20] and extensively exploited the analogy between the conformation of PE blocks in a corona and that in a spherical PE brush [25–33] or PE stars (see [10] for a review). The micellization and the responsive behavior of nanostructures formed by copolymers with pH-sensitive PE blocks have also been systematically studied in recent years [19, 21–23].

We present an overview of the statistical thermodynamic theories of self-assembly in aqueous media for amphiphilic diblock copolymers that are composed of one PE block and one hydrophobic block. In all theoretical models, the hydrophobic block is assumed to be “soft” enough to ensure the equilibrium character of self-assembly. We outline here the arguments that were presented in more detail in the corresponding original papers [18–23].

We start with a brief reminder of the theory of self-assembly in a selective solvent of non-ionic amphiphilic diblock copolymers. Here, the focus is on polymorphism of the emerging copolymer nanoaggregates as a function of the intramolecular hydrophilic/hydrophobic balance. We then proceed with a discussion of the structure of micelles formed by block copolymers with strongly dissociating PE blocks in salt-free and salt-added solutions. Subsequently, we analyze the responsive behavior of nanoaggregates formed by copolymers with pH-sensitive PE blocks. The predictions of the analytical models are systematically complemented by the results of a molecularly detailed self-consistent field (SCF) theory. Finally, the theoretical predictions are compared to the experimental data that exist to date.

## 2 Thermodynamic Principles of Micellization

### 2.1 Critical Micelle Concentration and Aggregation Number

The general principles of self-assembly of amphiphilic molecules into finite-sized aggregates (micelles) are described in a number of classic books [34–36]. In our analysis of micelle formation we apply the equilibrium “close association” model. That is, we assume first that only one population of micelles, with an aggregation number  $p$  (number of copolymers in one aggregate), is present in the system at any given concentration of amphiphiles in the solution, or that there are no micelles at all; and second, that the free energy per molecule in a micelle,  $F_p$ , exhibits a minimum at a certain value of the aggregation number,  $p = p_0$ .

The thermodynamic model of micellization, presented here, describes the association of any amphiphilic molecules, including low molecular weight surfactants or polymeric amphiphiles. The physical origin of the minimum in the free energy, as a function of  $p$ , is specified by the molecular architecture and the interactions between amphiphilic molecules involved in the assembly, and will be discussed in the corresponding sections. An extension of the model for the case of a continuous distribution of micelles with respect to aggregation number (polydispersity of the aggregates) involves the value of  $\partial^2 F_p / \partial p^2$ . If this quantity is small in the vicinity of  $p = p_0$ , then the micelle distribution is wide, and vice versa [37]. The approximation of micelle monodispersity is essential for application of the numerical SCF model which is discussed in Sect. 9.

We consider a solution with a volume  $V$  that contains  $N_p$  amphiphilic block copolymer molecules. The total number density of the amphiphiles is  $c = N_p/V$ . We assume that  $c_1$  is the concentration (number density) of the amphiphiles that are

found in the unimer (nonassociated) state, whereas  $c_{\text{mic}} = (c - c_1)/p$  is the number density of the monodisperse micelles with aggregation number  $p$ . The relevant thermodynamic potential is the Helmholtz free energy  $F(V, N_p, T)$ . Assuming that the solution is dilute and that intermicelle and micelle–unimer interactions can be ignored, the free energy of the system can be presented as:

$$F/Vk_B T = pc_{\text{mic}}F_p/k_B T + c_{\text{mic}}(\ln c_{\text{mic}} - 1) + c_1F_1/k_B T + c_1(\ln c_1 - 1), \quad (1)$$

wherein  $k_B$  is the Boltzmann constant and  $T$  is the temperature. Here, the first term represents the free energy of the micelles ( $F_p$  is the free energy of one amphiphile in a micelle comprising  $p$  molecules), the second term is the translational entropy of micelles, the third term is the free energy of unimers, and the last term is the translational entropy of unimers.

The minimization of the Helmholtz free energy,  $F$ , with respect to  $p$  and  $c_{\text{mic}}$ , ( $\partial F/\partial p = 0$ ,  $\partial F/\partial c_{\text{mic}} = 0$ ) leads to the following equations:

$$p \frac{\partial F_p}{\partial p} = \frac{k_B T}{p} \ln c_{\text{mic}}, \quad (2)$$

$$F_p + p \frac{\partial F_p}{\partial p} \equiv \frac{\partial(pF_p)}{\partial p} = \mu_1(c_1), \quad (3)$$

where:

$$\mu_1(c_1) = F_1 + k_B T \ln c_1 \quad (4)$$

is the chemical potential of unimer, and (3) implies the equality of chemical potentials of a free unimer and an amphiphile incorporated in a micelle.

Equations (2)–(4) determine the equilibrium aggregation number,  $p_{\text{eq}}$ , the number densities of unimers,  $c_1$ , and of micelles,  $c_{\text{mic}}$ , at a given value of the total number density of amphiphiles,  $c$ . With the account of (4), we can rewrite (2) as:

$$k_B T \ln c_{\text{mic}} = -[pF_p - p\mu_1(c_1)] = -\Omega(c_1), \quad (5)$$

where  $\Omega$  is (by definition) the grand potential of a micelle.

Note that the condition of thermodynamic stability requires that the free energy of a micelle,  $F_{\text{micelle}} \equiv pF_p$ , is a concave function of the aggregation number,  $p$ . That is:

$$\frac{\partial^2(pF_p)}{\partial p^2} > 0. \quad (6)$$

Therefore, as follows from (3) and (5), in a thermodynamically stable system:

$$\partial \mu_1(c_1)/\partial p \geq 0 \quad (7)$$

and:

$$\frac{\partial \Omega}{\partial p} = -p \frac{\partial \mu_1(c_1)}{\partial p} \leq 0. \quad (8)$$

Hence, under equilibrium conditions, the chemical potential of a unimer must be an increasing function of the aggregation number  $p$ , and the grand potential of a micelle,  $\Omega(p)$ , must be a decreasing function of  $p$ .

The minimal aggregation number,  $p = p_{\min}$ , in a thermodynamically stable micelle, is determined by the condition:

$$\left( \frac{\partial^2 (pF_p)}{\partial p^2} \right)_{p=p_{\min}} = 0. \quad (9)$$

That is,  $\partial\Omega/\partial p = \partial\mu_1/\partial p = 0$  at  $p = p_{\min}$ , and the micelles with  $p < p_{\min}$  are thermodynamically unstable.

A minimal micelle with  $p_{\text{eq}} = p_{\min}$  appears in the system at a certain (minimal) threshold concentration,  $c_{\min}$ , which can be identified as the “theoretical critical micellization concentration”. Below this threshold,  $c \leq c_{\min}$ , no micelles and only unimers are found in the solution. At amphiphile concentration  $c = c_{\min}$ , the number density of micelles,  $c_{\text{mic}}^{(\min)} = \exp[-\Omega(p_{\min})/k_B T]$ , is negligible with respect to the unimer density,  $c_1^{(\min)}$ . A subsequent increase in the concentration of amphiphiles,  $c \geq c_{\min}$ , leads to an increase in both the concentration of micelles,  $c_{\text{mic}}$ , and the concentration of unimers,  $c_1$ , and an increase in both the chemical potential of unimers and the aggregation number,  $p_{\text{eq}}$ .

Often, the critical micelle concentration (CMC) is defined as the total concentration of amphiphiles at which the number of unimers is equal to the number of amphiphiles incorporated into the micelles,  $p c_{\text{mic}} = c_1 = \text{CMC}/2$ . In this case, the CMC is specified by the equation:

$$k_B T \ln \left( \frac{\text{CMC}}{2} \right) = \left( \frac{\partial (pF_p)}{\partial p} \right)_{p=p_{\text{eq}}(\text{CMC})} - F_1, \quad (10)$$

where  $F_p$  is the free energy per chain in the equilibrium micelle with  $p = p_{\text{eq}}(\text{CMC})$ .

A frequently used simplifying approximation is based on neglecting the translational entropy of micelles (i.e., the second term in (1) is omitted). This approximation is justified as long as the aggregation number in an equilibrium micelle is large. Then, (2)–(4) reduce to:

$$\frac{\partial F_p(p)}{\partial p} = 0, \quad (11)$$

$$c_1 = \exp[(F_p(p_0) - F_1)/k_B T], \quad (12)$$

$$c_{\text{mic}} = \frac{c - c_1}{p_0}. \quad (13)$$

Within this approximation, (11) specifies the equilibrium aggregation number  $p_0$ , corresponding to the minimum of function  $F_p(p)$ , which does not depend on the concentration of amphiphiles. According to (12), the concentration of unimers,  $c_1$ , remains constant at  $c \geq \text{CMC}$ , irrespective of the total concentration of amphiphiles,  $c$ .

According to the above definition of CMC, an approximate expression for the CMC is given by:

$$k_B T \ln \left( \frac{\text{CMC}}{2} \right)_{\text{approx}} = F_p(p_0) - F_1 = \left( \frac{\partial(pF_p)}{\partial p} \right)_{p=p_0} - F_1. \quad (14)$$

As follows from (2),  $(\partial F_p / \partial p)_{p=p_{\text{eq}}} < 0$ . Because  $F_p$  exhibits a minimum at  $p = p_0$ , the equilibrium micelle is always smaller than that predicted by the approximate theory, i.e.,  $p_{\text{eq}} \leq p_0$ . An increase in the concentration of amphiphiles beyond the  $c_{\text{min}}$  threshold results in a progressive increase in the equilibrium aggregation number  $p_{\text{eq}}$ , that asymptotically approaches the value of  $p_0$ .

A comparison of (10) and (14) indicates that because of the stability condition, (8), the exact CMC [defined by (10)] is smaller than the CMC obtained from the approximate analytical model, (14). Accounting for the translational entropy of micelles leads, therefore, to a lower value of the aggregation number,  $p_{\text{eq}}(c) < p_0$ , and a lower CMC.

The statistical thermodynamic theory of self-assembly of amphiphilic ionic/hydrophobic diblock copolymers, reviewed in this chapter, is based on the simplifying approximation (11)–(13), which neglects the translational entropy of the micelles. In particular, we pre-assume that at the copolymer concentration beyond the CMC, the solution contains only micelles with the “optimal” aggregation number,  $p = p_0$ , which corresponds to the minimum of the free energy,  $F_p$ . As a result, the fluctuations around the most probable ground state,  $p = p_0$ , which give rise to the equilibrium distribution with respect to the aggregation number (polydispersity of the aggregates), are also neglected.

The simplified model enables one to account, in a straightforward way, for the effects of charge on the micellization of ionic amphiphiles. The electrostatic interactions between ionic groups of the amphiphilic molecules in a micelle are included in the free energy term,  $F_p$ . In a salt-free solution, the association of amphiphiles in aggregates is accompanied by the localization (“condensation”) of counterions, which are necessarily present in the system to ensure its total electroneutrality. While in solution of unimers (below the CMC), the counterions are distributed fairly uniformly, the formation of large aggregates leads to a restriction in the mobility of counterions. More specifically, a significant fraction of counterions are “trapped” in the vicinity of an aggregate due to the large local attractive electrostatic potential. This effect is well known for simple ionic amphiphiles, but becomes much more pronounced for polymeric species. Consistent with the discussion in [10], a major fraction of the counterions in PE micelles are entrapped in the highly hydrated PE coronas. Hence, the aggregation of PE copolymers in micelles is opposed not only by losses in the translational entropy of the polyamphiphiles but, much more significantly, by losses in the translational entropy of mobile counterions. Formally, the effect of counterions can be accounted for by adding the term:

$$F_{\text{ions}}/Vk_B T = c_1 Q [\ln(Qc_1) - 1] \quad (15)$$



to the free energy in (1). Here,  $Q$  is the number of elementary charged groups in one polyamphiphile and we assume that the “bare” charge,  $pQ$ , in the corona of a micelle with  $p$  copolymers, is totally neutralized by the localized counterions. The validity of this approximation is discussed in [10]. A more accurate analysis indicates that the degree of neutralization of the micelle charge by its counterions (the fraction of trapped counterions) is a function of  $p$ , which, however, approaches the plateau value of unity at large  $p \gg 1$ .

The free energy, (1), complemented by the contribution due to counterions, cf. (15), can be minimized with respect to  $c_{\text{mic}}$  and  $p$ . When the translational entropy of micelles is neglected, the optimal aggregation number,  $p = p_0$ , is still given by (11). The concentration of unimers that coexist with micelles, and thus the CMC, is, however, significantly larger than for neutral (uncharged) amphiphiles:

$$c_1 \approx \frac{1}{Q} \exp[(F_p(p_0) - F_1)/Qk_B T] \quad (16)$$

provided that  $Q \gg 1$ . This increase in the CMC upon an increase in  $Q$  is a direct consequence of the loss in translational entropy of a large number of counterions upon the aggregation of polyamphiphiles. A similar effect of significant increase in the CMC for ionic low molecular weight surfactants has been discussed in [38]. An addition of salt to the solution results in the decrease of excess electrostatic potential associated with the PE corona and, at sufficiently high ionic strengths, (11)–(13) apply for ionic polyamphiphiles.

## 2.2 Block Copolymer Micelles

As follows from Sect. 2.1, in order to find the optimal (equilibrium) aggregation number and the CMC, a theoretical model has to specify the functional form of the free energy  $F_p$  per amphiphile as a function of  $p$  in an aggregate of a given morphology. This free energy depends on the molecular architecture as well as on the interaction parameters, which, in general, can be affected by the environmental conditions (temperature, ionic strength, pH, etc.).

We consider a dilute solution of diblock copolymer, which is composed of a hydrophilic (non-ionic or ionic) block with a degree of polymerization  $N_A$  and a hydrophobic (associating) block with a degree of polymerization  $N_B$ . Here, we focus mostly on the specifics of self-assembly of the copolymer whose hydrophilic block  $A$  is charged.

A poor solubility of the hydrophobic blocks  $B$  in water provides the driving force for self-assembly of polymeric amphiphiles in aqueous media. This driving force is counterbalanced by repulsive interactions between the hydrophilic blocks, which ensure the formation of finite-sized aggregates in favor of a macroscopic phase separation at concentrations above the CMC. In these aggregates, blocks  $B$  associate in a dense hydrophobic core that is surrounded by a hydrated corona, formed by the

soluble blocks  $A$ . The preferred morphology of the core domain in the equilibrium aggregate is controlled by a subtle balance of solvophilic–solvophobic interactions, and the conformational entropy of both blocks.

Due to the strong hydrophobicity of the blocks  $B$ , the interface between the collapsed hydrophobic domain and the surrounding aqueous environment is narrow compared to the size of the core. Therefore, the coronal blocks  $A$  can be envisioned as tethered to the interface to form a polymer brush [33, 39, 40]. The hydration of the corona and the repulsion between different coronae ensure the solubility (aggregative stability) of the micelles in water.

### 2.2.1 Corona Domain

The conformational characteristics of the corona-forming blocks are controlled by the balance between repulsive monomer–monomer interactions and the conformational entropy penalty for chain stretching.

For uncharged coronal blocks  $A$ , the short-ranged (van der Waals) interactions between monomer units are described in terms of a virial expansion. The latter accounts for the monomer–monomer binary (pair) interactions, with second virial coefficient  $v_A a^3$ , or the ternary interactions with third virial coefficient  $w_A a^6$ . We assume that the monomer unit length,  $a$ , is the same for both blocks  $A$  and  $B$ . In the following, we use  $a$  as a unit length to make all lengths dimensionless and eliminate  $a$  in further equations. We also assume that the (dimensionless) second virial coefficient  $v_A \geq 0$  and that the third virial coefficient  $w_A \simeq 1$ .

The ionization of the soluble blocks  $A$  of the polymeric amphiphile introduces long-ranged repulsive interactions in the corona of a micelle. We discuss separately the cases of amphiphilic diblock copolymers containing strongly dissociating (“quenched”) and weakly dissociating (“annealing” or pH-sensitive) PE block  $A$  linked to the associating hydrophobic block  $B$ . In the former case, the fraction of charged monomer units,  $\alpha_b$ , in the block  $A$  is quenched according to its chemical sequence (as in the case of, e.g., partially sulfonated polystyrene). In the latter case, the fraction of charged monomer units,  $\alpha(\mathbf{r})$ , is controlled by the local pH (i.e., minus the log of the proton molar concentration), which depends on the bulk (buffer) pH, and the local electrostatic potential  $\Psi(\mathbf{r})$ . The degree of dissociation of the monomer unit,  $\alpha(\mathbf{r})$ , of a weak polyacid depends on the local concentration  $c_{H^+}(\mathbf{r})$  of hydrogen ions via the mass action law:

$$\frac{\alpha(\mathbf{r})}{1 - \alpha(\mathbf{r})} = \frac{K_a}{c_{H^+}(\mathbf{r})}, \quad (17)$$

where  $K_a$  is the acidic ionization constant for an isolated monomer. For a polybase, the ionization occurs through the protonation of the monomers, and a generalization of the theory is straightforward.

### 2.2.2 Core Domain

The compact core of a micelle is characterized by a uniform polymer density,  $\varphi(\chi_{BS})$ , chemical potential per monomer unit,  $k_B T \mu_B(\chi_{BS})$ , and excess free energy per unit area of the core–water interface,  $k_B T \gamma(\chi_{BS})$ . Here,  $\chi_{BS}(T)$  is the Flory–Huggins parameter of monomer (*B*)–solvent (*S*) interaction, and  $\chi_{BS}(T) \geq \chi_{BS}(\theta) = 1/2$  under poor solvent conditions for the monomer units of block *B*. Although the solubility of polymers in organic solvents usually decreases with a decrease in temperature,  $\partial\chi(T)/\partial T \leq 0$ , the situation is more complex in aqueous solutions. In particular, it appears that the solubility of thermosensitive block *B* in water typically decreases with an increase in temperature [11], and hence  $\partial\chi_{BS}(T)/\partial T \geq 0$ . In this case, the collapse of blocks *B* and the aggregation of the block copolymers into micelles occur at  $T \geq \text{LCST}$ , where LCST is the lower critical solution temperature.

Within this so-called volume approximation [41], all the partial parameters,  $\varphi(\chi_{BS})$ ,  $\mu_B(\chi_{BS})$ , and  $\gamma(\chi_{BS})$  are independent of the core size. This approximation is applicable as long as the width of the core–water interface,  $\Delta$ , is much smaller than the core size,  $R_{\text{core}}$ , i.e.,  $R_{\text{core}} \gg \Delta$ . The excess free energy of the core–water interface originates from an enhanced probability of unfavorable contacts between solvophobic monomer units of block *B* and solvent (water) molecules in the interfacial region. The surface tension  $\gamma$  also accounts for local conformational entropy losses in the segments of blocks *B* localized close to the core–solvent interface.

The explicit dependencies of  $\varphi(\chi_{BS})$ ,  $\mu_B(\chi_{BS})$ , and  $\gamma(\chi_{BS})$  on the  $\chi_{BS}$  parameter can be obtained [42] within the Flory theory of polymer solutions [43]. However, in the vicinity of the theta point (or LCST) for the core-forming block *B*,  $|\chi(\theta) - \chi(T)|/\chi(\theta) \approx |T - \theta|/\theta \ll 1$ , all the partial parameters can be expressed [41, 44] as power law functions of the dimensionless virial coefficients of monomer–monomer interactions for block *B*:

$$\varphi \approx -v_B/2w_B \cong \tau, \quad (18)$$

$$\gamma/k_B T \approx v_B^2/2^{7/2}3^{1/2}w_B^{3/2} \cong \tau^2. \quad (19)$$

Here, the second virial coefficient (excluded-volume parameter),  $v_B \cong [1 - 2\chi(T)] \leq 0$ , is negative because water is a poor solvent for the hydrophobic block *B*. The third virial coefficient,  $w_B$ , is positive, and  $\tau \equiv |T - \theta|/\theta$  is the relative deviation from the theta temperature. At small deviations from the theta point,  $\tau \ll 1$ , the surface tension  $\gamma$  and the polymer volume fraction  $\varphi$  are related as  $\gamma/k_B T \cong \varphi^2$ . However, at larger deviations from the theta point,  $\varphi$  becomes comparable to unity and the latter relationship breaks down. Because in a typical experimental situation  $\varphi \cong 1$ , we treat  $\varphi$  and  $\gamma$  as two independent parameters. Note that in a general case, surface tension  $\gamma$  and width  $\Delta$  of the core–corona interface depend on both the polymer–solvent interaction parameter  $\chi_{BS}(T)$  for the core-forming block and the incompatibility  $\chi_{AB}$  between monomers of blocks *A* and *B*. That is,  $\gamma$  could depend on the concentration of monomers of the coronal block *A* near the core surface. We, however, neglect this (weak) dependence and assume that the surface tension  $\gamma$  is not affected by conformations of the coronal blocks in a micelle.

The combination of packing constraints (constant concentration of  $B$  segments in the core and the localization of junctions between blocks  $B$  and  $A$  at the core–corona interface) implies the stretching of the core-forming blocks in the radial direction. This stretching leads to conformational entropy losses in the core-forming blocks. For a given core surface area per molecule, the stretching of a core block is maximal in a spherical geometry, and it decreases with decreasing curvature, i.e. going from spherical to cylindrical to lamellar geometries. Explicit expressions for the conformational entropy of core-forming blocks are presented below.

### 2.2.3 Free Energy

The free energy  $F$  per one block copolymer in a micelle can be presented as:

$$F = F_{\text{corona}} + F_{\text{interface}} + F_{\text{core}}. \quad (20)$$

Here, the term  $F_{\text{corona}}$  includes contributions due to the conformational entropy of the coronal blocks and the (repulsive) interactions in the coronal domain. The term  $F_{\text{interface}}$  is the excess free energy of the core–water interface. It is proportional to the interfacial area,  $s$ , per copolymer molecule:

$$F_{\text{interface}}/k_B T = \gamma s. \quad (21)$$

Finally, the term  $F_{\text{core}} \sim k_B T R_{\text{core}}^2 / N_B$  accounts for the conformational entropy of stretched core-forming blocks, for which the numerical prefactor depends on the particular morphology of the aggregate.

The volume contribution,  $N_B \mu_B$ , to the free energy of the collapsed core-forming block is independent of the aggregation number,  $p$ , and therefore is disregarded in subsequent equations.

The second term in (20) favors larger micelles (the area per chain,  $s$ , is a decreasing function of the aggregation number,  $p$ ), whereas the first and the last terms are increasing functions of  $p$ , and thus limit the growth of micelles.

As discussed below, the first two terms in (20) always dominate over the last term, i.e., the area per chain,  $s$ , is determined by the balance between the repulsive interactions in the corona and the excess free energy of the interface. The conformational entropy of the core-forming blocks, however, controls the morphology of the aggregates if the size of the core exceeds that of the corona (so-called crew-cut micelles, vesicles).

A minimization of the free energy, (20), with respect to its structural parameters, i.e., the aggregation number  $p$  or, equivalently, the core radius or area of the core–water interface per molecule, enables one to specify the values of structural parameters, corresponding to the minimum in the free energy of an aggregate of a given morphology. A subsequent comparison of the free energies, corresponding to the “optimal” aggregates of different morphologies, allows one to identify which morphology has the lowest free energy, i.e., which is the equilibrium morphology.

Finally, making use of the theory of polymer and PE brushes of different morphologies, one can calculate experimentally observable properties such as the radius of gyration and/or hydrodynamic radius of equilibrium aggregates.

### 3 Scaling Theory of Non-ionic Block Copolymer Micelles

#### 3.1 Spherical Non-ionic Micelles

We first review the main results of the scaling theory for micelles formed by block copolymers with a neutral (non-ionic) soluble block [37, 45–50].

In the case of strongly asymmetric block copolymers ( $N_A \gg N_B$ ), the size of the micellar core,  $R_{\text{core}}$ , is much smaller than the radius  $R_{\text{corona}}$  of the corona. In this case, “starlike” micelles with spherical cores are formed (Fig. 1a). In the opposite limit of short hydrophilic block,  $N_A \ll N_B$ , the size of micellar core,  $R_{\text{core}}$ , exceeds by far the thickness of the corona. The coronae of these crew-cut micelles can be viewed as quasi-planar polymer brushes [51, 52], see Fig. 1b.

In the framework of the scaling theory, the corona of a spherical micelle can be envisioned [53–56] as an array of concentric spherical shells of closely packed blobs. The blob size,  $\xi(r) \cong r/p^{1/2}$ , grows as a function of the radial distance  $r$  from the center of the core. Each blob comprises a segment of the chain within the local correlation length of the monomer density fluctuations [57], and corresponds to a  $\sim k_B T$  contribution to the free energy of steric repulsion between the coronal chains. After calculating the total number of blobs in the micellar corona, one finds the free energy (per coronal chain) as:

$$F_{\text{corona}}(p)/k_B T \cong p^{1/2} \ln \left( \frac{R_{\text{corona}}}{R_{\text{core}}} \right), \quad (22)$$

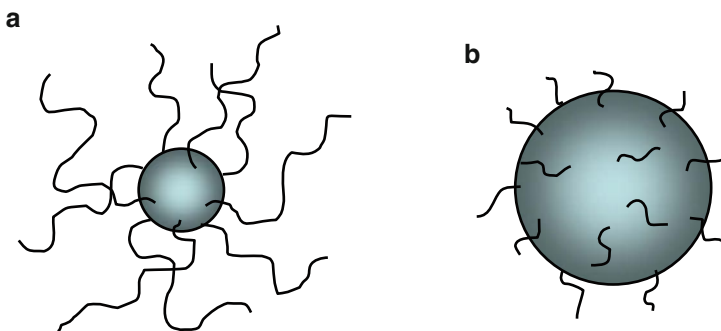


**Fig. 1** Spherical starlike (a) and crew-cut (b) block copolymer micelles

where:

$$R_{\text{core}} \cong (pN_B/\varphi)^{1/3} \quad (23)$$

is the radius of micellar core,  $R_{\text{corona}}$  is the outmost radius of the corona, and  $H_{\text{corona}} = R_{\text{corona}} - R_{\text{core}}$  is its thickness. The excess free energy of the core–corona interface is given by:

$$F_{\text{interface}}(p)/k_B T \cong \gamma s \cong \gamma \left( \frac{N_B}{\varphi} \right)^{2/3} p^{-1/3}, \quad (24)$$

where:

$$s \cong R_{\text{core}}^2/p \cong (N_B/\varphi)^{2/3} p^{-1/3} \quad (25)$$

is the area of the core–corona interface per chain.

Finally, the conformational entropy contribution of stretching in the radial direction of the core-forming block  $B$  scales as:

$$F_{\text{core}}(p)/k_B T \cong R_{\text{core}}^2/N_B. \quad (26)$$

### 3.1.1 Starlike Spherical Non-ionic Micelles

For strongly asymmetric copolymers,  $N_A \gg N_B$ , the structure of a micelle is controlled by the balance of the coronal free energy,  $F_{\text{corona}}$ , and the excess free energy of the core–corona interface,  $F_{\text{interface}}$ .

The minimization of the free energy with respect to  $p$  results in the equilibrium aggregation number:

$$p_{\text{eq}} \cong \gamma^{6/5} (N_B/\varphi)^{4/5} \left( \ln \frac{R_{\text{corona}}}{R_{\text{core}}} \right)^{-6/5}. \quad (27)$$

Here,  $R_{\text{corona}} \cong N_A^v p^{(1-v)/2} v_A^{2v-1}$  is the external radius of the corona, and  $v$  is the Flory exponent for the coronal block  $A$  ( $v \approx 3/5$  and  $v = 1/2$  under good and theta-solvent conditions, respectively).

With the accuracy of the logarithmic factors, the corona and the core radii are given by:

$$R_{\text{corona}} \cong N_A^v v_A^{2v-1} \gamma^{3(1-v)/5} \left( \frac{N_B}{\varphi} \right)^{2(1-v)/5} \quad (28)$$

and:

$$R_{\text{core}} \cong \gamma^{2/5} \left( \frac{N_B}{\varphi} \right)^{3/5} \quad (29)$$

respectively.

An important feature of (27), (29) is the absence of a power law dependence of the aggregation number  $p_{\text{eq}}$  and  $R_{\text{core}}$  on the length  $N_A$  of the coronal block. Micelles are starlike, i.e.,  $R_{\text{corona}} \gg R_{\text{core}}$ , provided that:

$$N_A \gg \gamma^{(3\nu-1)/5\nu} v_A^{(1-2\nu)/\nu} \left( \frac{N_B}{\phi} \right)^{(2\nu+1)/5\nu}. \quad (30)$$

By using (22), (24), and (27), one can calculate the free energy of the equilibrium micelle, and, by using (14), estimate the CMC as:

$$\ln \text{CMC} \approx -\gamma \left( \frac{N_B}{\phi} \right)^{2/3} + \gamma^{3/5} \left( \frac{N_B}{\phi} \right)^{2/5} \left( \ln \frac{R_{\text{corona}}}{R_{\text{core}}} \right)^{2/5}, \quad (31)$$

where  $F_{\text{interface}}(p=1)/k_B T \cong \gamma(N_B/\phi)^{2/3} \cong (N_B \tau^2)^{2/3}$  is the excess interfacial free energy of an individual block  $B$  collapsed in water. The latter provides the dominant contribution to the CMC [the first term in (31)]. The second term in (31) describes the repulsive interactions in the corona, balanced with the excess interfacial free energy, (24). As long as the aggregation number in the equilibrium micelle  $p_{\text{eq}} \gg 1$ , the second term in (31) is relatively small with respect to the first (dominant) term. Hence, in the case of non-ionic copolymer micelles, the CMC is determined mostly by the solubility of hydrophobic block  $B$  and is weakly affected by the properties of the coronal block  $A$ . An increase in length of the soluble block  $A$  leads to the logarithmic increase in the CMC via the increase in  $R_{\text{corona}}$ . These theoretical predictions are in qualitative agreement with experimental findings [58].

### 3.1.2 Crew-Cut Spherical Non-ionic Micelles

In the case of crew-cut micelles,  $H_{\text{corona}} \ll R_{\text{core}}$  and the logarithm in (22) can be expanded up to the term linear in  $H_{\text{corona}}/R_{\text{core}}$ , to give  $F_{\text{corona}}/k_B T \cong H_{\text{corona}}/s^{1/2} \cong H_{\text{corona}}/\xi$ . The thickness of the corona,  $H_{\text{corona}}$ , scales as  $H_{\text{corona}} \cong N_A s^{-(1-\nu)/2\nu} v_A^{(2\nu-1)/\nu}$ . In the framework of the Alexander–de Gennes blob model [51, 52], the micellar corona (the planar brush) can be envisioned as an array of closely packed blobs with size  $\xi \cong s^{1/2}$ , equal to the average distance between the coronal blocks. We note that a constant size of the blobs implies  $H_{\text{corona}} \sim N_A$ . The number of coronal blobs per chain  $\sim H_{\text{corona}}/\xi$  is proportional to the free energy of the interchain repulsion that equals  $F_{\text{corona}}/k_B T \cong N_A s^{-1/2\nu} v_A^{(2\nu-1)/\nu}$ .

Taking the relation  $s \cong (N_B/\phi_B)^{2/3} p^{-1/3}$  into account and minimizing the free energy with respect to  $p$ , one obtains the equilibrium aggregation number:

$$p_{\text{eq}} \cong \left( \frac{N_B}{\phi} \right)^2 \left( \frac{N_A}{\gamma} \right)^{-6\nu/(2\nu+1)} v_A^{-6(2\nu-1)/(2\nu+1)} \quad (32)$$

and the core radius, which determines the overall size of the crew-cut micelle:

$$R_{\text{core}} \cong \frac{N_B}{\varphi} \left( \frac{N_A}{\gamma} \right)^{-2\nu/(2\nu+1)} v_A^{-2(2\nu-1)/(2\nu+1)}. \quad (33)$$

The core–corona surface area per chain is given by

$$s_{\text{eq}} \cong \left( \frac{N_A}{\gamma} \right)^{2\nu/(2\nu+1)} v_A^{2(2\nu-1)/(2\nu+1)}. \quad (34)$$

Interestingly, this area is independent of the length of core-forming block  $B$ . In contrast to the case of starlike micelles, the equilibrium aggregation number and the core radius in a crew-cut micelle strongly decrease upon an increase in the degree of polymerization of the coronal block,  $N_A$ . The thickness of the corona is given by:

$$H_{\text{corona}} \cong N_A^{3\nu/(2\nu+1)} v_A^{3(2\nu-1)/(2\nu+1)} \gamma^{(1-\nu)/(2\nu+1)} \quad (35)$$

and it is easy to check that  $H_{\text{corona}} \leq R_{\text{core}}$  provided that:

$$N_A \leq \gamma^{(3\nu-1)/5\nu} v_A^{(1-2\nu)/\nu} (N_B/\varphi)^{(2\nu+1)/5\nu}. \quad (36)$$

Similarly to the case of starlike micelles, the CMC is controlled by the gain in free energy upon association of blocks  $B$  and is only weakly affected by the properties of coronal block  $A$ :

$$\ln \text{CMC} \cong -\gamma(N_B/\varphi)^{2/3} + (\gamma N_A^{2\nu})^{1/(2\nu+1)} v_A^{2(2\nu-1)/(2\nu+1)}. \quad (37)$$

An increase in the length of the core-forming block  $B$  leads to the progressive increase in the conformational entropy penalty for their stretching,  $F_{\text{core}}(p)$ , given by (26). However, before  $F_{\text{core}}(p)$  becomes comparable to the dominant terms in the free energy,  $F_{\text{corona}} + F_{\text{interface}}$ , the spherical crew-cut micelles change their morphology, i.e., they undergo a thermodynamic transition into cylindrical micelles, as discussed in the following section.

### 3.2 Polymorphism of Aggregates of Non-ionic Block Copolymers

For strongly asymmetric block copolymers with long hydrophobic blocks,  $N_B \gg N_A$ , the conformational entropy losses in the stretched core-forming blocks  $B$  determine the equilibrium morphology of an aggregate. Because for given surface area  $s$  per chain, the stretching of the core-forming blocks decreases from the spherical to the cylindrical and to the lamellar topology, one anticipates that copolymers with longer blocks  $B$  might form nonspherical aggregates.



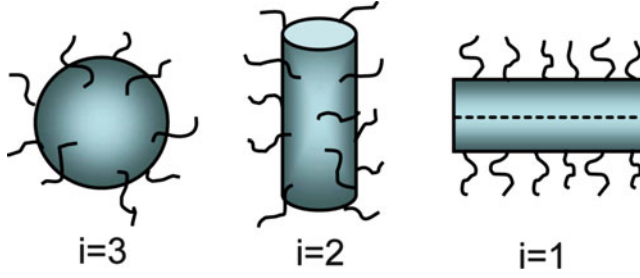


**Fig. 2** Self-assembled block-copolymers aggregates of different morphologies: spherical ( $i = 3$ ), cylindrical ( $i = 2$ ), lamellar ( $i = 1$ ). Hydrophobic blocks  $B$  and polyelectrolyte blocks  $A$  form the core and the corona of the micelle, respectively

The polymorphism of non-ionic block copolymer aggregates was theoretically analyzed by Zhulina and Rubinstein [50], and here we briefly summarize the main results.

The morphology of a block copolymer aggregate is specified by index  $i$ . We distinguish between spherical ( $i = 3$ ), cylindrical ( $i = 2$ ), and planar ( $i = 1$ ) morphologies (see Fig. 2). The latter describes lamellae, vesicles, discs, etc. Edge effects for nonspherical aggregates ( $i = 1, 2$ ) can be incorporated on the level of correction terms.

The condition of constant core density  $\varphi$  imposes a relation between the core radius,  $R_{\text{core}}$ , and the interfacial area per chain,  $s(R_{\text{core}})$ , in an aggregate of morphology  $i$  as:

$$s = s(R_{\text{core}}) = \frac{iN_B}{\varphi R_{\text{core}}} \quad i = 1, 2, 3. \quad (38)$$

The latter determines the excess interfacial free energy per chain as:

$$\frac{F_{\text{interface}}^{(i)}(R_{\text{core}})}{k_B T} = \gamma s(R_{\text{core}}), \quad i = 1, 2, 3. \quad (39)$$

The elastic free energy of a stretched block  $B$  in the core of an aggregate with morphology  $i$  yields:

$$\frac{F_{\text{core}}^{(i)}(R_{\text{core}})}{k_B T} = b_i \frac{R_{\text{core}}^2}{N_B}, \quad (40)$$

where:

$$b_i = \begin{cases} \pi^2/8, & i = 1 \\ \pi^2/16, & i = 2 \\ 3\pi^2/80, & i = 3 \end{cases}. \quad (41)$$

The values of the numerical coefficients in (41) account for the nonuniform and nonequal extension of the core blocks in micelles of different morphologies. They were first calculated by Semenov [59] for a dense micellar core,  $\varphi = 1$ , within

the so-called strong stretching approximation, i.e., when the chains are noticeably stretched with respect to their Gaussian size. The coefficients  $b_i$  in (41) remain valid also for a condensed core with  $\varphi \leq 1$  (provided that the polymer density profile in the core is uniform).

Finally, the coronal contribution,  $F_{\text{corona}}^{(i)}(R_{\text{core}})$ , to the free energy of an aggregate of morphology  $i$  is calculated as the free energy of a planar ( $i = 1$ ) or curved ( $i = 2, 3$ ) polymer brush. This is attained by a generalization of the blob model for the case of an arbitrary (finite) curvature of the grafting surface:

$$F_{\text{corona}}^{(i)}/k_B T = \int_{R_{\text{core}}}^{R_{\text{core}}+H_{\text{corona}}} \frac{s(r)dr}{\xi^3(r)}. \quad (42)$$

Here:

$$s(r) = s(R_{\text{core}}) \left( \frac{r}{R_{\text{core}}} \right)^{i-1}, \quad i = 1, 2, 3 \quad (43)$$

is the area per chain at a distance  $(r - R_{\text{core}})$  from the surface of the core, and  $k_B T \xi^{-3}(r) = f(r)$  is the free energy density in the corona. The latter accounts, in the scaling approximation, both for the conformational entropy losses and the monomer–monomer interactions, where  $\xi(r) \cong s(r)^{1/2}$  is the local correlation length in the corona. Note that at  $i = 3$ , (42) and (43) lead to (22).

It can be demonstrated that a spherical starlike micelle is always thermodynamically stable with respect to nonspherical aggregates. It has a lower free energy than the cylindrical micelle or the lamella, as long as the size of the corona exceeds that of the core,  $H_{\text{corona}} \gg R_{\text{core}}$ .

Morphological transitions sphere–cylinder–lamella occur, therefore, when the aggregates acquire the crew-cut shape. It is instructive to consider first a lamellar aggregate,  $i = 1$ . Here, the coronal contribution is given by the number of blobs per chain in a planar brush:

$$\frac{F_{\text{corona}}^{(1)}}{k_B T} \cong N_A s^{-1/(2\nu)} v_A^{(2\nu-1)/\nu}. \quad (44)$$

By balancing  $F_{\text{corona}}^{(1)} \simeq F_{\text{interface}}^{(1)}$ , one finds the equilibrium area per chain  $s$  in a planar lamella:

$$s \cong \left( \frac{N_A}{\gamma} \right)^{2\nu/(1+2\nu)} v_A^{2(2\nu-1)/(1+2\nu)}. \quad (45)$$

The thickness  $H_{\text{corona}}^{(1)}$  of the corona is given by:

$$H_{\text{corona}}^{(1)} \cong \gamma^{(1-\nu)/(1+2\nu)} N_A^{3\nu/(1+2\nu)} v_A^{3(2\nu-1)/(2\nu+1)} \quad (46)$$

while the free energy per chain yields:

$$\frac{F^{(1)}}{k_B T} \cong \gamma^{1/(1+2\nu)} N_A^{2\nu/(1+2\nu)} v_A^{2(2\nu-1)/(2\nu+1)}. \quad (47)$$

In a spherical or cylindrical crew-cut micelle ( $i = 2, 3$ ), the coronal free energy is lower than in a planar brush. At small curvatures of the core, the coronal contribution, given by (42), can be expanded with respect to the small parameter  $H_{\text{corona}}^{(1)}/R_{\text{core}} \ll 1$ , with an account of the normalization condition:

$$N_A = \int_{R_{\text{core}}}^{R_{\text{core}}+H_{\text{corona}}} c_p(r) s(r) dr. \quad (48)$$

Here,  $c_p(r)$  is the polymer concentration (number density of the  $A$  monomers) at a distance  $(r - R_{\text{core}})$  from the core, and one can use the scaling relation [57] between the local polymer concentration and the correlation length,  $c_p(r) \cong \xi^{(1-3\nu)/\nu} v_A^{(1-2\nu)/\nu}$ . Retention of the first (linear in  $H_{\text{corona}}^{(1)}/R_{\text{core}}$ ) term provides an approximate expression:

$$\begin{aligned} \frac{F_{\text{corona}}^{(i)}}{k_B T} &\approx \frac{F_{\text{corona}}^{(1)}}{k_B T} \left[ 1 - \frac{1}{2} \left( \frac{\partial \ln c_p(r)}{\partial \ln r} - \frac{\partial \ln f(r)}{\partial \ln r} \right) \frac{H_{\text{corona}}^{(1)}}{R_{\text{core}}} \right] = \\ &= \frac{F_{\text{corona}}^{(1)}}{k_B T} \left[ 1 - \frac{(i-1)}{4\nu} \frac{H_{\text{corona}}^{(1)}}{R_{\text{core}}} \right], \end{aligned} \quad (49)$$

where  $f(r) \sim \xi^{-3}(r) \sim r^{-3(i-1)/2}$  is the free energy density in the corona,  $H_{\text{corona}}^{(1)}$  is given by (46), and  $R_{\text{core}}$  is related to  $i$  and  $s$  via (38).

Within this line of approximations, the total free energy per chain in a crew-cut aggregate of morphology  $i$  yields:

$$\begin{aligned} \frac{F^{(i)}}{k_B T} &= \frac{F^{(1)}}{k_B T} - b_0 \frac{(i-1)}{2i} \gamma^{(2-3\nu)/(1+2\nu)} N_A^{7\nu/(1+2\nu)} v_A^{7(2\nu-1)/(2\nu+1)} \frac{\varphi}{N_B} \\ &\quad + b_i i^2 \frac{N_B}{\varphi^2} \left( \frac{N_A}{\gamma} \right)^{-4\nu/(1+2\nu)} v_A^{4(1-2\nu)/(2\nu+1)}. \end{aligned} \quad (50)$$

In this equation, the first (dominant) term is the free energy per chain in the equilibrium planar lamella ( $i = 1$ ). The second term is a decrease in coronal free energy due to curvature of the core (the numerical coefficient  $b_0 \simeq 1$  does not depend on  $i$ ). The third term gives the elastic free energy of the core block [the numerical coefficients  $b_i$  are specified in (41)]. The radius  $R_{\text{core}}$  of the core in a cylindrical ( $i = 2$ ) or spherical ( $i = 3$ ) micelle is calculated via (38) and (45), whereas the corona thickness  $H_{\text{corona}}^{(i)} \approx H_{\text{corona}}^{(1)}$ , cf. (46).

A morphological transition  $(i+1) \Rightarrow i$  is specified by the condition  $F^{(i+1)} = F^i$ , to give the following equation for the binodals:

$$\frac{b_0}{2i(i+1)[b_{i+1}(i+1)^2 - b_i i^2]} \frac{\varphi^3}{N_B^2} \gamma^{(2-7\nu)/(1+2\nu)} N_A^{11\nu/(1+2\nu)} v_A^{11(2\nu-1)/(2\nu+1)} = 1 \quad (51)$$

By substituting  $i = 1$  in (51) and solving it with respect to  $N_B$ , one finds the degree of polymerization of the insoluble block,  $N_B^{(l-c)}$ , corresponding to a lamella-to-cylinder transition:

$$N_B^{(l-c)} = \frac{\sqrt{2b_0}}{\pi} \varphi^{3/2} \gamma^{(2-7\nu)/(2+4\nu)} N_A^{11\nu/(2+4\nu)} v_A^{11(2\nu-1)/(4\nu+2)}. \quad (52)$$

Substitution of  $i = 2$  in (51) gives the degree of polymerization  $N_B^{(c-s)}$ , corresponding to a cylinder-to-sphere transition:

$$N_B^{(c-s)} = \frac{\sqrt{\frac{20}{21}b_0}}{\pi} \varphi^{3/2} \gamma^{(2-7\nu)/(2+4\nu)} N_A^{11\nu/(2+4\nu)} v_A^{11(2\nu-1)/(4\nu+2)}. \quad (53)$$

Because both binodals  $N_B^{(l-c)}$  and  $N_B^{(c-s)}$  obey the same power law dependencies on  $N_A$ ,  $\gamma$ ,  $v_A$ , and  $\varphi$ , the region of thermodynamic stability of the cylindrical micelles ( $N_B^{(c-s)} < N_B < N_B^{(l-c)}$ ) constitutes a narrow corridor with the boundaries that differ only in the numerical prefactor. Remarkably, the relative width of this corridor:

$$\frac{\Delta N_B}{N_B^{(l-c)}} = \frac{N_B^{(l-c)} - N_B^{(c-s)}}{N_B^{(l-c)}} = 1 - \sqrt{\frac{10}{21}} \approx 0.31 \quad (54)$$

is independent of the solvent strength (the value of  $\nu$ ). However, a weak dependence on the solvent quality is found for the inverted binodals (i.e., the degrees of polymerization of the coronal block,  $N_A^{(l-c)}(N_B, \gamma, \varphi)$  and  $N_A^{(c-s)}(N_B, \gamma, \varphi)$ , corresponding to the lamella-to-cylinder and the cylinder-to-sphere transitions, respectively):

$$\frac{\Delta N_A}{N_A^{(l-c)}} = \frac{N_A^{(c-s)} - N_A^{(l-c)}}{N_A^{(l-c)}} = \left(\frac{21}{10}\right)^{(1+2\nu)/11\nu} - 1 \approx \begin{cases} 0.28, & \nu = 3/5, \\ 0.31, & \nu = 1/2. \end{cases} \quad (55)$$

Hence, upon a progressive decrease in the solvent strength, a slight increase is predicted for the relative interval of molecular weights of soluble block A that corresponds to thermodynamically stable cylindrical micelles.

In Fig. 3 we present the theoretical diagram of states in  $N_A$ ,  $N_B$  coordinates, which specifies the stability regions of spherical (S), cylindrical (C), and lamellar (L) aggregates in dilute solutions of non-ionic block copolymer [50]. The binodals (solid lines) are calculated using the full expressions for the corresponding free energy of an aggregate of morphology  $i$ . The latter involves the numerical

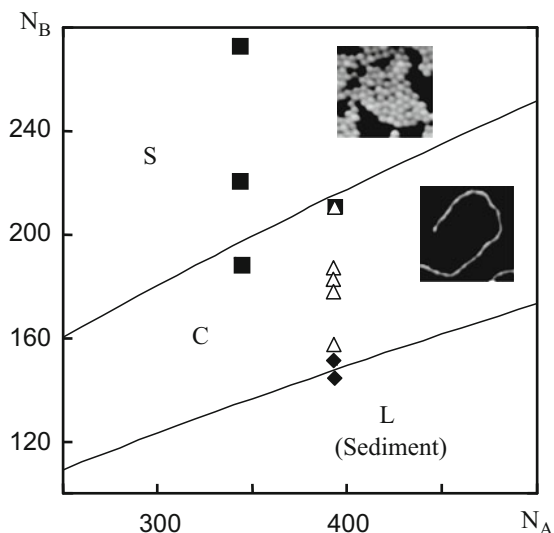


**Fig. 3** Diagram of states for non-ionic block copolymer with soluble  $A$  and insoluble  $B$  blocks with theoretically predicted stability regions of spherical (S), cylindrical (C), and lamellar (L) aggregates. Values of the theoretical parameters are adjusted for PS-PI copolymer in  $n$ -heptane [50]. Different symbols specify morphology of the experimental samples: spherical micelles (*squares*), cylindrical micelles (*triangles*), and insoluble aggregates, presumably lamellae (*diamonds*). AFM images of spherical and cylindrical micelles are adopted from [50]

values of all the parameters, adjusted for a specific block copolymer system, namely polyisoprene(PI)-polystyrene(PS) in  $n$ -heptane. Samples with different molecular weights of the soluble (PI) and insoluble (PS) blocks were examined by static and dynamic light scattering. The morphology  $i$  of the aggregates in each sample, specified by respective degrees of polymerization,  $N_A$  and  $N_B$ , of PI and PS blocks is indicated in the diagram by squares (spheres,  $i = 3$ ), triangles (cylinders,  $i = 2$ ), and diamonds (insoluble aggregates). The latter presumably correspond to associated lamellae ( $i = 1$ ) in the sediment. The shapes of soluble aggregates (spherical and cylindrical micelles of PI-PS diblock copolymer) are visualized by atomic force microscopy (AFM).

Note that for spherical (starlike as well as crew-cut) micelles, the most probable aggregation number [specified by (11)] is close to the average aggregation number. For large  $p \gg 1$ , the concentration-dependent corrections arising due to translational entropy of micelles are negligible. The thermal (equilibrium) fluctuations in the aggregation number (polydispersity of micelles) are controlled by the shape,  $\partial^2 F(p)/\partial p^2$ , of the free energy near the bottom of the minimum attained at  $p = p_0$ . By contrast, in the solution containing cylindrical micelles (at the total polymer concentration  $c \geq \text{CMC}$ ), the distribution with respect to the length (the aggregation number) is wide and follows an exponentially decaying function [35, 37]. The average length of a cylindrical micelle increases proportionally to the square root of the total polymer concentration,  $c$ , and grows exponentially as a function of excess free energy of the end-cap of the cylindrical micelle [35, 60].

## 4 Scaling Theory of Micelles with Polyelectrolyte Corona

The structure and the basic thermodynamics of micelles formed by amphiphilic block copolymers with a PE coronal block  $A$  can be analyzed using the blob model. However, the ionization of block  $A$  in a polymeric amphiphile introduces long-ranged repulsive interactions in the corona of a micelle. As a result, the blob picture for the micellar corona has to be modified, as explained in this section.

### 4.1 Starlike Micelles with Quenched Polyelectrolyte Corona

We start with the case of a salt-free dilute solution that contains asymmetric ( $N_A \geq N_B$ ) ionic/hydrophobic block copolymers with a long quenched PE block. These copolymers associate into starlike micelles. The corona of such micelle resembles a star-branched PE [61–64], discussed in detail in [10].

Long-ranged repulsive Coulomb interactions between the coronal blocks  $A$  dominate over short-ranged excluded-volume monomer–monomer repulsions, provided that the fraction of charged monomer units is sufficiently large. The block copolymer solution also contains mobile counterions that spread fairly uniformly over the volume of the solution if the aggregation number  $p$  is small,  $p \leq \alpha_b^{-1/2} l_B^{-1}$ . Here,  $l_B = e^2 / a \epsilon k_B T$  is the Bjerrum length measured in units of monomer length  $a$ ,  $e$  is the elementary charge, and  $\epsilon$  is the dielectric permittivity of the solvent. By contrast, a micelle with large aggregation number,  $p \gg \alpha_b^{-1/2} l_B^{-1}$ , retains the majority of its counterions inside the corona. The coronal contribution to the free energy is dominated by Coulomb repulsions between charged blocks  $A$  in the former case, and by the translational entropy of counterions confined in the corona in the latter case (the so-called osmotic regime). The combined action of Coulomb repulsion and osmotic pressure of counterions entrapped in the corona results in a uniform radial stretching of the coronal blocks  $A$ ,  $R_{\text{corona}} \sim N_A$ . If Gaussian entropic elasticity of the coronal chains is assumed,  $F_{\text{elastic}} \cong k_B T R_{\text{corona}}^2 / N_A$ , then each coronal block can be envisioned as a string of Gaussian electrostatic blobs with constant size:

$$\xi \cong \begin{cases} (\alpha_b^2 l_B)^{-1/3} p^{-1/3}, & p \ll \alpha_b^{-1/2} l_B^{-1}, \\ \alpha_b^{-1/2}, & p \gg \alpha_b^{-1/2} l_B^{-1}. \end{cases} \quad (56)$$

Hence, the radius of the corona is given by:

$$R_{\text{corona}}(p) \cong \frac{N_A}{\xi} \cong \begin{cases} N_A (\alpha_b^2 l_B)^{1/3} p^{1/3}, & p \ll \alpha_b^{-1/2} l_B^{-1}, \\ N_A \alpha_b^{1/2}, & p \gg \alpha_b^{-1/2} l_B^{-1} \end{cases} \quad (57)$$

and the free energy is given by:

$$F_{\text{corona}} / k_B T \cong \frac{N_A}{\xi^2}. \quad (58)$$

Balancing the coronal free energy,  $F_{\text{corona}}$ , with the excess free energy of the core–corona interface [cf. (24)] leads to the equilibrium aggregation number:

$$p_{\text{eq}} \cong \begin{cases} \gamma(N_B/\varphi)^{2/3} N_A^{-1} (\alpha_b^2 l_B)^{-2/3}, & p_{\text{eq}} \ll \alpha_b^{-1/2} l_B^{-1}, \\ \gamma^3 (N_B/\varphi)^2 (N_A \alpha_b)^{-3}, & p_{\text{eq}} \gg \alpha_b^{-1/2} l_B^{-1} \end{cases} \quad (59)$$

the radius of the core:

$$R_{\text{core}} \cong \begin{cases} \gamma^{1/3} (N_B/\varphi)^{5/9} N_A^{-1/3} (\alpha_b^2 l_B)^{-2/9}, & p_{\text{eq}} \ll \alpha_b^{-1/2} l_B^{-1}, \\ \gamma (N_B/\varphi) (N_A \alpha_b)^{-1}, & p_{\text{eq}} \gg \alpha_b^{-1/2} l_B^{-1} \end{cases} \quad (60)$$

and the corresponding radius of the corona:

$$R_{\text{corona}} \cong \begin{cases} N_A^{2/3} \gamma^{1/3} (N_B/\varphi)^{2/9} (\alpha_b^2 l_B)^{1/9}, & p_{\text{eq}} \ll \alpha_b^{-1/2} l_B^{-1}, \\ N_A \alpha_b^{1/2}, & p_{\text{eq}} \gg \alpha_b^{-1/2} l_B^{-1} \end{cases} \quad (61)$$

which determines the experimentally measurable (e.g., in dynamic light scattering experiments) size of the micelle.

As in the case of micelles formed by copolymers with non-ionic coronal blocks, the aggregation number  $p$  increases as a power law function of the length  $N_B$  of the core-forming block. A new feature, introduced by ionic interactions in the corona, is, however, a strong decrease in the aggregation number as a function of the length  $N_A$  of the coronal block  $A$  and its degree of ionization,  $\alpha_b$ . As follows from (59), micelles with a small aggregation number,  $p_{\text{eq}} \leq \alpha_b^{-1/2} l_B^{-1}$ , that release counterions from their barely charged coronae into the bulk of the solution, are formed if  $N_A^3 \alpha_b^{5/2} \geq \gamma^3 (N_B/\varphi)^2 l_B$ . In the case of shorter coronal and/or longer core-forming blocks,  $N_A^3 \alpha_b^{5/2} \ll \gamma^3 (N_B/\varphi)^2 l_B$ , osmotic micelles with larger aggregation numbers,  $p_{\text{eq}} \gg \alpha_b^{-1/2} l_B^{-1}$  are formed, which retain most of their counterions in the coronal domain. This situation usually occurs in experimental systems. Remarkably, as follows from (61), the radius of the micellar corona in the osmotic regime is controlled (in terms of its power law dependence) solely by the length,  $N_A$ , and the degree of ionization,  $\alpha_b$ , of the coronal block.

Another specific feature of osmotic micelles in salt-free solutions is the strong increase of the CMC as a function of  $N_A$  and  $\alpha_b$ . As follows from (16), the dominant term for the CMC of micelles in the osmotic regime is given by:

$$\ln \text{CMC} \approx -\gamma (N_B/\varphi)^{2/3} (\alpha_b N_A)^{-1}. \quad (62)$$

As discussed in Sect. 2.1, the origin of this increase in the CMC is the translational entropy penalty for the localization of counterions in the corona upon the association of block copolymers into micelles.

For micelles with a small aggregation number,  $p \leq \alpha_b^{-1/2} l_B^{-1}$ , screening effects of low molecular weight salt that is added to the micellar solution, become important when the salt-controlled Debye screening length becomes smaller than the

micellar size,  $r_D \leq R_{\text{corona}}$ . For micelles with a large aggregation number, whose coronae are found in the osmotic regime, the effect of salt on the self-assembly becomes essential when the (bulk) salt concentration  $\Phi_{\text{ion}}$  exceeds the concentration of counterions entrapped in the corona,  $\Phi_{\text{ion}} \geq p\alpha_b^{-1/2}N_A^{-2}$ . As discussed in detail in [18, 62], in the salt-dominated regime, the micellar corona can be subdivided into several concentric regions that differ with respect to local structural properties (e.g., radial dependence of the coronal blob size). Importantly, the size of the coronal blobs in salt added solution is an increasing function of the distance from the center of a micelle, though the blobs are not closely packed [18, 62]. However, with a good (experimentally accessible) accuracy, the effect on the self-assembly of the screening of the electrostatic interactions in the micellar corona, can be accounted for within the mean-field approximation, as explained in Sect. 6.

## 4.2 Crew-Cut Micelles with Quenched Polyelectrolyte Corona

Strongly asymmetric copolymers with long hydrophobic blocks form crew-cut micelles with  $H_{\text{corona}} \ll R_{\text{core}}$ . The coronae of such micelle can be treated as quasi-planar PE brushes [25–33].

A detailed analysis shows [30] that when the surface area per coronal chain is sufficiently small, the majority of counterions are localized inside the brush. The free energy of such corona is dominated by the translational entropy loss of the entrapped counterions (the corona is equivalent to the “osmotic” PE brush). More specifically, this is the case when  $H_{\text{corona}} \gg \Lambda$ , where  $\Lambda = s/2\pi l_B \alpha_b N_A$  is the Gouy–Chapman length. In the opposite limit of a relatively sparsely “grafted” corona formed by blocks  $A$  that have few charged groups,  $H_{\text{corona}} \ll \Lambda$ , and most of the counterions escape from the corona, but are retained in the proximity of the core within a distance  $\sim \Lambda$  provided that  $\Lambda \ll R_{\text{core}}$ . We assume that the corona of a crew-cut PE micelle is in the osmotic regime (this situation is typical for experimental systems).

For crew-cut PE micelles, the coronal chains can be presented as being composed of strings of Gaussian electrostatic blobs of size  $\xi \cong \alpha_b^{-1/2}$ . The average distance between the coronal chains,  $\sim s^{1/2}$  exceeds the blob size  $\xi$ . This implies that the electrostatic blobs in the quasi-planar corona of a crew-cut micelle are also not closely packed. Remarkably, in the osmotic regime, the size of the electrostatic blob and, consequently, the corona thickness,  $H_{\text{corona}} \cong N_A/\xi \cong N_A \alpha_b^{1/2}$ , are independent (in terms of power law dependencies) of the aggregation number  $p$  (i.e., independent of area  $s(R_{\text{core}})$  per PE block  $A$  at the core–corona interface).

As a result, the equilibrium aggregation number and the core radius in a crew-cut spherical micelle are given (with the accuracy of numerical factors) by the same expressions [second lines in (59) and (60)] as for a starlike spherical micelle in the osmotic regime:

$$p_{\text{eq}} \cong \gamma^3 (N_B/\varphi)^2 (N_A \alpha_b)^{-3}, \quad (63)$$

$$R_{\text{core}} \cong \gamma (N_B/\varphi) (\alpha_b N_A)^{-1}. \quad (64)$$



The aggregation number and the core size increase as a function of the length of the hydrophobic block,  $N_B$  and decrease as a power law function of the length of the PE block,  $N_A$ . The surface area per chain:

$$s_{\text{eq}} \cong \alpha_b \frac{N_A}{\gamma} \quad (65)$$

is independent of the length  $N_B$  of the core block [cf. (34)]. The CMC for the crew-cut micelles in a salt-free solution is also given by (62).

The condition  $H_{\text{corona}} \ll R_{\text{core}}$  holds as long as  $N_A \ll (N_B \gamma / \varphi)^{1/2} \alpha_b^{-3/4}$ . In the opposite limit,  $N_A \gg (N_B \gamma / \varphi)^{1/2} \alpha_b^{-3/4}$ , the micelles are starlike,  $H_{\text{corona}} \gg R_{\text{core}}$ .

Addition of salt in the solution leads to the screening of electrostatic repulsions between the coronal chains and a decrease in the excess osmotic pressure, as soon as the corona is found in the salt-dominated regime [28]. This regime is entered when the bulk concentration of added salt exceeds significantly the concentration of counterions trapped inside the corona,  $\Phi_{\text{ion}} \gg \alpha_b^{1/2} s^{-1} \cong \gamma \alpha_b^{-1/2} N_A^{-1}$ . Here, one can use the local electroneutrality mean-field approximation, discussed in Sect. 5.

## 5 Mean-Field Theory of Block Copolymer Micelles: Boxlike Model

The mean-field approach provides a convenient framework for the analysis of copolymer self-assembly leading to micellar structures. Combining the mean-field approach with the local electroneutrality approximation (LEA) enables us to generalize the theory for micelles with ionic coronal blocks that feature stimuli-responsive properties.

The LEA assumes that the charge of coronal chains is compensated by the (excess) local concentration of counterions. The LEA is applicable provided that the number of copolymer chains in one micelle is sufficiently large that the excess electrostatic potential is great enough to retain the mobile counterions inside the corona, even at low salt concentrations in the solution. In the LEA framework, the electrostatic interactions manifest themselves through the entropy of the ions, disproportionated between the interior of the corona and the bulk solution. The mean-field theory in combination with the LEA scheme gives a route wherein one can account explicitly for the ionization equilibrium and the interplay of electrostatic and nonelectrostatic interactions in the micellar corona. This is of key importance for the analysis of stimuli-induced structural transitions in micelles formed by copolymer that contains a weakly ionizable (pH-sensitive) PE block. The latter demonstrate a strong coupling between the ionization and aggregation state of the block copolymer.

Within a mean-field approximation, the interaction part of the free energy density in the corona,  $f_{\text{int}}\{c_p(r)\}$ , can be presented as a function of the local concentration

of monomer units,  $c_p(r)$ . It comprises the contributions  $f_{\text{ev}}\{c_p(r)\}$  and  $f_{\text{ion}}\{c_p(r)\}$  that arise due to the repulsive short-ranged (excluded volume) monomer–monomer interactions and due to the charges along the coronal chains:

$$f_{\text{int}}\{c_p(r)\} = f_{\text{ev}}\{c_p(r)\} + f_{\text{ion}}\{c_p(r)\}. \quad (66)$$

Here:

$$f_{\text{ev}}\{c_p(r)\}/k_B T = v_A c_p^2(r) + w_A c_p^3(r) + \dots, \quad (67)$$

whereas the ionic contribution,  $f_{\text{ion}}\{c_p(r)\}$ , is specified below in Sects. 6 and 7. Since solvent is assumed to be good for uncharged monomer units of the block *A*, we retain only the first term in (67) (to account for binary short-ranged repulsions).

At this stage, we neglect the radial gradients in the polymer density distribution within the corona and in the elastic stretching of the *A* and *B* chains. In other words, we implement a boxlike model wherein the average concentration of monomer units inside the corona is given by:

$$c_p = \frac{3pN_A}{4\pi(R_{\text{corona}}^3 - R_{\text{core}}^3)} \quad (68)$$

and the free energy of a spherical micelle with arbitrary size ratio,  $R_{\text{corona}}/R_{\text{core}} \equiv H_{\text{corona}}/R_{\text{core}} + 1$ , can be presented as:

$$\frac{F}{k_B T} \cong \frac{3R_{\text{core}}^2}{2N_B} + \frac{3(R_{\text{corona}} - R_{\text{core}})^2}{2N_A} + \frac{3\gamma N_B}{R_{\text{core}}\varphi} + \frac{F_{\text{int}}(c_p)}{k_B T}. \quad (69)$$

In this equation, the first and the second terms describe the respective conformational entropies of stretched core and coronal blocks, whereas the third term,  $\sim \gamma s(R_{\text{core}})$ , accounts for excess interfacial free energy [here,  $s(R_{\text{core}})$  is specified by (38)]. The last term in (69) accounts for repulsive interactions in the corona,

$$F_{\text{int}}(c_p) = (4\pi/3)(R_{\text{corona}}^3 - R_{\text{core}}^3)f_{\text{int}}(c_p). \quad (70)$$

The radii of the core,  $R_{\text{core}}$ , and of the corona,  $R_{\text{corona}}$ , are related as:

$$\frac{R_{\text{corona}}}{R_{\text{core}}} = \left(1 + \frac{N_A\varphi}{N_B c_p}\right)^{1/3}. \quad (71)$$

When (71) is substituted into (69), one can formulate the free energy of a micelle as a function of two independent variables,  $R_{\text{core}}$  and  $c_p$ . The minimization of this free energy with respect to  $R_{\text{core}}$  provides a relation between  $c_p$  and  $R_{\text{core}}$ :

$$R_{\text{core}} = \left(\frac{\gamma N_B^2}{\varphi}\right)^{1/3} \left\{1 + \frac{N_B}{N_A} \left[\left(1 + \frac{N_A\varphi}{N_B c_p}\right)^{1/3} - 1\right]^2\right\}^{-1/3} \quad (72)$$

and [using the packing condition, (23)] between  $c_p$  and the aggregation number  $p$ :

$$p = \frac{4\pi\gamma N_B}{3} \left\{ 1 + \frac{N_B}{N_A} \left[ \left( 1 + \frac{N_A\varphi}{N_B c_p} \right)^{1/3} - 1 \right]^2 \right\}^{-1} \quad (73)$$

in the equilibrium micelle. Correspondingly, the free energy per chain in a micelle becomes a function of a single structural parameter,  $c_p$ :

$$\frac{F(c_p)}{k_B T} = \frac{9}{2} \left( \frac{\gamma}{\varphi} \right)^{2/3} N_B^{1/3} \left\{ 1 + \frac{N_B}{N_A} \left[ \left( 1 + \frac{N_A\varphi}{N_B c_p} \right)^{1/3} - 1 \right]^2 \right\}^{1/3} + \frac{F_{\text{int}}(c_p)}{k_B T}. \quad (74)$$

In the limiting cases of starlike ( $N_A\varphi/N_B c_p \gg 1$ ) and crew-cut ( $N_A\varphi/N_B c_p \ll 1$ ) micelles, the free energy in (74) can be approximated as:

$$\frac{F(c_p)}{k_B T} \approx \frac{F_{\text{int}}(c_p)}{k_B T} + \begin{cases} \frac{9}{2} \gamma^{2/3} \left( \frac{N_B}{\varphi} \right)^{4/9} N_A^{-1/9} c_p^{-2/9}, & N_A\varphi/N_B c_p \gg 1, \\ \frac{9^{2/3}}{2} \gamma^{2/3} N_A^{1/3} c_p^{-2/3}, & N_A\varphi/N_B c_p \ll 1. \end{cases} \quad (75)$$

A closer inspection of the free energy (74) and (75) as a function of  $c_p$  allows us to specify the structural properties (aggregation number and size) of the equilibrium micelle as a function of the copolymer composition (values of  $N_B$  and  $N_A$ ) and the external parameters that control the strength of interactions in the coronal domain.

### 5.1 Non-ionic Block Copolymer Micelles

In the case of non-ionic or weakly charged coronal chains, the excluded-volume repulsions in the corona dominate over ionic interactions. In this case, the ionic contribution can be neglected and the corresponding contribution to the free energy can be presented as:

$$\frac{F_{\text{int}}(c_p)}{k_B T} = v_A N_A c_p. \quad (76)$$

The minimization of the free energy, (74) or (75), with respect to  $c_p$  gives the structural properties of a spherical micelle with a quasi-neutral corona. For a starlike micelle one finds:

$$p_{\text{eq}} \cong \gamma^{15/11} \left( \frac{N_B}{\varphi} \right)^{10/11} N_A^{-3/11} v_A^{-6/11}, \quad (77)$$

$$R_{\text{corona}} \cong \gamma^{3/11} \left( \frac{N_B}{\phi} \right)^{2/11} N_A^{6/11} v_A^{1/11}, \quad (78)$$

$$R_{\text{core}} \cong \gamma^{5/11} \left( \frac{N_B}{\phi} \right)^{7/11} N_A^{-1/11} v_A^{-2/11}. \quad (79)$$

The micelles are starlike, i.e.  $R_{\text{core}} \ll R_{\text{corona}}$ , as long as block A is sufficiently long:

$$N_A \gg \gamma^{2/7} \left( \frac{N_B}{\phi} \right)^{5/7} v_A^{-3/7} \quad (80)$$

In the range of block lengths specified by (80), starlike spherical micelles are thermodynamically most favorable. Copolymer aggregates with other morphologies (cylindrical micelles, vesicles) are metastable (i.e., have a larger free energy per chain). The most important factor that contributes to the stability of spherical micelles with relatively long  $N_A$  is that overlap, and therefore repulsions, between coronal blocks are minimal in the spherical geometry. The ionization of coronal chains results in their additional stretching as compared to quasi-neutral micelles. Therefore, the micelles with ionized corona remain spherical (starlike), provided (80) is fulfilled.

For the crew-cut quasi-neutral micelles with  $H_{\text{corona}} \ll R_{\text{core}}$ , that are formed by strongly asymmetric copolymers with short coronal blocks,  $N_A \ll \gamma^{2/7} (\frac{N_B}{\phi})^{5/7} v_A^{-3/7}$ , one finds:

$$p_{\text{eq}} \cong (\gamma/N_A)^{9/5} \left( \frac{N_B}{\phi} \right)^2 v_A^{-6/5}, \quad (81)$$

$$R_{\text{core}} \cong (\gamma/N_A)^{3/5} \left( \frac{N_B}{\phi} \right) v_A^{-2/5}, \quad (82)$$

$$H_{\text{corona}} \cong \gamma^{1/5} N_A^{4/5} v_A^{1/5}. \quad (83)$$

Due to the mean-field approximation used to account for excluded-volume interactions in the coronal domain, the power law exponents in (77)–(82) differ slightly from those obtained in the scaling framework in Sect. 3.1. This is because the mean-field approach neglects the local density correlations and overestimates the free energy of the micellar corona.

## 6 Mean-Field Theory of Block Copolymer Micelles with Quenched Polyelectrolyte Corona

Structural rearrangements in a micelle with quenched PE corona can be investigated using the mean-field approach (described in Sect. 5) in combination with the local electroneutrality approximation (LEA). As before, we neglect here the radial gradients in the polymer density and mobile ion distributions (i.e., implement the boxlike model). Moreover, we omit the contribution due to nonelectrostatic

(excluded volume) repulsions. In such a framework, the free energy of a quenched PE corona is formulated as:

$$\begin{aligned} \frac{F_{\text{ion}}(c_p)}{k_B T} &= \alpha_b N_A \left[ \left( 1 - \sqrt{1 + (\alpha_b c_p / \Phi_{\text{ion}})^2} \right) / (\alpha_b c_p / \Phi_{\text{ion}}) + \text{Arsh}(\alpha_b c_p / \Phi_{\text{ion}}) \right] \\ &\approx \begin{cases} \alpha_b N_A [\ln(2\alpha_b c_p / \Phi_{\text{ion}}) - 1], & \alpha_b c_p / \Phi_{\text{ion}} \gg 1, \\ N_A \frac{\alpha_b^2 c_p}{2\Phi_{\text{ion}}}, & \alpha_b c_p / \Phi_{\text{ion}} \ll 1, \end{cases} \end{aligned} \quad (84)$$

where:

$$\Phi_{\text{ion}} \equiv \sum_j c_{bj} \quad (85)$$

is the total concentration of (monovalent) ionic species in the bulk of the solution (including  $H^+$  and  $OH^-$  ions) and  $\text{Arsh}(x) \equiv \ln(x + \sqrt{x^2 + 1})$  is the inverse hyperbolic sine function.

Combining (84) and (74), one finds a closed expression for the free energy of a spherical micelle with a quenched PE corona as a function of a single structural parameter,  $c_p$ .

In the low salt limit,  $\alpha_b c_p \gg \Phi_{\text{ion}}$ , the coronal contribution to the free energy is dominated by the translational entropy of counterions entrapped inside the corona,  $F_{\text{int}} \cong k_B T \alpha_b N_A (\ln c_p - 1)$ . In this case, all results of the blob model are recovered both for osmotic starlike and crew-cut spherical micelles (59), (61), and (62).

In the high salt limit,  $\alpha_b c_p \ll \Phi_{\text{ion}}$ , the contribution of the translational entropy of mobile ions, disproportionated between the interior and the exterior of the corona, is equivalent to a renormalization of the second virial coefficient of monomer–monomer interactions, as  $v_A \rightarrow v_{\text{eff}} = v_A + \alpha_b^2 / 2\Phi_{\text{ion}}$ , [see (84)].

At any salt concentration,  $\Phi_{\text{ion}}$ , the  $F(c_p)$  curve exhibits a single minimum as a function of  $c_p$  that corresponds to a single population of equilibrium micelles. Using approximate expressions in (75), one can derive the power law dependencies for the structural properties of starlike and crew-cut micelles on the block lengths,  $N_A$  and  $N_B$ , the degree of ionization  $\alpha_b$ , the hydrophobicity of the block  $B$ , and the salt concentration, as discussed in the following section.

## 6.1 Starlike Micelles with Quenched Polyelectrolyte Corona

Within the mean-field approximation, the coronal contribution to the free energy in the salt-dominated regime can be calculated as:

$$F_{\text{int}}(p)/k_B T \cong v_{\text{eff}} N_A c_p = \left( v_A + \frac{\alpha_b^2}{2\Phi_{\text{ion}}} \right) N_A c_p, \quad (86)$$

where  $v_{\text{eff}} = v_A + \alpha_b^2 / 2\Phi_{\text{ion}}$  is the salt-dependent effective second virial coefficient. The equilibrium aggregation number and the core size in a starlike PE micelle

increase as a function of the salt concentration  $\Phi_{\text{ion}}$  according to the following equations:

$$p_{\text{eq}}(\Phi_{\text{ion}}) \cong \gamma^{15/11} (N_B/\varphi)^{10/11} N_A^{-3/11} \left( v_A + \frac{\alpha_b^2}{\Phi_{\text{ion}}} \right)^{-6/11}, \quad (87)$$

$$R_{\text{core}}(\Phi_{\text{ion}}) \cong \gamma^{5/11} (N_B/\varphi)^{7/11} N_A^{-1/11} \left( v_A + \frac{\alpha_b^2}{2\Phi_{\text{ion}}} \right)^{-2/11}. \quad (88)$$

An increase in the aggregation number  $p_{\text{eq}}(\Phi_s) \sim \Phi_{\text{ion}}^{6/11}$ , accompanied by a decrease in the strength of repulsive electrostatic interactions (due to added salt ions), results in a very weak decrease in the coronal size in a starlike PE micelle as a function of the salt concentration:

$$R_{\text{corona}}(\Phi_{\text{ion}}) \cong \gamma^{3/11} (N_B/\varphi)^{2/11} N_A^{6/11} \left( v_A + \frac{\alpha_b^2}{2\Phi_{\text{ion}}} \right)^{1/11}. \quad (89)$$

The micelles are starlike, i.e.,  $R_{\text{corona}} \gg R_{\text{core}}$  as long as  $N_A \gg \gamma^{2/7} (N_B/\varphi)^{5/7} (v_A + \alpha_b^2/2\Phi_{\text{ion}})^{-3/7}$ .

Under the so-called salt dominance conditions, the association of block copolymers into micelles does not lead to significant losses in the translational entropy of counterions (whose concentrations inside the corona and in the bulk of the solution are approximately equal). Therefore, within the accuracy of the main term, the CMC is controlled by the hydrophobicity of the block  $B$ :

$$\ln \text{CMC} \approx -\gamma (N_B/\varphi)^{2/3} + \gamma^{6/11} (N_B/\varphi)^{4/11} N_A^{1/11} \left( v_A + \frac{\alpha_b^2}{2\Phi_{\text{ion}}} \right)^{2/11}. \quad (90)$$

An increase in the salt concentration  $\Phi_{\text{ion}}$ , leads only to a decrease in the second (correction) term and to a mild decrease in the CMC.

At high salt concentrations  $\Phi_{\text{ion}} \gg v_A^{-1} \alpha_b^2$ , the structural properties (e.g.,  $p_{\text{eq}}(\Phi_{\text{ion}})$ , and  $R_{\text{corona}}(\Phi_{\text{ion}})$ ) approach the values that are found for starlike micelles with non-ionic corona, (77), (78).

Because an increase in salt concentration leads to the increase in the core size,  $R_{\text{core}}$ , and in the simultaneous decrease in the corona size,  $R_{\text{corona}}$ , the starlike micelle can transform into the crew-cut micelle with an increase in the salt concentration.

## 6.2 Crew-Cut Micelles with Quenched Polyelectrolyte Coronae

In the salt-dominated regime, the free energy of the quasi-planar corona of a crew-cut micelle is given by:

$$F_{\text{int}}/k_B T \cong N_A s^{-2/3} v_{\text{eff}}^{2/3} = N_A s^{-2/3} \left( v_A + \frac{\alpha_b^2}{2\Phi_{\text{ion}}} \right)^{2/3}. \quad (91)$$

It decreases as a function of the salt concentration. Balancing the free energy, (91), with the excess free energy of the core–corona interface, (24), gives the equilibrium interfacial area per copolymer chain:

$$s_{\text{eq}} \cong (N_A/\gamma)^{3/5} \left( v_A + \frac{\alpha_b^2}{2\Phi_{\text{ion}}} \right)^{2/5} \quad (92)$$

and the equilibrium aggregation number in a salt-dominated crew-cut micelle:

$$p_{\text{eq}}(\Phi_{\text{ion}}) \cong (\gamma/N_A)^{9/5} (N_B/\varphi)^2 \left( v_A + \frac{\alpha_b^2}{2\Phi_{\text{ion}}} \right)^{-6/5}. \quad (93)$$

As expected, the aggregation number increases with increasing salt concentration  $\Phi_{\text{ion}}$ . The corresponding power law exponent, 6/5, is remarkably larger than in the case of starlike micelles. This is due to stronger repulsive interactions between PE blocks in the quasi-planar corona of a crew-cut micelle as compared to those in a starlike corona. Similarly to the case of a starlike micelle, the thickness of the corona,  $H_{\text{corona}}$ , in a crew-cut micelle decreases as a function of the salt concentration,  $\Phi_{\text{ion}}$ , although the area  $s(\Phi_{\text{ion}})$  per PE chain at the core–corona interface decreases:

$$H_{\text{corona}}(\Phi_{\text{ion}}) \cong \gamma^{1/5} N_A^{4/5} \left( v_A + \frac{\alpha_b^2}{2\Phi_{\text{ion}}} \right)^{1/5}. \quad (94)$$

The size of the core, which dominates the overall dimensions of a crew-cut micelle, grows upon an increase in salt concentration as:

$$R_{\text{core}}(\Phi_{\text{ion}}) \cong (\gamma/N_A)^{3/5} (N_B/\varphi) \left( v_A + \frac{\alpha_b^2}{2\Phi_{\text{ion}}} \right)^{-2/5}. \quad (95)$$

Upon further increase in the salt concentration,  $\Phi_{\text{ion}} \gg v_A^{-1} \alpha_b^2$ , the structural properties of crew-cut micelles with a quenched PE corona asymptotically approach these of micelles with a non-ionic corona, (81)–(83).

Similarly to the case of crew-cut micelles composed of non-ionic block copolymers, an increase in the length of the core-forming block  $B$  leads to an increase in entropic penalty for stretching the chains. As a result, copolymers with longer insoluble block  $B$  might associate in nonspherical aggregates (e.g., cylindrical crew-cut micelles). These morphological changes will be discussed in detail in Sect. 10.

## 7 Mean-Field Theory of Block Copolymer Micelles with Annealing Polyelectrolyte Corona

Within the framework of the boxlike model, the free energy of the corona of micelle with annealing PE block can be formulated as:

$$\begin{aligned} \frac{F_{\text{ion}}(c_p)}{k_B T} &= N_A \left[ \left( 1 - \sqrt{1 + (\alpha c_p / \Phi_{\text{ion}})^2} \right) + \ln(1 - \alpha) \right] \\ &\approx N_A \cdot \begin{cases} -\alpha + \ln(1 - \alpha), & \alpha_b c_p / \Phi_{\text{ion}} \gg 1, \\ \frac{\alpha_b^2 c_p}{2\Phi_{\text{ion}}} + \ln(1 - \alpha_b), & \alpha_b c_p / \Phi_{\text{ion}} \ll 1. \end{cases} \end{aligned} \quad (96)$$

Here, the average degree of ionization  $\alpha$  of the coronal block  $A$  depends not only on the pH (via  $\alpha_b$ ), but also on the ionic strength in the bulk solution (buffer), and the average polymer concentration in the corona,  $c_p$ , as:

$$\frac{\alpha}{1 - \alpha} \cdot \frac{1 - \alpha_b}{\alpha_b} = \sqrt{1 + (\alpha c_p / \Phi_{\text{ion}})^2} - \alpha c_p / \Phi_{\text{ion}}, \quad (97)$$

where  $\alpha_b$  is the degree of ionization of a single monomer in the bulk solution of given pH:

$$\alpha_b = \frac{10^{\text{pH} - \text{p}K_a}}{10^{\text{pH} - \text{p}K_a} + 1}. \quad (98)$$

Equation (97) can be used to obtain approximate expressions for the degree of ionization of the monomer units of the coronal block  $A$  in the limiting cases of low and high salt concentrations:

$$\alpha \cong \begin{cases} \left( \frac{\alpha_b}{1 - \alpha_b} \cdot \frac{\Phi_{\text{ion}}}{2c_p} \right)^{1/2}, & \alpha c_p / \Phi_{\text{ion}} \gg 1, \\ \alpha_b \left[ 1 - \frac{\alpha_b c_p}{\Phi_{\text{ion}}} (1 - \alpha_b) \right], & \alpha c_p / \Phi_{\text{ion}} \ll 1. \end{cases} \quad (99)$$

The coupling between the ionization of the coronal block  $A$  and the association equilibrium of the copolymers gives rise to unique features for the self-assembly of amphiphilic block copolymers with a weak (pH-sensitive) PE block. In other words, the levels of ionization for unimers in solution and for copolymers incorporated in micelles, can be noticeably different due to different values of the pH inside micellar corona and in the bulk solution. Furthermore, the strength of the electrostatic repulsion in the corona can be affected not only by variations in the ionic strength (as it is for micelles with quenched PE corona), but also by variations in the pH, which affect the ionization of the coronal chains.

Moreover, the effect of added salt on the self-assembly of block copolymers with an annealing PE block is more complicated than for copolymers with a quenched PE block. The reason for this is that at  $\text{pH} \cong \text{p}K$ , an addition of small amounts of salt into the bulk solution leads to substitution of  $H^+$  (or  $OH^-$ ) counterions in the micellar corona by salt ions. The latter promotes ionization of the coronal chains and affects the strength of repulsive interactions between the corona-forming blocks. At low salt concentrations, ionization of the monomer units in coronae of micelles formed by copolymers with an annealing PE block can be strongly suppressed. As a result, the coronal contribution to the free energy of the micelle might be dominated by nonelectrostatic excluded-volume repulsions between corona-forming blocks (the so-called quasi-neutral micelle regime).



## 7.1 Structural Transitions in Starlike Micelles with Annealing PE Corona

The block copolymer chains with a strongly asymmetric composition,  $N_A \gg \gamma^{2/7}(N_B/\varphi)^{5/7}v_A^{-3/7}$ , form starlike micelles at an arbitrary small degree of ionization of the coronal block. The free energy per chain in a starlike micelle with an annealing PE coronal block is given by:

$$\frac{F}{k_B T} \cong \frac{9}{2} \gamma^{2/3} \left( \frac{N_B}{\varphi} \right)^{4/9} N_A^{-1/9} c_p^{-2/9} + N_A \left[ v_A c_p + \left( 1 - \sqrt{1 + (\alpha c_p / \Phi_{\text{ion}})^2} \right) + \ln(1 - \alpha) \right], \quad (100)$$

where the degree of ionization  $\alpha(\alpha_b, \Phi_{\text{ion}}, c_p)$  is determined from (97).

Further analysis of the free energy as a function of  $c_p$  (or  $\alpha$ ), (100) and (97), indicates the existence of a single minimum at both low,  $\Phi_{\text{ion}} \ll \alpha_b c_p$ , and high,  $\Phi_{\text{ion}} \gg \alpha_b c_p$ , salt concentrations. This minimum corresponds to a single population of micelles that coexist with unimers either at low or at high salt concentration in the solution. At intermediate salt concentrations,  $F(c_p)$  might exhibit two minima as a function of  $c_p$ . The presence of two minima in the free energy indicates the possibility of abrupt (quasi-first order) salt- and pH-induced structural transitions in block copolymer micelles. These transitions are discussed below in Sect. 7.1.3.

### 7.1.1 Quasi-neutral Micelles

At low salt concentrations,  $\Phi_{\text{ion}} \ll \alpha_b c_p$ , the ionization of A segments in the micelle corona is low,  $\alpha \ll \alpha_b$ . In this case, the excluded-volume repulsions (binary interactions) give the dominant contribution to the free energy of the corona. As a result, the structural properties of the quasi-neutral micelles approximately coincide with those formed by non-ionic block copolymers and are given by (77) and (78).

An increase in the salt concentration leads to the progressive replacement of  $H^+$  ions in the micellar corona by, e.g.,  $Na^+$  ions of the added salt (i.e., increases the local pH in the corona). This promotes the increase in the degree of ionization  $\alpha$  of the coronal blocks as:

$$\alpha \cong \left( \frac{\alpha_b}{1 - \alpha_b} \cdot \Phi_{\text{ion}} \right)^{1/2} \gamma^{-3/11} \left( \frac{N_B}{\varphi} \right)^{-2/11} N_A^{5/11} v_A^{9/22}. \quad (101)$$

The latter leads to a slight decrease (on the level of the correction terms) in the aggregation number, and an increase in the radius of the corona.

The free energy per chain in a quasi-neutral micelle is given by:

$$F_{\text{quasi-neutral}}/k_B T \cong \gamma^{6/11} (N_B/\varphi)^{4/11} N_A^{1/11} v_A^{2/11} + N_A \ln(1 - \alpha). \quad (102)$$

Here, the first term is dominant because  $\alpha$ , given by (101), is small.

Although at low salt concentrations the structural parameters of quasi-neutral micelles formed by copolymers with an annealing PE block are close to those of micelles formed by non-ionic block copolymers, the CMC for the former is significantly larger than that for the latter. Indeed, the degree of ionization of the annealing PE blocks in the unimer state of copolymer,  $\alpha_b$ , is significantly larger than that of the copolymers incorporated in micelles. Hence, the association of copolymers into micelles is accompanied by an additional free energy penalty (recombination of significant fraction of counterions with the acidic groups of the annealing PE blocks). As a result, the CMC increases as a function of  $N_A$  and  $\alpha_b$  according to the equation:

$$\begin{aligned} \ln \text{CMC}_{\text{quasi-neutral}} &\approx -\gamma(N_B/\varphi)^{2/3} + \gamma^{6/11}(N_B/\varphi)^{4/11}N_A^{1/11}v_A^{2/11} - N_A \ln(1 - \alpha_b) \\ &= \ln \text{CMC}_{\text{neutral}} - N_A \ln(1 - \alpha_b). \end{aligned} \quad (103)$$

Here, the first two terms specify the CMC for equivalent uncharged (neutral) block copolymer with lengths of blocks,  $N_A$  and  $N_B$ :

$$\ln \text{CMC}_{\text{neutral}} \approx -\gamma(N_B/\varphi)^{2/3} + \gamma^{6/11}(N_B/\varphi)^{4/11}N_A^{1/11}v_A^{2/11}, \quad (104)$$

and we have neglected the  $N_A(1 - \alpha)$  term in the free energy of the coronae of the quasi-neutral micelles as well as the contribution due to intramolecular repulsive interactions and the stretching of the block  $A$  in unimers.

Equation (103) demonstrates that the CMC for quasi-neutral micelles is a strongly increasing function of  $\alpha_b$ , i.e., it is strongly affected by the value of the bulk pH. When  $-N_A \ln(1 - \alpha_b) \geq \gamma(N_B/\varphi)^{2/3}$ , quasi-neutral micelles do not form at any copolymer concentration in the solution.

### 7.1.2 Charged Micelles

In the opposite limit of high salt concentration,  $\Phi_{\text{ion}} \gg \alpha_b c_p$ , the difference between the pH in the bulk solution and inside the micellar corona is negligible. At a given solution pH,  $\alpha_b$  is specified according to (98), and the monomer units of blocks  $A$  in the micellar corona approach their maximal at given pH degree of ionization,  $\alpha \approx \alpha_b$ . The corona is indistinguishable from that formed by quenched PE chains with a degree of ionization  $\alpha_b$  in the salt-dominated regime. The evolution of the structural parameters of the micelles follows the same trends as described above: the aggregation number increases and the coronal dimensions decrease upon an increase in the salt concentration according to (87) and (89), respectively. An increase in  $\alpha_b$  (an increase in the pH) enhances repulsive interactions in the corona and thus leads to a progressive decrease in the aggregation number and an increase in the coronal dimensions.

The free energy of micelles in the salt-dominated regime is formulated as:

$$F/k_B T \cong \gamma^{6/11} (N_B/\varphi)^{4/11} N_A^{1/11} (\alpha_b^2/2\Phi_{\text{ion}} + v_A)^{2/11} + N_A \ln(1 - \alpha_b), \quad (105)$$

whereas the CMC is given by:

$$\begin{aligned} \ln \text{CMC}_{\text{charged}} &\approx -\gamma (N_B/\varphi)^{2/3} + \gamma^{6/11} (N_B/\varphi)^{4/11} N_A^{1/11} \left( v_A + \frac{\alpha_b^2}{2\Phi_{\text{ion}}} \right)^{2/11} \\ &= \ln \text{CMC}_{\text{neutral}} + \gamma^{6/11} (N_B/\varphi)^{4/11} N_A^{1/11} v_A^{2/11} \\ &\quad \times \left[ \left( 1 + \frac{\alpha_b^2}{2\Phi_{\text{ion}} v_A} \right)^{2/11} - 1 \right]. \end{aligned} \quad (106)$$

### 7.1.3 Micelle-to-Micelle Transition

Remarkably, in the intermediate range of salt concentrations, starlike micelles formed by block copolymer with an annealing PE block exhibit a discontinuous variation of their structural parameters upon a smooth variation in either the salt concentration,  $\Phi_{\text{ion}}$ , or the pH of the solution.

Analysis of (100) indicates that at moderate salt concentrations, the free energy versus  $c_p$  curves might exhibit two minima, one corresponding to a quasi-neutral (weakly ionized) micelle with high aggregation number, and the other corresponding to a micelle with strongly charged corona,  $\alpha \approx \alpha_b$ , and low aggregation number. These two minima correspond to two populations of micelles that coexist in the solution in a certain range of salt concentrations.

When the two minima are equally deep, the transition from large (quasi-neutral) to small (charged) micelle occurs as a jump-wise quasi-first order phase transition. (A more accurate analysis [23] points at a finite interval of salt concentrations wherein the two types of micelles coexist). Using (102) and (105) for the free energy of quasi-neutral and charged micelle, and assuming  $\alpha_b^2/\Phi_{\text{ion}} v_A \gg 1$ , the characteristic salt concentration at the transition point can be evaluated as:

$$\Phi_{\text{ion}}^* \cong \alpha_b^{-7/2} \gamma^3 \left( \frac{N_B}{\varphi} \right)^2 N_A^{-5}. \quad (107)$$

Decomposition of large micelles into many smaller ones is accompanied by an abrupt increase in the degree of ionization of the corona from  $\alpha \approx \alpha_b (\Phi_{\text{ion}}^*/\alpha_b c_p)^{1/2}$  to  $\alpha_b$ , accompanied by a substantial drop in the aggregation number:

$$\frac{p_{\text{quasi-neutral}}}{p_{\text{charged}}} \cong \left( 1 + \frac{\alpha_b^2}{2v_A \Phi_{\text{ion}}^*} \right)^{6/11}. \quad (108)$$

A combined action of the decrease in the number of coronal chains and the increase in their ionization results in a relatively small jump up in the coronal dimensions:

$$\frac{R_{\text{corona,charged}}}{R_{\text{corona,quasi-neutral}}} \cong \left( 1 + \frac{\alpha_b^2}{2\nu_A \Phi_{\text{ion}}^*} \right)^{1/11}. \quad (109)$$

The diagram of states of the solution of block copolymer that forms starlike micelles is presented using as coordinates either polymer concentration versus salt concentration ( $\Phi_{\text{ion}}$ ) (Fig. 4a) or polymer concentration versus bulk degree of ionization ( $\alpha_b$ ) (Fig. 4b).

When the polymer concentration is below  $\text{CMC}_{\text{quasi-neutral}}^{\text{quasi-neutral}}$  ( $\text{CMC}_{\text{qn}}$ ), micelles do not form in the range of  $\Phi_{\text{ion}}$  to the left of the  $\text{CMC}_{\text{charged}}^{\text{charged}}$  ( $\text{CMC}_{\text{ch}}$ ) line. When the  $\text{CMC}_{\text{ch}}$  line is crossed, starlike micelles with charged,  $\alpha \approx \alpha_b$  coronae appear in the solution.

When the polymer concentration exceeds  $\text{CMC}_{\text{qn}}$ , quasi-neutral micelles with weakly ionized,  $\alpha \ll \alpha_b$ , coronae are found in the range of low salt concentrations (small  $\Phi_{\text{ion}}$ ). At the transition concentration,  $\Phi_{\text{ion}} = \Phi_{\text{ion}}^*$ , these micelles abruptly rearrange into micelles with smaller aggregation number, but stronger charged coronae. Further increase in salt content,  $\Phi_{\text{ion}} > \Phi_{\text{ion}}^*$ , leads to progressive increase in the micelle aggregation number.

Alternatively, decomposition of large quasi-neutral micelles into smaller charged micelles (upon crossing of  $\Phi_{\text{ion}}^*(\alpha_b)$  line) may be triggered by an increase in the pH (i.e., in  $\alpha_b$ ) at the polymer concentration above  $\text{CMC}_{\text{qn}}$ . An increase in the pH both below and above the transition threshold, leads to a continuous decrease in the aggregation number and an increase in the span of the corona. At polymer concentrations below  $\text{CMC}_{\text{ch}}$ , only unimers are found in the solution at high pH ( $\alpha_b \approx 1$ ). A decrease in pH leads to a decrease in chain ionization and in Coulomb repulsions between unimers, and may trigger micellization upon crossing the  $\text{CMC}_{\text{ch}}$  or the  $\text{CMC}_{\text{qn}}$  lines.

Figure 5 demonstrates the diagram of states for starlike micelles in the  $\Phi_{\text{ion}}, \alpha_b$  coordinates. We delineate four regions, denoted as  $S_{\text{qn}}, S_{\text{qn}'}, S_{\text{ch}}$  and  $U$ . In region  $S_{\text{qn}}$ , the starlike micelles are quasi-neutral, and their structural parameters are given by (77), (78), and (101). The dotted line divides region  $S_{\text{qn}}$  into two parts. To the left of the dotted line, the  $\text{CMC}_{\text{qn}}$  is virtually unaffected by the polyelectrolyte nature of the coronal chains (it coincides with the CMC for the equivalent neutral copolymer). To the right of the dotted line, the  $\text{CMC}_{\text{qn}}$  is shifted according to (103).

In region  $S_{\text{ch}}$ , the coronal blocks are charged,  $\alpha \approx \alpha_b$ , and the parameters of equilibrium micelles are given by (87) and (89). The bold line separating regions  $S_{\text{ch}}$  and  $S_{\text{qn}}$  is the line of abrupt rearrangements of the micelles,  $\Phi_{\text{ion}} = \Phi_{\text{ion}}^*(\alpha_b)$ . In region  $S_{\text{qn}'}$ , the coronal blocks  $A$  are ionized,  $\alpha \approx \alpha_b$ , but the electrostatic interactions are strongly screened due to the high salt concentration. As a result, the structural parameters of the micelles are the same as in region  $S_{\text{qn}}$ .

Finally, in region  $U$  the micelles are unstable, and only free ionized unimers (with  $\alpha = \alpha_b$ ) are found in the solution for any polymer concentration.

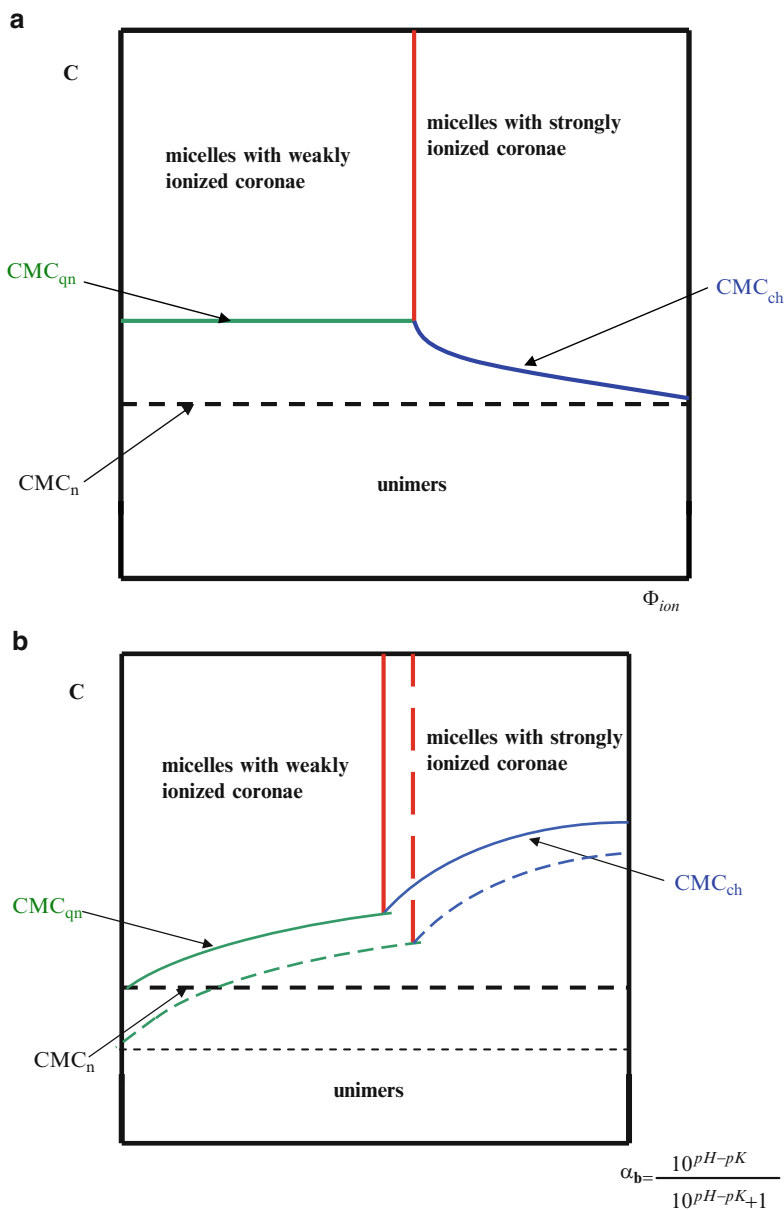


**Fig. 4** Diagram of states for solution of block copolymers with pH-sensitive PE blocks. Coordinates are (a) polymer concentration  $C$  and salt concentration  $\Phi_{ion}$  (at constant buffer pH); (b) polymer concentration  $C$  and pH (at constant salt concentration). Dashed lines in (b) indicate shift of the boundaries of different regimes upon increasing hydrophobicity of the blocks  $B$

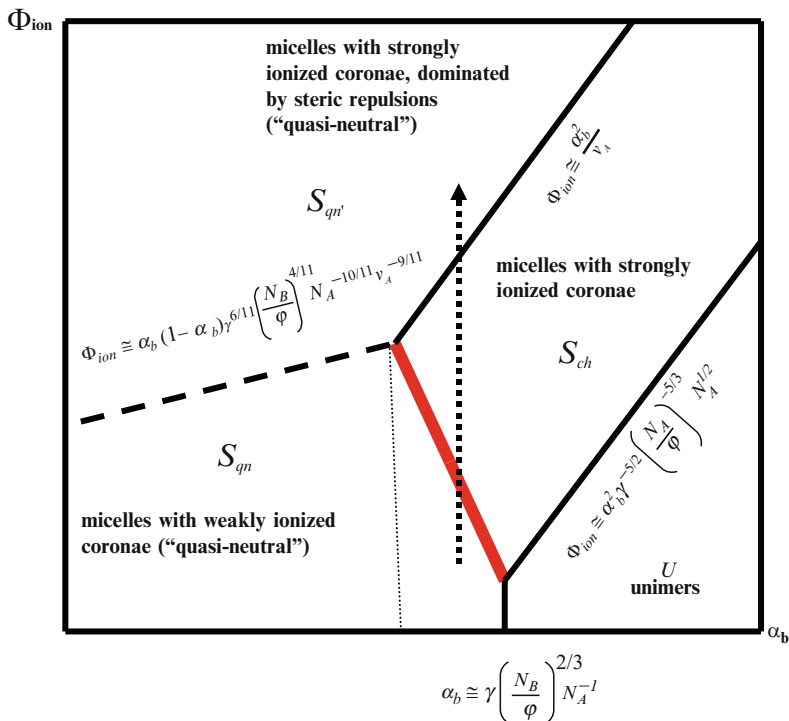


**Fig. 5** Diagram of states in  $\alpha_b, \Phi_{ion}$  coordinates for dilute solution of block copolymers with pH-sensitive PE blocks, that associate in starlike micelles,  $N_A \gg \gamma^{2/7} (\frac{N_B}{\phi})^{5/7} v_A^{-3/7}$ . The dotted arrow indicates cross-section of the diagram corresponding to the evolution of the micelle parameters as a function of salt concentration presented in Fig. 6a, b

Figure 6 shows the evolution of both the aggregation number and the radius of the corona for starlike micelles upon variations in the salt concentration (6a, b) and in the pH (6c,d). All the structural properties of starlike micelles with pH-sensitive coronal blocks exhibit a non-monotonous and discontinuous variation as a function of  $\Phi_{ion}$ : the aggregation number exhibits a minimum (with a jump down at  $\Phi_{ion} \approx \Phi^*$ ), whereas the coronal dimensions exhibit a weak maximum (with a jump up at  $\Phi_{ion} \approx \Phi^*$ ).

## 7.2 Crew-Cut Micelles with Annealing Polyelectrolyte Coronae

Crew-cut micelles with  $H_{corona} \ll R_{core}$  are formed by copolymers with comparatively long hydrophobic and short hydrophilic blocks,  $N_A \ll \gamma^{2/7} (\frac{N_B}{\phi})^{5/7} v_A^{-3/7}$ . The latter condition ensures that quasi-neutral micelles have a crew-cut shape. As we

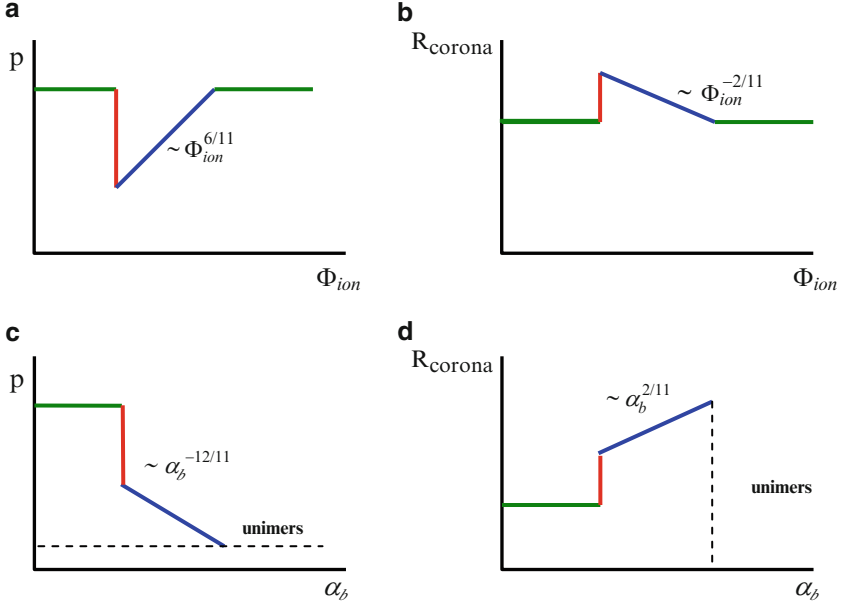


**Fig. 6** Dependency of (a) aggregation number  $p$ ; (b) radius of the corona  $R_{corona}$  for starlike micelles with annealing coronal block as a function of salt concentration. The pH is fixed according to the position of the dotted arrow in Fig. 5. Dependency of (c)  $p$  and (d)  $R_{corona}$  as a function of pH

will show, the progressively increasing role of electrostatic interactions at intermediate salt concentrations leads to the decrease in the size ratio,  $R_{core}/H_{corona}$ , which suggests possible transformation of crew-cut into starlike micelles.

The corona of a crew-cut micelle can be viewed as a quasi-planar annealing PE brush, as long as  $R_{core} \gg H_{corona}$ . The ionization-recombination balance and the structural properties of a planar PE brush were discussed in detail in [31]. Here, we focus on the evolution of crew-cut micelles caused by an increase in the salt concentration,  $\Phi_{ion}$ , and pH.

Using (75) (at  $N_A \phi_B / N_B c_p \ll 1$ ) and (96), we find that with the accuracy of numerical coefficients:

$$\frac{F}{k_B T} \cong \frac{9^{2/3}}{2} \gamma^{2/3} N_A^{1/3} c_p^{-2/3} + N_A \left[ v_A c_p + \ln(1 - \alpha) - \frac{\Phi_{ion}}{c_p} \left( \sqrt{1 + (\alpha c_p / \Phi_{ion})^2} - 1 \right) \right], \quad (110)$$

where  $\alpha(c_p, \Phi_{ion})$  is determined by (97).

In the low salt limit,  $\Phi_{\text{ion}} \ll \alpha_b c_p$ , the coronal chains are weakly ionized, i.e.,  $\alpha \ll \alpha_b \leq 1$ . Making use of (96), we represent the free energy in (110) as:

$$\frac{F}{k_B T} \cong \frac{9^{2/3}}{2} \gamma^{2/3} N_A^{1/3} c_p^{-2/3} + N_A [v_A c_p + \ln(1 - \alpha) - \alpha]. \quad (111)$$

At very low salt concentrations  $\alpha \ll \alpha_b \leq 1$ , and the last two terms in (111) are negligible compared to the second term (steric repulsions). The structure of micelles is determined by the competition between steric repulsions (the second term) and excess free energy of the core–corona interface (the first term). Balance of these terms indicates that the structural parameters are given by (81)–(83) for quasi-neutral crew-cut micelles.

The degree of ionization of the coronal chains increases as a function of the salt concentration (99) and is given by:

$$\alpha \cong \left( \frac{\alpha_b \Phi_{\text{ion}}}{1 - \alpha_b} \right)^{1/2} \frac{N_A^{1/5} v_A^{3/10}}{\gamma^{1/5}}. \quad (112)$$

As long as steric repulsions  $\sim c_p v_A$  in the corona dominate over the ionic contributions  $\sim \alpha$ , the increase in  $\alpha$  does not affect the structure of the micelles.

The ionic contributions start to dominate over steric repulsions at:

$$\Phi_{\text{ion}} \geq \Phi_{\text{ion}}^{(1)} \equiv \frac{1 - \alpha_b}{\alpha_b} \left( \frac{\gamma}{N_A} \right)^{6/5} v_A^{1/5}. \quad (113)$$

The equilibrium structure of the micelle is now determined by a balance between the osmotic pressure of counterions in the corona and excess interfacial free energy of the core–corona boundary. Here, the micellar corona is equivalent to a quasi-planar PE brush in the annealing osmotic regime [31].

The aggregation number and the thickness of the corona depend on the degree of ionization  $\alpha$  in the same way as for crew-cut micelles with osmotic quenched PE corona:

$$p \cong \gamma^3 (N_B / \varphi)^2 (N_A \alpha)^{-3}, \quad (114)$$

$$H_{\text{corona}} \cong a N_A \alpha^{1/2}, \quad (115)$$

$$s \cong \alpha \frac{N_A}{\gamma}, \quad (116)$$

but now the degree of ionization  $\alpha$  of the coronal blocks depends on the ionic strength,  $\Phi_{\text{ion}}$ , and on the polymer concentration in the corona  $c_p \cong N_A / s H_{\text{corona}}$  via (99), which leads to:

$$\alpha \cong \left( \frac{\alpha_b}{1 - \alpha_b} \frac{N_A \Phi_{\text{ion}}}{\gamma} \right)^2. \quad (117)$$

Hence,  $\alpha$  rapidly increases as a function of  $\Phi_{\text{ion}}$ .



An increase in the degree of ionization of blocks  $A$  leads to an increase in osmotic repulsion in the corona, and the aggregation number rapidly decreases as:

$$p_{\text{eq}} \cong \left( \frac{N_B}{\varphi} \right)^2 \left( \frac{\gamma}{N_A} \right)^9 \left( \frac{1 - \alpha_b}{\alpha_b \Phi_{\text{ion}}} \right)^6. \quad (118)$$

The extension of coronal chains is therefore given by:

$$H_{\text{corona}} \cong \alpha^{1/2} N_A \cong \frac{N_A^2}{\gamma} \frac{\alpha_b \Phi_{\text{ion}}}{1 - \alpha_b}, \quad (119)$$

i.e., the corona thickness increases with increasing salt concentration  $\Phi_{\text{ion}}$ , while the size of the core:

$$R_{\text{core}} \cong \left( \frac{N_B}{\varphi} \right) \left( \frac{\gamma}{N_A} \right)^3 \left( \frac{1 - \alpha_b}{\alpha_b \Phi_{\text{ion}}} \right)^2 \quad (120)$$

decreases with  $\Phi_{\text{ion}}$  due to the decrease in aggregation number, (118). As a result, the ratio  $R_{\text{core}}/H_{\text{corona}}$  decreases with increasing salt concentration as  $\sim 1/(\Phi_{\text{ion}})^3$ .

The annealing osmotic regime holds as long as  $\alpha \ll \alpha_b$ , i.e., in the range of salt concentrations:

$$\Phi_{\text{ion}} \ll \Phi_{\text{ion}}^{(2)} \equiv \frac{\gamma}{N_A} \alpha_b^{-1/2} (1 - \alpha_b). \quad (121)$$

At  $\Phi_{\text{ion}} \cong \Phi_{\text{ion}}^{(2)}$ , the coronal blocks reach maximal ionization,  $\alpha \approx \alpha_b$ , and maximal extension,  $H_{\text{corona}} \cong \alpha_b^{1/2} N_A$ . In contrast, the aggregation number reaches its minimal value, which coincides with the aggregation number for a quenched PE micelle with  $\alpha = \alpha_b$  in a salt-free solution and is given by (63).

The ratio  $R_{\text{core}}/H_{\text{corona}}$  also passes through a minimum at  $\Phi_{\text{ion}}^{(2)}$ :

$$\left( \frac{R_{\text{core}}}{H_{\text{corona}}} \right)_{\Phi_{\text{ion}}^{(2)}} \cong \frac{N_B}{\varphi} \frac{\gamma}{N_A^2} \alpha_b^{-3/2}. \quad (122)$$

At larger salt concentrations,  $\Phi_{\text{ion}} \gg \Phi_{\text{ion}}^{(2)}$ , the corona is found in the salt-dominated regime. Here,  $\alpha \approx \alpha_b$  and the structural parameters of these micelles coincide with those of crew-cut micelles with a quenched PE coronal block, given by (93)–(95). The CMC of copolymers with an annealing PE block at high salt concentration also coincides with that for copolymers with quenched PE block.

In the range of salt concentrations  $\Phi_{\text{ion}}^{(2)} \ll \Phi_{\text{ion}} \ll \alpha_b^2/\nu_A$ , the electrostatic contribution of  $\nu_{\text{eff}}$  dominates over the steric contribution, and  $\nu_{\text{eff}} = \nu_A + \alpha_b^2/\Phi_{\text{ion}} \cong \alpha_b^2/\Phi_{\text{ion}}$ . At higher salt content,  $\Phi_{\text{ion}} \gg \alpha_b^2/\nu_A$ , the electrostatic interactions are screened, and the micelles are found in the quasi-neutral regime (81)–(83).

The scenario of crew-cut micelle evolution (described above) holds if  $H_{\text{corona}} \ll R_{\text{core}}$  in the whole range of salt concentrations (including  $\Phi_{\text{ion}}^{(2)}$ , where  $R_{\text{core}}$  and  $H_{\text{corona}}$  reach their minimal and maximal values, respectively).

The condition  $H_{\text{corona}} \ll R_{\text{core}}$  can, however, break down at relatively high values of  $\alpha_b$  and/or for moderately asymmetric block copolymers, i.e., at  $\alpha_b \geq (\gamma N_B / N_A^2 \varphi)^{2/3}$ . In this case, the stronger electrostatic interactions in the corona transform crew-cut micelles whose coronae are in the osmotic annealing regime,  $\Phi_{\text{ion}} \geq \Phi_{\text{ion}}^{(1)}$ , into salt-dominated starlike micelles when the bulk concentration of salt reaches the value of  $\Phi_{\text{ion}} = \Phi_{\text{ion}}^* \leq \Phi_{\text{ion}}^{(2)}$ .

The transition point  $\Phi_{\text{ion}}^*$  is specified by (107), and this rearrangement occurs abruptly (as the first-order phase transition). In the transition range two population of micelles, quasi-neutral crew-cut micelles and charged starlike micelles coexist in the solution.

The equilibrium parameters of the micelles after the transition coincide with those for charged starlike micelles.

In Fig. 7 the diagram of states for crew-cut micelles is presented in the  $\Phi_{\text{ion}}, \alpha_b$  coordinates. The diagram contains regions  $CC_{\text{qn}}$ ,  $CC_{\text{qn}'}$ ,  $CC_{\text{osm}}$ ,  $CC_{\text{ch}}$  and  $S_{\text{ch}}$ . In region  $CC_{\text{qn}}$ , the micelles are quasi-neutral, and the coronae are weakly ionized,  $\alpha \ll \alpha_b$ . The dotted line indicates the value of  $\alpha_b$  above which the CMC<sub>qn</sub>

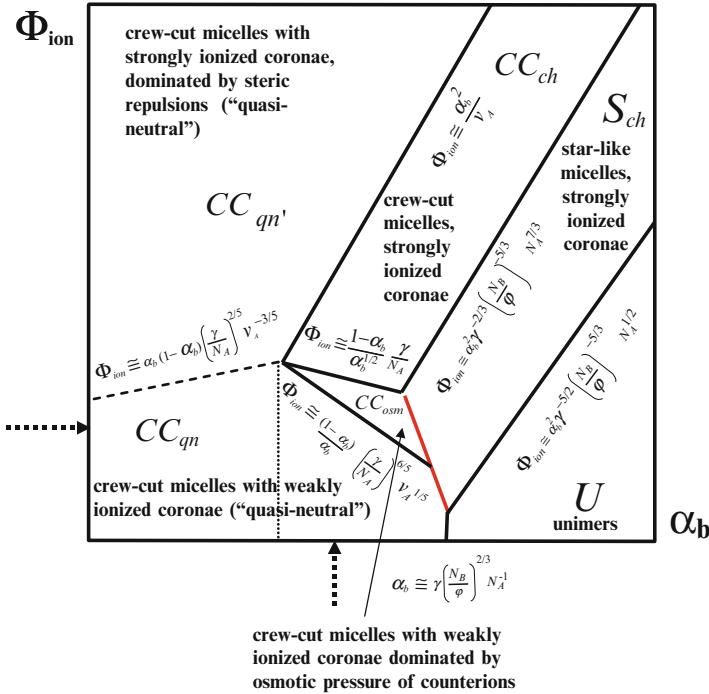


**Fig. 7** Diagram of states in  $\alpha_b, \Phi_{\text{ion}}$  coordinates for dilute solution of block copolymers with pH-sensitive PE blocks, that associate in crew-cut spherical micelles,  $N_A \ll \gamma^{2/7} \left( \frac{N_B}{\varphi} \right)^{5/7} v_A^{-3/7}$ . Vertical and horizontal dotted arrows indicate fixed values of pH and salt concentration corresponding to Fig. 8a, b and Fig. 8c, d, respectively

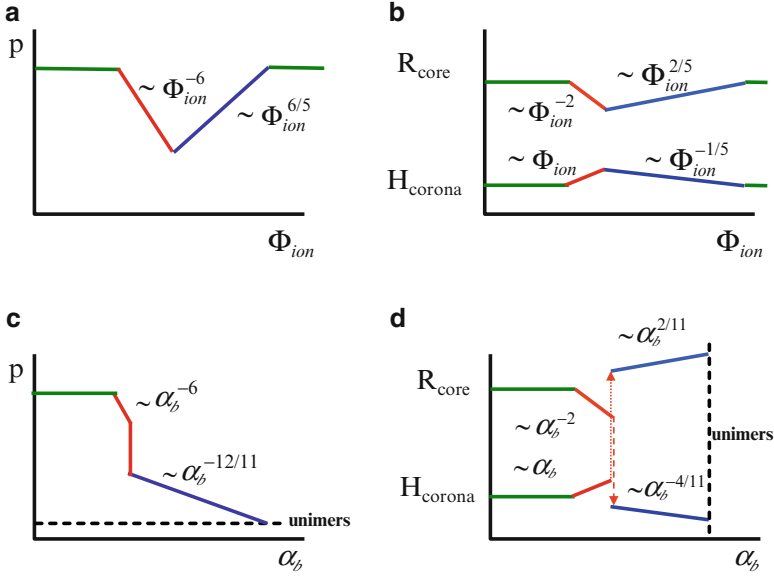


**Fig. 8** Dependency of (a) aggregation number  $p$ ; (b) radius of the core  $R_{core}$  and thickness of the corona  $H_{corona}$  in crew-cut spherical micelles with pH-sensitive coronal block as a function of salt concentration. The pH is fixed according to the position of the vertical dotted arrow in Fig. 5. Dependency of (c)  $p$ , and (d)  $R_{core}$  and  $H_{corona}$  as a function of pH. Salt concentration is fixed according to the position of horizontal dotted arrow in Fig. 7

deviates from  $CMC_n$ , cf. (103). In region  $CC_{qn'}$ , the coronal blocks are ionized,  $\alpha \approx \alpha_b$ , but the electrostatic interactions are strongly screened due to high salt concentration, and structural parameters of the micelles are the same as in region  $CC_{qn}$ . Line  $\Phi_{ion}^{(1)}$  separates regions  $CC_{qn}$  and  $CC_{osm}$ . The bold line indicates the transition line  $\Phi_{ion} = \Phi_{ion}^*(\alpha_b)$ , where weakly ionized osmotic crew-cut micelles abruptly transform into strongly charged starlike micelles (region  $S_{ch}$ ). In region  $CC_{ch}$ , the charged micelles acquire crew-cut shape. Line  $\Phi_{ion}^{(2)}$  separates regions  $CC_{osm}$  from  $CC_{ch}$ . Upon crossing this line, a continuous transformation of micelles occurs.

The evolution in aggregation number, core radius, degree of dissociation, and extension of the coronal chains in a crew-cut micelle, as a function of salt concentration and pH, are schematically presented in Fig. 8.

In contrast to a nonmonotonous behavior of the equilibrium parameters of crew-cut micelles, the CMC decreases monotonously as a function of the bulk salt concentration,  $\Phi_{ion}$ . Namely:

$$\ln CMC_{CC} \cong -\gamma(N_B/\varphi)^{2/3} + \begin{cases} -N_A \ln(1 - \alpha_b) - N_A^3 [\alpha_b \Phi_{ion} / \gamma (1 - \alpha_b)]^2, & \Phi_{ion} \ll \Phi_{ion}^{(2)}, \\ N_A^{3/5} \gamma^{2/5} (v_A + \alpha_b^2 / 2\Phi_{ion})^{2/5}, & \Phi_{ion} \gg \Phi_{ion}^{(2)}. \end{cases} \quad (123)$$

## 8 Micelles with Quenched and Annealing Polyelectrolyte Coronae: Nonlocal Mean-Field Approach

The mean-field approach combined with the local electroneutrality approximation (LEA) can be extended beyond the boxlike model. To calculate the free energy of a micellar corona with the radial gradients in polymer density, we assume that all the free ends of blocks  $A$  are located at the corona periphery and are equally stretched. Within this model, the free energy of a micelle of morphology  $i$  ( $i = 1, 2, 3$ ), can be explicitly calculated for both quenched and annealing PE coronae. We outline here only a general scheme of the approach, whereas the details can be found in [22, 32].

The Gibbs free energy per chain in the corona of morphology  $i$  is formulated as:

$$F_{\text{corona}}^{(i)} = \frac{3k_{\text{B}}T}{2} \int_{R_{\text{core}}}^{R_{\text{corona}}} \left( \frac{dr}{dn} \right) dr + \int_{R_{\text{core}}}^{R_{\text{corona}}} f_{\text{int}}\{c_p(r)\}s(r)dr. \quad (124)$$

Here, the first term accounts for the nonuniform stretching of the coronal block, whereas the second term accounts for the excluded-volume interactions, the translational entropy of mobile ions, and (in the case of an annealing PE block) the free energy gain due to corona ionization, as specified by (66), (67).

The local chain stretching at distance  $r$  from the center of micelle,  $dr/dn$ , is related to local polymer density,  $c_p(r)$ , as:

$$c_p(r) = \frac{dn}{s(r)dr}, \quad (125)$$

where:

$$s(r) = s(R_{\text{core}}) \left( \frac{r}{R_{\text{core}}} \right)^{i-1}, \quad i = 1, 2, 3. \quad (126)$$

This enables one to represent the free energy of the corona, (124), in the form:

$$F_{\text{corona}}^{(i)} = \int_{R_{\text{core}}}^{R_{\text{corona}}} f\{c_p(r), r\}s(r)dr, \quad (127)$$

where the free energy density in the corona is given by:

$$f\{c_p(r), r\} = \frac{3k_{\text{B}}T}{2c_p(r)s^2(r)} + f_{\text{int}}\{c_p(r)\}. \quad (128)$$

The outermost radius  $R_{\text{corona}}$  of the corona follows from the normalization condition:

$$\int_{R_{\text{core}}}^{R_{\text{corona}}} c_p(r)s(r)dr = N_A. \quad (129)$$

Minimization of the coronal free energy, (127), under the constraint given by (129) leads to the following equations for polymer density profile,  $c_p(r)$ , and for the radius of the corona,  $R_{\text{corona}}$ :

$$\frac{\delta}{\delta c_p(r)} f\{c_p(r), r\} = \lambda, \quad (130)$$

$$\left( c_p(r) \frac{\delta}{\delta c_p(r)} f\{c_p(r), r\} - f\{c_p(r), r\} \right)_{r=R_{\text{corona}}} = 0, \quad (131)$$

where  $\lambda$  is the (exchange) chemical potential of monomer unit of the coronal block. For specified density of the interaction free energy,  $f_{\text{int}}\{c_p(r) = f_{\text{ev}}\{c_p(r)\} + f_{\text{ion}}\{c_p(r)\}$ , the coronal free energy,  $F_{\text{corona}}^{(i)}$ , can be calculated with the account of (127)–(131) at arbitrary radius of the core,  $R_{\text{core}}$ . The density of the free energy of non-ionic interactions,  $f_{\text{ev}}\{c_p(r)\}$ , is given by (66). Within the LEA, the ionic contribution,  $f_{\text{ion}}\{c_p(r)\}$ , can be obtained from (84) or (96) for a quenched and an annealing corona, respectively, by replacing  $c_p \rightarrow c_p(r)$ ,  $\alpha \rightarrow \alpha(r)$ . In the latter case, the degree of ionization of the coronal chains  $\alpha(r)$  becomes also a function of the radial coordinate,  $r$ , and is related to local polymer concentration,  $c_p(r)$ , by (97) and (99).

Compared to the boxlike model, the nonlocal mean-field approach provides deeper insights in the structure of a micellar corona. In particular, in starlike micelles ( $R_{\text{corona}} \gg R_{\text{core}}$ ), the polymer density,  $c_p(r)$ , decays as a power law function of  $r$  in the central regions of the corona. At low salt concentration, the local degree of ionization in the corona increases as a power law function of  $r$ , according to the relation between  $c_p(r)$  and  $\alpha(r)$ , specified by (99). In both limits of starlike ( $H_{\text{corona}} \gg R_{\text{core}}$ ) and crew-cut ( $H_{\text{corona}} \ll R_{\text{core}}$ ) micelles, the asymptotic power law expressions for the coronal size and the free energy, obtained in the framework of the boxlike model, are recovered. In addition, explicit numerical prefactors for both properties can be calculated [22].

Analysis of the radial gradients in polymer and free energy densities in the corona of aggregate with morphology  $i$  enables one to obtain linear in curvature correction terms for the coronal free energy of crew-cut micelles,  $H_{\text{corona}} \ll R_{\text{core}}$ . As we demonstrate below in Sects. 10 and 11, the magnitude of these curvature-dependent terms can be tuned by variations in the pH and ionic strength in the solution. As a result, morphological transformations of block copolymer aggregates can take place.

## 9 Self-Consistent Field Modeling of Micelle Formation

Scaling approaches to predicting structural dependencies for micelles are useful to reveal power law behavior, but lack the precision with respect to numerical coefficients. The mean-field theory for self-assembly, as discussed above, unravels the general trends for these complex micellar systems, but implements major approximations. In particular, the boxlike model neglects gradients in the local densities in both the core and corona regions. A more advanced nonlocal mean field model

accounts for radial gradients in the coronal density profile and in local stretching of both the coronal and the core-forming blocks, but implements the strong stretching approximation. Moreover, large-scale fluctuations in stretching of the coronal chains (distribution of the free ends) are neglected. Therefore, one cannot expect truly accurate molecularly detailed results from these analytical theories. In this section we discuss the numerical self-consistent field (SCF) approach to self-assembly of block copolymers [65–69]. The SCF approach is also of the mean-field type and thus has a known tendency to overestimate the free energy of the unimers, as well as the free energy for the polymer brushes that make up the micelle coronae. In contrast to the box model, one can account for all relevant gradients in densities in the micelle [70–73] because it includes the statistical weights of all possible chain conformations within a freely jointed chain approximation [74] and therefore is able to account for molecular details. Not surprisingly, the equations need to be solved numerically [75], and the calculations really become challenging for weakly charged and pH-dependent systems, especially in the limit of low salt concentrations. As computations are more demanding, the SCF approach should be seen to complement the analytical approaches rather than to replace them.

The scaling laws and the analytical dependencies that are discussed in this review, are expected to hold in the limit of long chains. In stark contrast, well-defined block copolymers that form responsive micelles often have a limited molecular weight. The analytical theory is only expected to give some guidance and trends for micelles composed of short polymers because several of its premises are not met. From this perspective, there exists a need to forward approaches that can give accurate information on self-assembly for relatively short copolymers [76]. As computational difficulties are gradually overcome, Monte Carlo and molecular dynamics computer simulations are used to generate results for self-assembly of copolymers in selective solvents. Accurate results are expected for short copolymers, but detailed analysis for micellization of amphiphilic ionic copolymers is not yet available.

Numerical SCF theory can be used to probe the self-assembly of both long and short copolymers [72, 73, 77], for non-ionic [78–82] as well as ionic systems [83–86]. For long polymers, we can use the numerical SCF theory to check the scaling predictions and to test the validity of the analytical approximations. For short chains, the numerical theory is still expected to give reasonable predictions and results can be used to analyze experiments on the one hand, and to complement computer simulation results on the other hand.

## ***9.1 Spherical Micelles: Implementation of Numerical SF-SCF Method***

Here, we discuss results from the SF-SCF model wherein the SCF equations are implemented using the discretization scheme of Scheutjens and Fleer. Details of this approach have been presented in the literature [74]. Here, we only specify the

main approximations of the model and focus on diblock copolymers  $A_{N_A}B_{N_B}$  in a selective monomeric solvent  $S$  that may contain monovalent salt ions as well as hydroxyl and hydrogen ions.

Calculations are done in a spherical coordinate system wherein lattice sites are organized in layers with spherical geometry [70, 87, 88], resulting in measurable radial volume fraction profiles for all the components  $\phi(r)$ . Generalizations to other geometries are straightforward and one can therefore use the SCF approach to study micelle–cylinder–lamelle transitions. To date, the SCF work in this direction has been limited to surfactant systems [70, 88]. In this review, we thus focus on the block copolymer micelles of spherical geometry. Besides the volume fractions  $\phi(r)$ , the SCF theory features radial segment potential profiles  $u(r)$  for each type of segment  $X = A, B, S, \dots$ . Using these profiles, the free energy  $F$  can be computed. The optimization of this free energy results in the self-consistent field machinery:

$$u[\phi(r)] \leftrightarrow \phi[u(r)]. \quad (132)$$

The left-hand side of this equation indicates that the segment potentials are uniquely computed from the volume fractions. First of all we have a Lagrange field, which is coupled to the incompressibility relation  $\sum_X \phi_X(r) = 1$  implemented for all coordinates  $r$ . In addition there are the excluded volume interactions. These are accounted for using the Bragg–Williams approximation, where the interactions are parameterized by Flory–Huggins  $\chi$  parameters. When the segments are charged they give rise to an electrostatic contribution,  $e\Psi(r)/k_B T$ , where  $\Psi$  is the local electrostatic potential. The potentials follow from solving, for a specified charge distribution  $q(r)$ , the Poisson equation. In these systems we introduce a 1:1 electrolyte wherein the ions take up the same volume as a solvent molecule [89]. A two-state model is implemented when the  $A$  segments are weakly charged. Depending on the local proton concentration and the  $pK_a$  value, a segment can either be in the state with a negative charge or in a neutral form. These two states are equilibrated with the account of the autodissociation of water. In this way, the degree of dissociation of a monomer unit  $A$ ,  $\alpha$ , is a function of the radial coordinate [90]. For such system, we introduce proton and hydroxyl ions (both of the same size as the water molecules) into the system and fix the bulk concentration of hydrogen ions to set the (bulk) pH.

The right-hand side of (132) indicates that the segment volume fractions are uniquely computed from the segment potentials. As mentioned above, we implement a freely jointed chain model, which ensures the chain connectivity, but which does not prevent backfolding of the chain to previously occupied lattice sites. For this chain model, the volume fractions can be computed efficiently using a propagator formalism, which is intimately related to the Edwards equation [91].

The free energy of  $n$  micelles in a volume (which is assumed to be incompressible) that has a solvent, copolymers, etc. ( $j = 1, 2, \dots$ ) as its molecular species, is given by  $F = \Omega n + \sum_j n_j \mu_j$  where  $n_j$  and  $\mu_j$  are the number and chemical potential of molecules of type  $j$ . The optimization of the free energy with respect to the number of micelles leads to the condition of equilibrium for micelles, i.e.,  $\Omega = 0$  [36, 92]. The SCF model gives access to the grand potential  $\Omega_m$  of the micelle that

is pinned at the center of the computational box. When the micelle is sufficiently large, we may ignore the translational entropy and define stable micelles having  $\Omega_m \approx \Omega = 0$  (cf. (5) with  $\ln c_{mic} \approx 0$ ). Unless mentioned otherwise, we follow this Ansatz in this section. By doing so we give an upper limit of the micelle size and aggregation number (see discussion in Sect. 2.1).

We will focus on spherical micelles formed by copolymers in a monomeric solvent. The default parameters are consistent with a selective solvent  $\chi_{BS} = \chi_{AB} = 1.5$  and  $\chi_{AS} = 0$ . The discretization length (size of a lattice site = size of a segment)  $a$  is equal to 0.5 nm, which is chosen to be close to the Bjerrum length for aqueous solutions around room temperature. The relative dielectric constant  $\epsilon$  is set equal to 80 for all species except for apolar species, for which  $\epsilon_B = 2$ . Further details are given in the relevant sections.

The radial density profile (polymer volume fraction  $\phi_A$ ) in the corona of micelle can unambiguously be used to find the aggregation number  $p$ . The sizes of core and corona are less trivially obtained. To help define the micellar dimensions we have incorporated two molecular markers at both ends of the hydrophilic block, named  $X_2$  (at the junction between  $A$  and  $B$  segments) and  $X_1$  (at the free end of the  $A$  block). The first moment  $\langle X_k \rangle$ :

$$\langle X_k \rangle \equiv \frac{\sum_r L(r) r \phi_{X_k}(r)}{\sum_r L(r) \phi_{X_k}(r)} \quad k = 1, 2, \quad (133)$$

where  $L(r) \propto r^2$  is the number of lattice sites at coordinate  $r$ , is a measure for the average position of the marker. The  $X_2$  is typically at the boundary between the core and the corona and  $\langle X_2 \rangle$  is a measure for the core size,  $R_{core}$ . The average position of the first marker is a measure of the overall size of the micelle,  $R_{corona}$ . The difference between these two average positions is a measure for the dimension of the corona,  $H_{corona}$ .

The CMC of the copolymer system can also be extracted from the radial profile  $\phi_A$  because it corresponds to the concentration of copolymers in the limit of  $r \rightarrow \infty$ .

## 9.2 Neutral Micelles of Amphiphilic Block Copolymers

The SF-SCF approach has been used to consider many aspects of amphiphile self-assembly [77, 82, 88, 93–96]. Here, we focus on results that are relevant for the self-assembly of non-ionic copolymers in spherical micelles. The self-assembly of non-ionic copolymers is characterized by relatively few parameters, and we will use this system to show the micellar properties as a function of the most relevant molecular parameters.

In Fig. 9 we give, as an example, the radial density (volume fraction) profiles through a spherical micelle composed of  $A_{200}B_{50}$  copolymers with a four times longer hydrophilic block than the hydrophobic block. Inspection of the radial profile



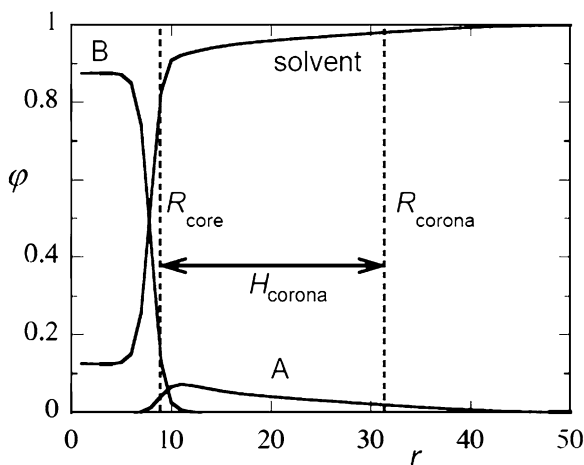


**Fig. 9** Radial volume fraction profiles for the core-forming (*B*) segments, the corona-forming (*A*) segments, and the monomeric solvent *S* for copolymer  $A_{200}B_{50}$ . The vertical *dashed lines* specify the core size  $R_{\text{core}}$ , the overall size of the micelle  $R_{\text{corona}}$ , and the size of the corona  $H_{\text{corona}}$ . These measures are found by two markers placed in the molecule. One of the markers,  $X_1$ , is positioned between blocks *A* and *B*; the second marker,  $X_2$ , is at the end of the hydrophilic block *A*. The first moments of the density distributions of these markers are indicated by the two vertical *dashed lines*. The Flory–Huggins parameters have the default values  $\chi_{BS} = \chi_{AB} = 1.5$  and  $\chi_{AS} = 0$ . The grand potential  $\Omega_m = 0$ , which represents equilibrium when translational entropy of the micelle is ignored

for the core-forming block *B* exemplifies that, as anticipated above, the core has a homogeneous density. The density in the core is an increasing function of  $\chi_{BS}$ . In contrast to the assumption in the boxlike model, the volume fraction profile in the corona has a clear dependence on *r*. Analysis of the latter profile indicates the following generic features: For very small cores, the profile represents that of a starlike micelle and the volume fraction of monomers *A* decays as a power law near the micelle center, in accordance to the predictions of the analytical theory. At larger distances (at the periphery of the corona), the profile is quasi-parabolic. The core–solvent interface is sharp and becomes progressively sharper with increasing  $\chi_{BS}$ , but also when the repulsion between *A* and *B* (specified by the value of  $\chi_{AB}$ ) increases. In Fig. 9 we also show the sizes of the micelle,  $R_{\text{corona}}$ , and of the core,  $R_{\text{core}}$  (dashed vertical lines), and the thickness of the corona,  $H_{\text{corona}}$ , obtained as explained above.

The dependence of the aggregation number and the CMC on the lengths of the polar blocks are given in Fig. 10a, b, respectively, for two values of the core-forming block and for two values of the solvent quality of the corona-forming block. The scaling theory and also the boxlike model give different dependencies for these quantities, depending on the geometry of micelle (crew-cut or starlike). The size of the core,  $R_{\text{core}}$ , and that of the corona,  $H_{\text{corona}}$ , are presented as a function of the length of the soluble block *A* in Fig. 10c. As can be seen in Fig. 10c, the size of the core decreases and that of the corona increases with increasing length of the coronal

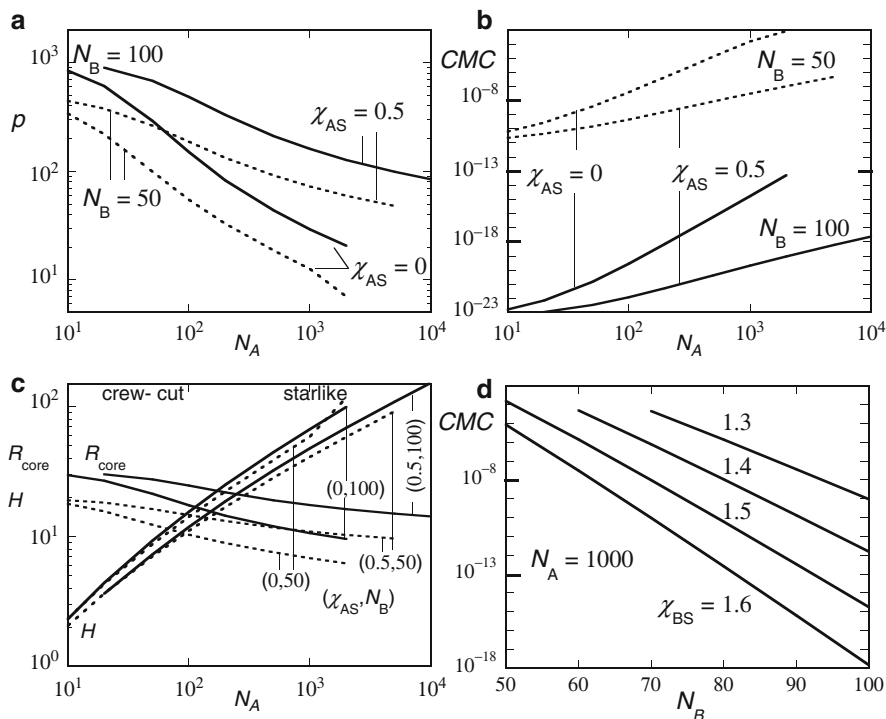


**Fig. 10** (a) The micellar aggregation number  $p$  as a function of the length of the polar block  $N_A$ ; (b) CMC (volume fraction of copolymer in the bulk) as a function of the block length  $N_A$ ; and (c) the core size  $R_{\text{core}}$  and corona size  $H$  as a function of  $N_A$  for equilibrium micelles ( $\Omega_m = 0$ ) with  $N_B = 50$  (dotted lines) and  $N_B = 100$  (solid lines) and  $\chi_{AS}$  values of 0 (good solvent) and 0.5 (theta solvent). Other parameters have the default values. (d) CMC as a function of the length of the core-forming block  $N_B$  for  $N_A = 1000$  and for different values of the solvent quality of the core-forming block  $\chi_{BS}$  as indicated

block. The boundary from crew-cut to starlike shape appears around  $N_A \approx 100$  for  $N_B = 50$  and is about twice as high for  $N_B = 100$ . Over a wide range of  $N_A$  values, the core and corona dimensions are comparable and therefore there is a wide range of parameters for which the micelle is in the crossover from crew-cut to starlike regimes. Starlike micelles occur over a wider range of parameters when the solvent quality for the corona chains is better.

From Fig. 10a, b it is difficult to extract clear power law dependencies. Therefore, we only qualitatively discuss the trends that are in qualitative agreement with the scaling analysis. The longer the polar block  $A$ , the smaller the aggregation number and the higher the CMC, (31). Inferior solvent quality for the polar block makes these trends less pronounced. The decrease in the aggregation number with increasing length of the polar block approximately follows a power law dependence, where the apparent exponent is highest in the crossover regime. The slope of the dependence  $p(N_A)$  is not a strong function of the length of the core-forming block. It is more steep for good solvent than for theta solvent conditions.

In Fig. 10d we show that the CMC depends exponentially on the length  $N_B$  of the core-forming block. The slope of this dependence is proportional to the  $\chi_{BS}$ , and is well documented in the surfactant literature. We note that the dependence of the CMC on the length of the core block (Fig. 10d) is much stronger than that of the corona (Fig. 10b). In passing, we note that the SCF theory assumes that the chains in the bulk are ideal and are fully surrounded by the solvent. The method thus ignores the possibility that the core-forming block of unimers is collapsed. In such a state, the unimer also avoids most contacts with the solvent and we conclude that the SF-SCF approach overestimates the free energy of unimers. Collapse of the hydrophobic block of unimer would increase CMC according to (31), (37).

### 9.3 Micelles with Quenched Polyelectrolyte Corona

For block copolymers comprising ionic hydrophilic blocks one has, in addition to the parameters discussed in the previous section, several new parameters that influence the micelle characteristics. Here, we focus on how these new parameters, i.e., the charge density in the corona and the ionic strength influence the micelle characteristics. In this section we therefore focus on a given molecular composition and we opt for a symmetric case,  $A_{200}B_{200}$ , and fixed the values for the excluded-volume interactions parameters:  $\chi_{BS} = \chi_{NaB} = \chi_{ClB} = \chi_{AB} = 1.5$  and  $\chi_{AS} = \chi_{NaS} = \chi_{ClS} = 0$ . Hence, we choose for the scenario that the ions have similar excluded-volume interactions with the polymer segments as the solvent. Note that in practice ions might have some specific affinity for either the core or the coronal blocks, and this situation could be also addressed in frames of the SF-SCF model.

In Fig. 11 we show an example of the relevant radial distributions for an equilibrium micelle composed of a symmetric ionic/non-ionic diblock copolymer with a

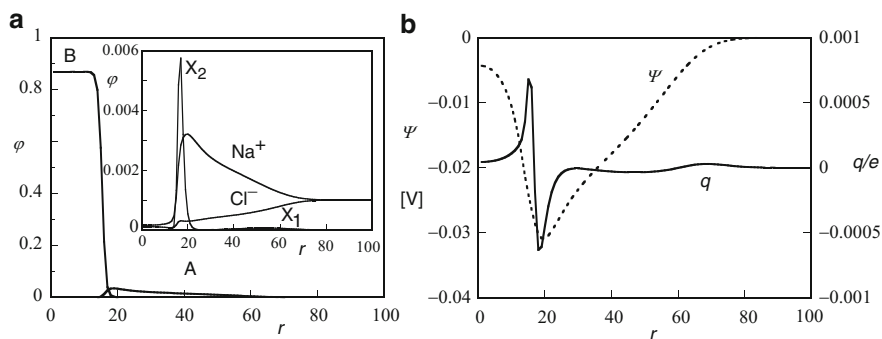


**Fig. 11** (a) Radial volume fraction profiles for apolar block  $B$  and charged coronal block  $A$  with  $\alpha = 0.2$  (every fifth segment along the coronal block has a negative charge  $-e$ ). Inset shows radial distributions for the two markers and for the 1:1 electrolyte for which the bulk concentration is  $\Phi_s = 0.001$ . (b) Corresponding radial electrostatic potential profile  $\Psi(r)$  (left ordinate) in volts and the dimensionless radial charge density  $q(r)/e$  (right ordinate)

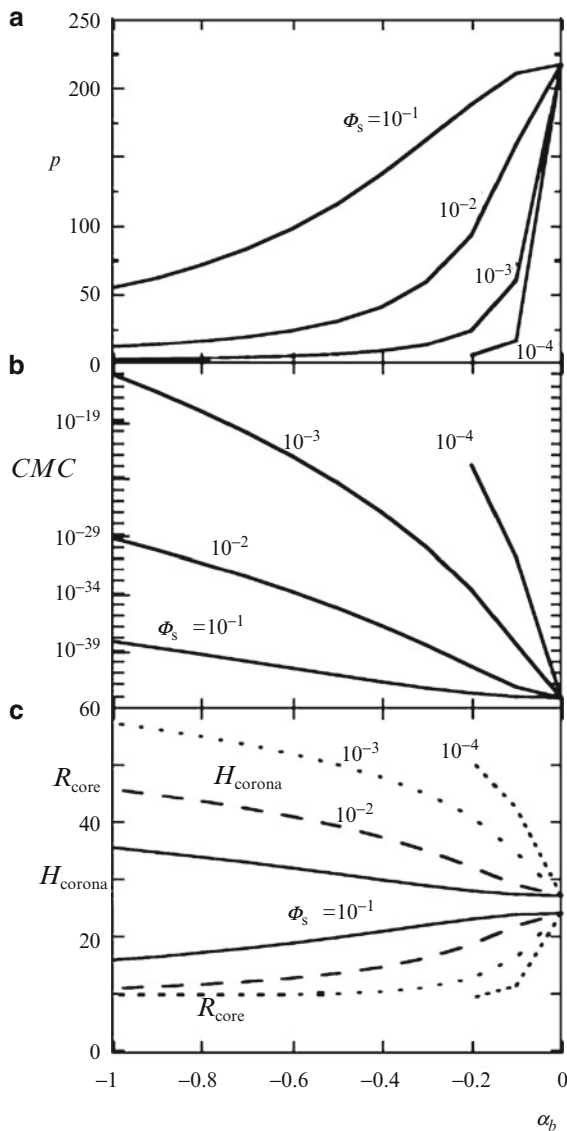
charge density of  $-0.2$  charges per segment in the coronal chain in a  $\Phi_s = 0.001$  salt solution. In Fig. 11a, the volume fractions of the polar and apolar blocks are shown in combination with that of the two markers. The distributions of the salt ions are given as well (in the inset). Compared to Fig. 9 we show here a result for which the core is larger. In the corona the counterions ( $Na$ ) accumulate and the co-ions ( $Cl$ ) are depleted with respect to the bulk concentrations. Both co- and counterions avoid the core because they interact with  $B$  monomers as molecules of a poor solvent.

In Fig. 11b the radial distribution of the electrostatic potential is shown in combination with the overall distribution of the charge density. As, in this case, the charge along the chain is quenched, the charge distribution due to the polymers in the micelle simply follows the distribution of the  $A$  segments. The total charge profile is now computed from  $q(r)/e = -0.2\phi_A(r) + \phi_{Na}(r) - \phi_{Cl}(r)$ . As seen in Fig. 11b, the overall charge in the corona chain is very low, proving that the LEA is accurate in this case. The radial electrostatic potential in the micelle is negative throughout the micelle, as expected. One can systematically investigate the radial profile of the electrostatic potential and one then finds that the electrostatic potential is approximately parabolic in the corona region. As compared to Fig. 9 the average density of segments in the corona is significantly lower in the case of the charged micelle than for the non-ionic case. The accumulation of counterions in the corona causes a local high osmotic pressure, which, in turn, swells the corona region. This is typical for micelles with a PE corona.

Copolymers with quenched PE blocks form micelles that strongly respond to variations in the ionic strength in solution. To illustrate this behavior, which is already anticipated above from the scaling theory and the boxlike model, we show the micelle characteristics in Fig. 12. In these graphs, we plot the aggregation number, the CMC and the sizes of the core and corona as a function of the fractional charge along the corona block for various values of the salt concentration  $\Phi_s$ .

Inspection of the results of Fig. 12 shows that in the limit of high ionic strength and low charge density, the micelle parameters go to the limit of non-ionic micelles. With increasing charge and decreasing ionic strength, rather dramatic changes in micellar properties are predicted. As illustrated in Fig. 12a, the aggregation number dramatically drops to very low values. More specifically, when  $\Phi_s = 10^{-4}$  the micelles disappear when the fractional charge is more negative than  $-0.1$ . Correspondingly, the CMC is a very strong function of the charge density along the  $A$  chain, especially when the ionic strength is low. This strong dependence is traced to the loss in translational entropy of the entrapped counterions. As the density of segments in the core is not a strong function of the aggregation number, the size of the core follows the aggregation number. Hence,  $R_{\text{core}}$  is a strongly decreasing function of the charge density. On the other hand, the size of the corona increases with increasing charge density. The higher the charge density in the corona, the more counterions are localized in the corona, with corresponding consequences for the osmotic driving force that swells the corona. At the same time, the effective second virial coefficient of monomer–monomer interactions in the corona is a strongly increasing function of the charge density and a decreasing function of the ionic strength.

**Fig. 12** (a) Dependence of the aggregation number  $p$ ; (b) CMC; and (c) core size  $R_{\text{core}}$  and corona size  $H_{\text{corona}}$  as a function of the fractional charge  $\alpha_b$  for quenched PE block at  $\Phi_s$  values of  $10^{-1}$ ,  $10^{-2}$ ,  $10^{-3}$ , and  $10^{-4}$ . Both blocks have the length of 200 segments.  $\Omega_m = 0$  and the interaction parameters have the default values



From the above it is clear that one needs relatively long core-forming blocks in order to generate a strong enough associating force to keep highly charged coronal chains in the micelle. This observation explains why, in the next section, we focus on copolymers with a longer apolar block.

### 9.4 Micelles with Annealing Polyelectrolyte Corona

When the charge density in the corona chains is pH-dependent (i.e., the charges are annealing), the micelles are even more responsive. Here, we consider micelles composed of a relatively long hydrophobic block,  $N_B = 300$ , and a shorter acidic coronal block,  $N_A = 100$ , to illustrate the properties of these systems. It is assumed that the  $A$  segments have an (intrinsic)  $pK_a$  and when the  $pH \gg pK_a$ , all the segments release a proton so that each one acquires a negative charge ( $-e$ ) and  $\alpha_b = 1$ . For  $pH \ll pK_a$  all segments are in the protonated (neutral) state, i.e.  $\alpha_b = 0$ . The difference  $\Delta pH = pK_a - pH$  is important. When the chargeable segments are isolated in the bulk solution, half the segments will be charged at  $pH = pK_a$  (i.e.,  $\alpha_b = 0.5$ ), as described by (98). In the corona, however, the locally high electrostatic potential suppresses the degree of dissociation and, typically, the effective  $pK_a^{\text{eff}}$  (defined as the pH at which half the groups are titrated) is shifted by several pH units with respect to the intrinsic  $pK_a$ .

The radial volume fraction profiles of monomer units in such micelle at a pH one unit below the intrinsic  $pK_a$  and for a salt concentration of  $\Phi_s = 10^{-3}$  are shown in Fig. 13. In this case, the degree of dissociation in the bulk is  $\alpha_b \approx 0.1$ . As shown in Fig. 13 (right ordinate), the degree of dissociation is significantly suppressed in the corona region of the micelle. This is due to the negative electrostatic potential in the corona. As shown for quenched micelles, the electrostatic potential is low outside the corona of the micelle (i.e., both in the core and in the bulk solution) and this is why  $\alpha(r)/\alpha_b \approx 1$  in these regions. In this particular example, the corona block is rather small and the ionic strength is not too low. This is why in this case the core size exceeds that of the corona. Hence in this example the micelle is in the crew-cut regime. For such a micelle, the curvature in the coronal part of the micelle is not very important and the profile is close to that in a planar PE brush. Such a brush is known [30] to have a parabolic profile of the electrostatic potential.

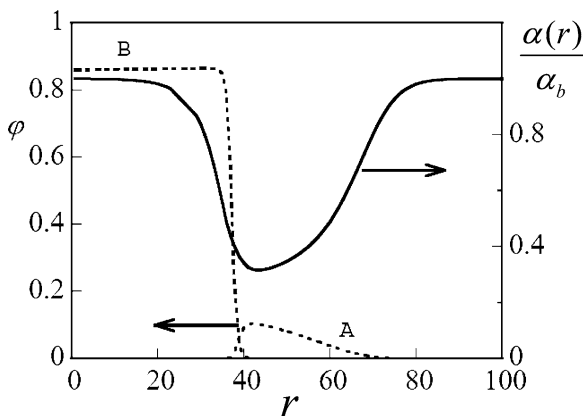


**Fig. 13** Radial density profiles for  $A$  and  $B$  segments (*left ordinate*), and radial distribution of the degree of dissociation normalized to the dissociation of an  $A$  segment in the bulk,  $\alpha(r)/\alpha_b \approx 1$  (*right ordinate*), for  $A_{100}B_{300}$ ,  $\Phi_s = 10^{-3}$ , and  $pH - pK_a = -1$

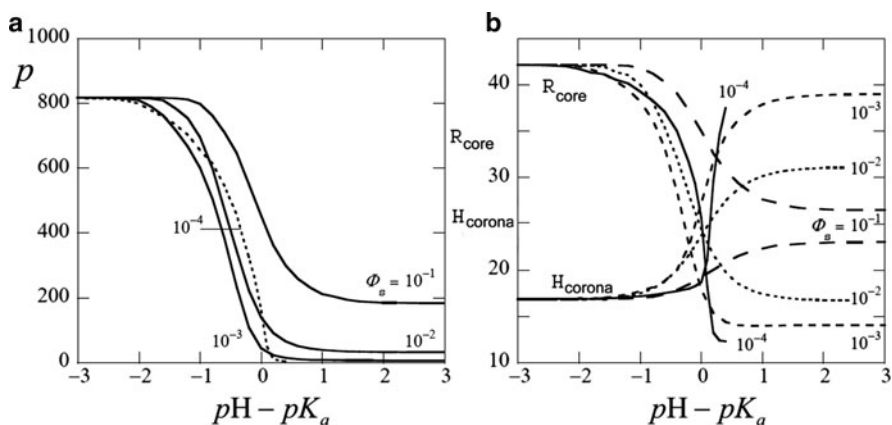


**Fig. 14** (a) Aggregation number  $p$ , and (b) core size  $R_{core}$  and corona size  $H_{corona}$  as a function of the difference between pH and  $pK_a$  for  $\Phi_s = 10^{-4}$ ,  $10^{-3}$ ,  $10^{-2}$ , and  $10^{-1}$  as indicated. The copolymer chain  $A_{100}B_{300}$  has polar A segments with annealing charges. Other parameters have the default values

For micelles composed of diblock copolymers with pH-sensitive coronal blocks, all measurable characteristics become a strong function of the pH and ionic strength in solution. In Fig. 14 we show how the aggregation number and the sizes of the core and corona change over a wide range of these parameters. With increasing pH, the polyacid chains become gradually more charged, (117), and the response of the micelles is to decrease the aggregation number as well as the core size [cf. (118), (120)]. At the same time the corona size increases, (119) so that the overall size of the micelle is a much weaker function of the pH.

As illustrated in Fig. 14 there is a nontrivial salt concentration dependence for the aggregation number and core size: both pass through a minimum at low salt concentration, if  $pH \approx pK_a$  (cf. predictions of the analytical theory schematically depicted in Fig. 8). In all cases, the drop in aggregation number, as well as the size changes are more dramatic for lower ionic strengths. Furthermore, the major changes occur near  $pH \approx pK_a$ ; however, in the series  $\Phi_s = 10^{-1}$ ,  $10^{-2}$  and  $10^{-3}$  the drop in  $p$  and  $R_{core}$  and the rise in  $H_{corona}$  occur at gradually lower pH values, but this trend reverses for even lower ionic strength. More specifically, for  $\Phi_s = 10^{-4}$  the drop occurs very close to  $pH \approx pK_a$  at a value of the pH that is larger than for  $\Phi_s = 10^{-3}$ . For even lower ionic strengths this upward shift continues (not shown). It is relevant to mention that for these low ionic strengths, no stable micelles are present when pH is much larger than  $pK_a$ .

Comparing the core and corona sizes as presented in Fig. 14 we see that for these rather asymmetric copolymers with a much longer apolar block than polar block, the micelles remain in the crew-cut regime for all pH values ( $R_{core} > H_{corona}$ ) at high ionic strength. For lower ionic strengths, there is a transition from a crew-cut to a starlike micelle that takes place around  $pH \approx pK_a$ . Typically, the overall size of the crew-cut micelles ( $R_{corona} = R_{core} + H_{corona}$ ) decreases with pH due to the dominant decrease in  $R_{core}$ . However, for very low ionic strengths, the overall micelle size

goes through a minimum around the crossover from crew-cut to starlike micelles. This minimum appears due to interplay of the opposite trends in evolution of  $R_{\text{core}}$  and  $H_{\text{corona}}$  as a function of pH. The transition from crew-cut to starlike micelles becomes progressively sharper the lower the ionic strength in the solution.

From Fig. 14 it is noticed that the crew-cut to starlike micelle transition becomes sharper with decreasing ionic strength. In Fig. 14 we focused on micelles with a vanishing grand potential, and that have the property that  $\partial\Omega_m/\partial p < 0$  [see (8)]. As discussed in Sect. 7.2, below some threshold ionic strength the crew-cut to starlike micelle transition becomes jump-like and, under certain conditions, both the starlike and the crew-cut micelles coexist in equilibrium. We illustrate this coexistence with a study on micelles at low salt concentration,  $\Phi_s = 10^{-5}$ . For more details we refer to the literature where the transition is analyzed in depth for a slightly different case [23].

The coexistence between crew-cut and starlike micelles is demonstrated for micelles composed of  $A_{50}B_{300}$  copolymers using the default solvency parameters. We selected the low ionic strength conditions,  $\Phi_s = 10^{-5}$ . In this case, the pH-induced micelle-to-micelle jump-like transition occurs around  $\text{pH} - \text{p}K_a \approx 1$ , i.e., for a pH just above the  $\text{p}K_a$ . It is illustrated in Fig. 15a that in a narrow pH range, the grand potential  $\Omega_m$  develops a new region of stability at small values of  $p$  (indicated by the conditions  $\Omega_m > 0$  and  $\partial\Omega_m/\partial p < 0$ ). For lower values of the pH (upper curve in Fig. 15a), the grand potential becomes an increasing function of  $p$ , which signals that these micelles are unstable. For higher values of the pH (lower curves in Fig. 15a), the grand potential becomes negative for small values of  $p$ , implying that these small micelles spontaneously disintegrate. For coexistence between starlike and crew-cut micelles, it is further necessary that the chemical potentials of the copolymers in both aggregates match. As proven in Fig. 15b, it is possible to find such conditions. For stable micelles, the condition  $\partial \ln \phi^b / \partial p > 0$  should be fulfilled and, as can be seen in Fig. 15b, this occurs both for small values of  $p$  (starlike micelle) and for much larger values (crew-cut micelle). For the value of  $\text{pH} - \text{p}K_a = 1$ , we therefore find a corridor of micelle sizes for which the two types of micelles coexist at the same chemical potential (indicated by the shaded area). For lower values of the pH, it is found from the chemical potentials that crew-cut micelles are more favorable than the starlike micelles (not shown), whereas at higher pH values the opposite occurs. Indeed, the coexistence region (in terms of a pH interval) is very narrow.

In Fig. 15c,d we show the radial volume fraction profiles for  $A$  and  $B$  segments. By visual inspection of the two profiles, it is clear that the coronal size is much larger than the core size in Fig. 15c (starlike micelle) and the opposite occurs in Fig. 15d (crew-cut micelle). For the starlike micelle, the density in the corona is much lower than in the crew-cut case. Due to the curvature, the corona of a starlike micelle layer has two regions: near the core the density drops as a power law function of the distance from the center of the core and near the periphery the shape of the profile resembles that in a planar-like corona. These trends are in line with predictions of the analytical theory.

In the SCF results discussed in this section, it was pre-assumed that the geometry of the micelles is spherical. Especially for the cases that the micelles are in the crew-



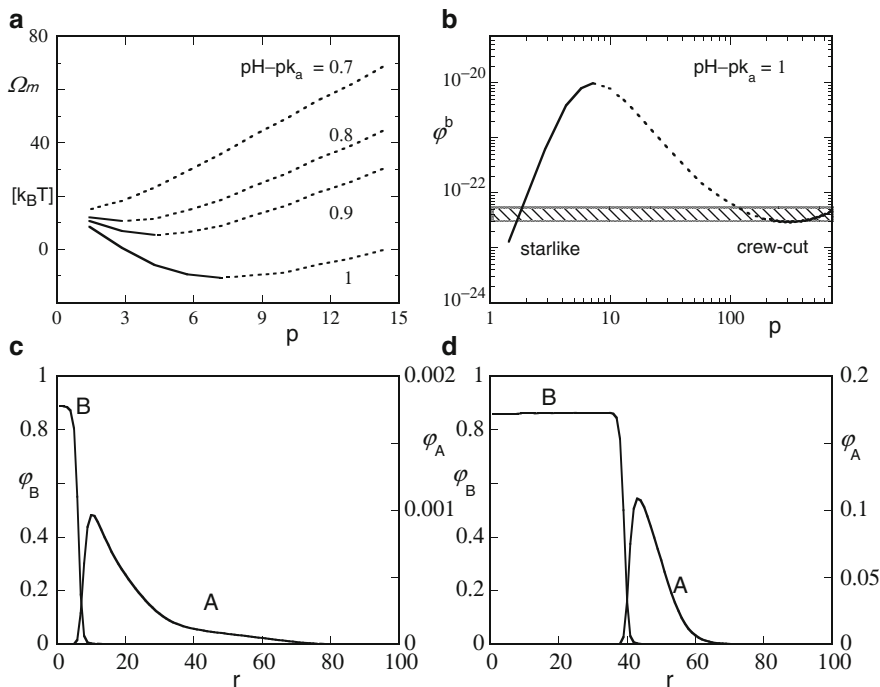


**Fig. 15** (a) Grand potential  $\Omega_m$  of a micelle composed of  $A_{50}B_{300}$  copolymers and fixed in the center of the coordinate system as a function of the aggregation number  $p$ . (b) The volume fraction of the unimers  $\phi^b$  that are in equilibrium with the micelles, as a function of the aggregation number  $p$  for given values of pH. The unstable parts of the curves of (a) and (b) are *dotted*. The stable parts are shown by *solid* lines. The *shaded* area in (b) represents the coexistence region where starlike and crew-cut micelles coexist. In (c, d), the radial volume fraction profiles for the apolar (B) and annealing charged (A) segments are shown for a typical starlike ( $p = 3$ ) and a typical crew-cut ( $p = 700$ ) micelle, respectively. The two micelles have almost identical grand potential  $\Omega_m$  (very close to zero) and their copolymers have (almost) the same chemical potentials. In all panels  $\Phi_s = 10^{-5}$

cut regime, one should consider the relative stability of the aggregates of the same copolymers, being in the same physical chemical conditions, but with a different geometry (cylindrical or lamellar). Although such analysis is possible, systematic SCF analysis of nonspherical block copolymer aggregates is currently lacking in the literature.

## 10 Polymorphism of Self-Assembled Aggregates of Block Copolymers with Quenched Polyelectrolyte Blocks

Similarly to the case of non-ionic micelles, micelles with a charged corona can demonstrate shape transformations. The physical origin of these morphology

changes is the same as in non-ionic micelles. That is, an increase in curvature of the micellar core decreases the coronal electrostatic interactions (with respect to a planar PE corona) at the cost of an additional stretching of the insoluble core blocks. These changes in the coronal and core free energies become comparable when the size of the core,  $R_{\text{core}}$ , becomes larger than that of the corona,  $R_{\text{core}} \geq H_{\text{corona}}$ . Therefore, one anticipates morphological transformations (under both low and high salt conditions), when spherical micelles acquire the crew-cut shape. In the case of ionic coronal block, the morphological transitions can be triggered by tuning the strength of repulsive interactions in the corona, e.g., by variation in the ionic strength of the solution.

To specify the range of thermodynamic stability of micelles with morphology  $i$ , at a given salt concentration,  $\Phi_{\text{ion}}$ , we go beyond the boxlike model and incorporate polymer density gradients in the coronal domain and account for a nonuniform stretching of the blocks. We follow here the arguments of [20, 22].

In a crew-cut aggregate with morphology  $i$ , the free energy per chain is given by  $F^{(i)} = F_{\text{core}}^{(i)} + F_{\text{interface}}^{(i)} + F_{\text{corona}}^{(i)}$ , where the first two terms are specified by (40), (41), and (39), whereas the coronal contribution is approximated if the core of the aggregate is weakly curved,  $H_{\text{corona}}/R_{\text{core}} \approx H_{\text{corona}}^{(1)}/R_{\text{core}} \ll 1$ , as:

$$F_{\text{corona}}^{(i)} \approx F_{\text{corona}}^{(1)} - \frac{3(i-1)}{2} \left( \frac{H_{\text{corona}}^{(1)}}{N_A^{1/2}} \right)^2 \frac{H_{\text{corona}}^{(1)}}{R_{\text{core}}}. \quad (134)$$

Here,  $H_{\text{corona}}^{(1)}$  and  $F_{\text{corona}}^{(1)}$  are the respective thickness and free energy (per chain) in a planar brush with grafting area  $s(R_{\text{core}}) = iN_B/\phi R_{\text{core}}$ . The specific expressions for  $H_{\text{corona}}^{(1)}$  and  $F_{\text{corona}}^{(1)}$  are determined by the state of a PE brush (osmotic, salt-dominated, or quasi-neutral). By substituting the corresponding expressions for  $H_{\text{corona}}^{(1)}$  and  $F_{\text{corona}}^{(1)}$  in (134), one finds the coronal free energy per chain,  $F_{\text{corona}}^{(i)}$ , in an aggregate of morphology  $i$  and, subsequently, the equilibrium value of the free energy,  $F^{(i)}$ , in a weakly curved crew-cut aggregate. The binodals, separating stability regions of aggregates with morphologies  $i$  and  $i+1$ , are derived from the condition  $F^{(i)} = F^{(i+1)}$ .

## 10.1 Salt-Free Solution

We first find the binodals in a salt-free solution of block copolymers with a quenched PE block A. Assuming Gaussian elasticity of the stretched coronal blocks, and taking advantage of the LEA (all mobile counterions are entrapped inside the corona), one finds [22]:

$$\frac{F_{\text{corona}}^{(1)}}{k_B T} = \alpha_b N_A \left[ \ln \left( \frac{\sqrt{3\alpha_b}}{s(R_{\text{core}})} \right) - \frac{1}{2} \right] \quad (135)$$

and:

$$H_{\text{corona}}^{(1)} = \frac{1}{\sqrt{3}} \alpha_b^{1/2} N_A. \quad (136)$$

Note that the LEA can be safely applied in salt-free solutions of the ionic/hydrophobic block copolymers at concentrations sufficiently larger than the CMC to insure finite electrostatic screening length in the solution.

The free energy per chain,  $F^{(i)}$ , in an aggregate of morphology  $i$  yields:

$$\frac{F^{(i)}}{k_B T} \approx \frac{F_{\text{corona}}^{(1)}}{k_B T} + \gamma s(R_{\text{core}}) - \frac{(i-1)}{2i\sqrt{3}} \frac{\alpha_b^{5/2} N_A^3 \phi}{\gamma N_B} + b_i \frac{i^2 N_B \gamma^2}{\phi^2 \alpha_b^2 N_A^2}. \quad (137)$$

Here, the first two terms are the free energy of the planar corona and core–water interface, respectively. The third term is the reduction of coronal free energy due to curvature, while the last term accounts for the elastic stretching of the core blocks. Similarly to the case of non-ionic micelles, the area  $s$  per chain is determined by balancing the dominant free energy contributions (the first and the second terms in (137)). Correspondingly, the binodals are specified from balancing the correction terms [the third and forth terms in (137)] in the free energies of aggregates with morphology  $i$  and  $i+1$ , as:

$$\frac{\alpha_b^{9/2} N_A^5 \phi^3}{N_A^2 \gamma^3} = 2\sqrt{3}i(i+1) [b_{i+1}(i+1)^2 - b_i i^2] \quad i = 1, 2. \quad (138)$$

The transition from morphology  $i$  to  $i+1$  (i.e., lamella to cylinder or cylinder to sphere) occurs upon an increase in the degree of ionization of the coronal blocks,  $\alpha_b$ , and/or an increase in  $N_A$ /decrease in  $N_B$ . These molecular parameters are specified by the block copolymer composition. Therefore, to detect the predicted structural transformations, one has to use a series of block copolymer with finely tuned molecular weights of the blocks. As follows from (138), the relative width of the corridor, delineating the stability range of cylindrical micelles in a low salt solution,  $(N_A^{(c-s)} - N_A^{(l-c)})/N_A^{(l-c)} \approx 0.16$ , is rather small. Moreover, the absolute width of the corridor,  $N_A^{(c-s)} - N_A^{(l-c)}$ , is also small due to the typically short length of block  $A$ . A more practical route to search for morphological transitions in diblock copolymers with quenched PE block is to exploit the response of charged micelles to variations in the content of added salt.

## 10.2 Salt-Dominated Solution

Under salt dominance conditions (i.e., when the concentration of salt,  $\Phi_{\text{ion}}$ , exceeds by the far the concentration of counterions in salt-free osmotic corona), the electrostatic interactions in the corona are described via an effective second

virial coefficient of binary monomer–monomer interactions,  $v_{\text{eff}}$ . The structure of a planar brush, wherein the interactions are determined by binary contacts between monomers, is specified by the free energy per chain:

$$\frac{F_{\text{corona}}^{(1)}}{k_B T} = \frac{3^{4/3}}{2} N_A v_{\text{eff}}^{2/3} s (R_{\text{core}})^{-2/3} \quad (139)$$

and the brush thickness:

$$H_{\text{corona}}^{(1)} = \frac{1}{3^{1/3}} N_A v_{\text{eff}}^{1/3} s (R_{\text{core}})^{-1/3}, \quad (140)$$

where  $s(R_{\text{core}})$  is the grafting area per chain. By using (39), (40), (41), and (134), and by optimizing the free energy with respect to area  $s$ , we find the equilibrium free energy per chain,  $F^{(i)}$ , in a weakly curved crew-cut aggregate of morphology  $i$  [20]. Within the accuracy of linear in curvature terms:

$$\frac{F^{(i)}}{k_B T} \approx \frac{5}{2} 3^{1/5} N_A^{3/5} v_{\text{eff}}^{2/5} \gamma^{2/5} - \frac{(i-1)}{2i} \frac{N_A^2 \varphi v_{\text{eff}}}{N_B} + b_i \frac{i^2 N_B}{3^{2/5} \varphi^2} \left( \frac{\gamma}{N_A v_{\text{eff}}^{2/5}} \right)^{6/5} \quad (141)$$

for  $i = 1, 2, 3$ . Here, the first term is the free energy of a planar PE corona balanced with the surface free energy, the second term specifies the reduction in coronal free energy caused by the core curvature, and the third term is due to elastic stretching of core blocks  $B$ . An approximate expression for the binodals that separate regions of thermodynamic stability of aggregates with morphology  $i$  and  $i+1$ , are given by:

$$v_{\text{eff}} = v_A + \alpha_b^2 / 2\Phi_{\text{ion}} \approx \frac{N_B^{10/9}}{N_A^{16/9}} \frac{\gamma^{2/3}}{\varphi^{5/3}} \left\{ \frac{2i(i+1)}{3^{2/5}} [b_{i+1}(i+1)^2 - b_i i^2] \right\}^{5/9} \quad i = 1, 2. \quad (142)$$

A progressive increase in the salt concentration,  $\Phi_{\text{ion}}$ , leads first to the sphere-to-cylinder and then to cylinder-to-lamella transitions, which occur almost at a constant surface area per chain,  $s$ .

The regions of thermodynamic stability of the aggregates of different morphologies are presented in Fig. 16a, b as a function of variable length of the ionic and hydrophobic blocks, respectively. As follows from Fig. 16, spherical micelles are stable in a wide range of salt concentrations if  $N_A \gg N_B$  and even if  $N_A \leq N_B$ . Cylindrical micelles and vesicles (or lamellar structures) are found in a narrow range of (high) salt concentration for strongly asymmetric,  $N_B \gg N_A$  copolymers. For each morphology  $i$ , an increase in salt concentration leads to the progressive decrease in the corona thickness,  $H_{\text{corona}}$ , and in a simultaneous increase in the radius of the core  $R_{\text{core}}$ . At the transition (sphere-to-cylinder and cylinder-to-lamella) points, these smooth dependencies are interrupted by a drop in the core size (which enables relaxation of the elastic tension in the core blocks) and in a simultaneous jump up in the thickness of the corona. The ratio  $H_{\text{corona}}/R_{\text{core}}$  monotonically decreases as a

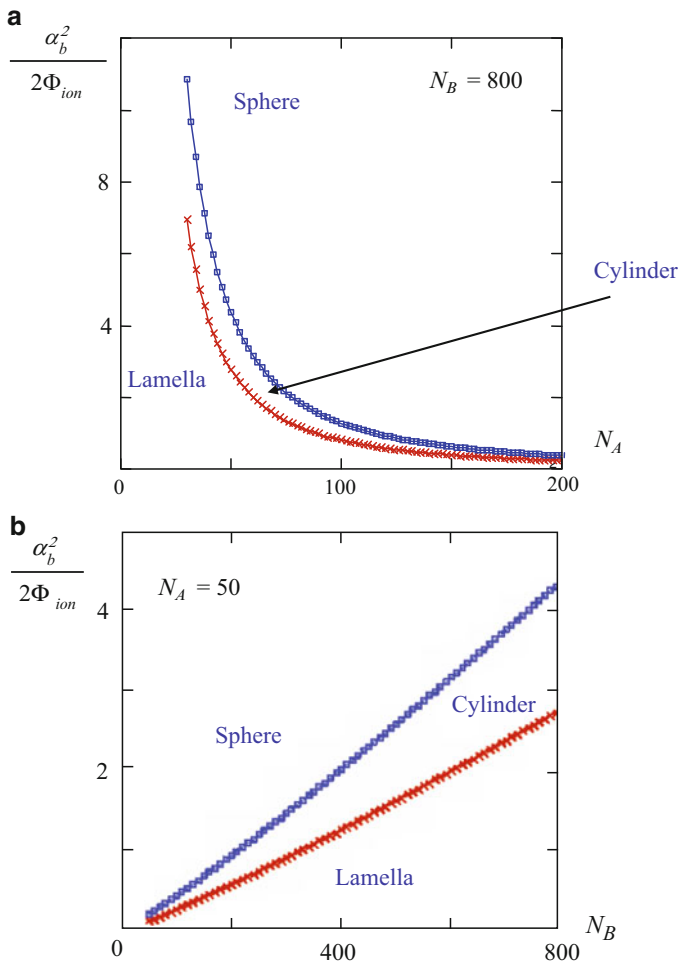
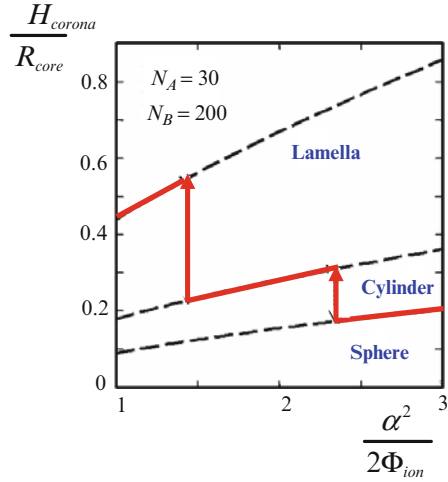


**Fig. 16** Phase diagrams of the solution of ionic/hydrophobic diblock copolymers as a function of salt concentration and the length of the hydrophilic (A) (a) and hydrophobic (B) (b) blocks

function of salt concentration for each particular morphology, but jumps up at the transition point, as demonstrated in Fig. 17.

We emphasize that it is a reduction in elastic stretching of the core blocks  $B$ , that drives the change in micelle morphology. Similarly to the case of salt-free solutions, both the elastic stretching of the core blocks and the reduction in electrostatic interactions in weakly curved corona constitute only small corrections to the major free energy terms: the surface free energy at core–corona interface, balanced with the ionic contribution in a quasi-planar corona [the first term in (141)]. However, the interplay between these corrections dictate the morphology  $i$  of crew-cut aggregates.

**Fig. 17** Ratio of the coronal thickness  $H_{\text{corona}}$  to the core radius  $R_{\text{core}}$ , as a function of the salt concentration (via the effective second virial coefficient  $\alpha_b^2/2\Phi_{\text{ion}}$ ) in the aggregates of different morphologies. Arrows indicate transitions from spherical to cylindrical, and from cylindrical to lamellar morphology



Salt-induced transitions between charged aggregates of different morphologies were also considered in [17]. In contrast to our findings, the transitions sphere-to-cylinder and cylinder-to-lamella were predicted in the starlike regime of charged aggregates with corona thickness  $H_{\text{corona}} \geq R_{\text{core}}$ . (We refer to such aggregates as starlike irrespective of morphology  $i$ .) The origin of this discrepancy is traced to an inadequate extrapolation of the asymptotic expressions for the free energy of a starlike corona (that are valid only in the limit  $H_{\text{corona}} \gg R_{\text{core}}$ ) to the range  $H_{\text{corona}} \simeq R_{\text{core}}$ . As a result of such treatment, the free energies of the spherical ( $i = 3$ ), cylindrical ( $i = 2$ ), and lamellar ( $i = 1$ ) starlike aggregates intersect when  $H_{\text{corona}} \geq R_{\text{core}}$ , resulting in improper location of the sphere-to-cylinder and cylinder-to-lamella morphological transitions. These transitions were erroneously attributed in [17] to the gain in entropy of counterions. Remarkably, if the finite size of the core is taken into account, but the conformational entropy of the core-forming blocks  $B$  is disregarded, a spherical shape of the micelle provides the minimal free energy at any values of the interaction parameters. As emphasized earlier, the driving force for morphological transitions is the successive relaxation of the elastic stretching of the core blocks going from a spherical to cylindrical and finally to the lamellar topology. Without this effect, a spherical micelle with a quenched PE corona would be stable at any salt concentration [20].

## 11 Re-entrant Morphological Transitions in Aggregates of Block Copolymers with Annealing Polyelectrolyte Block

Remarkably, in micelles with weakly dissociating (pH-sensitive) coronae an increase in the salt concentration,  $\Phi_{\text{ion}}$ , might invert the sequence of morphological transformations from sphere–cylinder–lamella to lamella–cylinder–sphere [21].

This “unusual” sequence of transitions occurs under low salt conditions, when the coronal ionization is strongly coupled to the conformations of the soluble block  $A$ . The physical origin of inverted morphological transitions is the same as for non-ionic micelles and micelles with quenched PE corona. The elastic stretching of the core-forming blocks increases in the series lamella–cylinder–sphere, whereas the average coronal concentration of ionizable monomer units decreases upon an increase in curvature of coronal domain. As a result, the ionization of the coronal blocks,  $\alpha$ , increases, and the corresponding ionic contribution to the free energy decreases. When gains in the ionic contribution in the corona of micelle become comparable to the losses in elastic stretching of core blocks, micelles might change morphology. To specify the binodals, separating the regions of thermodynamic stability for aggregate of morphology  $i$ , we use (134). As is discussed earlier, this equation approximates the coronal free energy of a crew-cut aggregate with a weakly curved core,  $R_{\text{core}} \gg H_{\text{corona}}^{(1)}$ . Recall that  $H_{\text{corona}}^{(1)}$  and  $F_{\text{corona}}^{(1)}$  in (134) are the thickness and the free energy of a planar corona under the corresponding conditions (i.e., for pH-sensitive chains with varying  $\alpha$ ).

When the degree of ionization of monomer units in the corona is relatively small,  $\alpha \ll \alpha_b \leq 1$ , the effect of short-ranged interactions is not negligible. Therefore, in a weakly dissociating corona, both ionic and nonelectrostatic binary interactions (specified by the second virial coefficient  $v_A$ ) should be taken into account. In this case, the corresponding expressions for  $H_{\text{corona}}^{(1)}$  and  $F_{\text{corona}}^{(1)}$  can be represented as [22, 97]:

$$H_{\text{corona}}^{(1)} = \frac{1}{3^{1/3}} N_A v_A^{1/3} s(R_{\text{core}})^{-1/3} \frac{z^{1/3}}{(\sqrt{1+z}-1)^{2/3}}, \quad (143)$$

$$\frac{F_{\text{corona}}^{(1)}}{k_B T} = \frac{3^{4/3}}{2} N_A v_A^{2/3} s(R_{\text{core}})^{-2/3} \frac{\sqrt{1+z}-3}{z^{1/3} (\sqrt{1+z}-1)^{1/3}}, \quad (144)$$

where the combination of parameters:

$$z = \frac{24v_A}{s(R_{\text{core}})^2} \frac{1-\alpha_b}{\alpha_b \Phi_{\text{ion}}}$$

depends on both area per chain,  $s(R_{\text{core}})$ , and the strength of steric and electrostatic repulsions (via  $v_A$  and  $\alpha_b$ ).

The coronal free energy in a weakly curved aggregate of morphology  $i$  is then specified as [22]:

$$F_{\text{corona}}^{(i)} \approx F_{\text{corona}}^{(1)} \left[ 1 - (i-1) \frac{H_{\text{corona}}^{(1)}}{3R_{\text{core}}} \frac{z}{(\sqrt{1+z}-3)(\sqrt{1+z}-1)} \right]. \quad (145)$$

We now introduce the new combinations of the parameters,  $t$  and  $u$ :

$$t = \frac{s(R_{\text{core}})}{3^{1/5} v_A^{2/5}} \left( \frac{\gamma}{N_A} \right)^{3/5}; \quad u = \frac{24v_A^{1/5}}{3^{2/5}} \left( \frac{\gamma}{N_A} \right)^{6/5} \frac{1-\alpha_b}{\alpha_b \Phi_{\text{ion}}}. \quad (146)$$

Here,  $t$  is proportional to the still-unknown area per chain,  $s(R_{\text{core}})$ , whereas  $u$  specifies the relative strength of non-ionic and ionic interactions. When electrostatic interactions are weak compared to nonelectrostatic interactions,  $u \rightarrow \infty$ . In the opposite limit, i.e., when electrostatic interactions dominate,  $u \rightarrow 0$ .

By balancing the dominant contribution in the coronal free energy,  $F_{\text{corona}}^{(i)} \approx F_{\text{corona}}^{(1)}$ , with the surface free energy,  $F_{\text{interface}}^{(i)} = \gamma s k_B T$ , we find the equilibrium area,  $s(R_{\text{core}})$ , or, equivalently, the relation between  $t$  and  $u$ :

$$\frac{u^{2/3}}{t^3 \left( \sqrt{1 + u/t^2} - 1 \right)^{4/3}} = 1. \quad (147)$$

The equation for binodals is obtained along the same lines as before. One finds [22]:

$$\frac{N_B^2 \gamma^{6/5}}{\phi^3 N_A^{16/5} v_A^{9/5} t(u)^{9/2}} \left\{ \frac{2}{3^{2/5}} i(i+1) [(i+1)^2 b_{i+1} - i^2 b_i] \right\} = 1 \quad i = 1, 2, \quad (148)$$

where  $t(u)$  is the solution of (147).

When electrostatic interactions are weak,  $u \rightarrow \infty$  (or, equivalently,  $\alpha_b \rightarrow 0$ ), the solution of (147),  $t(u) \rightarrow 1$ , and one finds asymptotic expressions for the binodals in the quasi-neutral limit. Note that due to the mean-field nature of the model used here, the exponents are slightly different from these in (51), obtained for non-ionic micelles in the scaling framework. The difference is, however, minor.

When  $u \rightarrow 0$  (the so-called osmotic annealing limit),  $t(u) \approx 16/u^2$ . Here, one finds the asymptotic expressions for the binodals as:

$$\frac{\alpha_b \Phi_{\text{ion}}}{1 - \alpha_b} = 3^{5/9} 2^{10/9} \frac{N_B^{2/9} \gamma^{4/3}}{\phi^{1/3} N_A^{14/9}} i(i+1) [(i+1)^2 b_{i+1} - i^2 b_i] \quad i = 1, 2. \quad (149)$$

As follows from (149), an increase in  $\Phi_{\text{ion}}$  triggers the lamella–cylinder–sphere transformations in a crew-cut micelle with an annealing osmotic corona. As discussed earlier, an increase in  $\Phi_{\text{ion}}$  leads to an enhanced ionization of the coronal blocks, driven by the substitution of hydrogen ions by the salt ions and, thereby, decreasing local pH inside the corona. As a result, the ionic contribution to the coronal free energy decreases, and the spherical shape of the aggregate is stabilized. In other words, in order to transform a cylindrical aggregate into spherical micelles, one has to increase the concentration of salt ions in the solution. Recall that such behavior is expected only under low salt conditions, when salt-induced screening of electrostatic interactions is negligible.

In a salt-dominated solution, the behavior of weakly and strongly dissociating PEs becomes indistinguishable,  $\alpha \approx \alpha_b$ . Here, the addition of salt leads predominantly to an enhanced screening of electrostatic interactions in the corona (via the decrease in the effective virial coefficient,  $v_{\text{eff}} = v_A + \alpha_b^2/2\Phi_{\text{ion}}$ ). Therefore,



block copolymer with a pH-sensitive block demonstrates under these conditions the conventional sequence of morphological transitions (see Sect. 10). The corresponding binodals are specified by (142).

Figure 18a demonstrates the diagram of states in  $N_B$ ,  $\Phi_{\text{ion}}$  coordinates for block copolymer with the length of pH-sensitive block  $N_A = 50$ , and  $\text{pH} = \text{p}K_a$  (i.e., for  $\alpha_b = 0.5$ ). Solid lines indicate the binodals calculated according to (148) and (142). A smaller value of  $\alpha_b = 0.1$  is used in Fig. 18b. The diagrams localize the stability regions of three main morphologies of block copolymer aggregates: spherical, S ( $i = 3$ ), and cylindrical C ( $i = 2$ ) micelles, and lamellae L ( $i = 1$ ). The latter can further associate due to Van der Waals forces, and precipitate from the solution.

Comparison of diagrams of Fig. 18a, b indicates that morphology  $i$  of aggregate formed by pH-sensitive block copolymers can be tuned by variations in both concentration of added salt,  $\Phi_{\text{ion}}$  and pH in solution. For example, when  $\text{pH} < \text{p}K_a$  (e.g., at  $\alpha_b = 0.1$ , Fig. 18b), a copolymer with lengths of the blocks,  $N_A = 50$  and  $N_B = 125$ , retains the cylindrical (C) morphology at any salt concentration,  $\Phi_{\text{ion}}$ . In contrast, when  $\text{pH} = \text{p}K_a$  ( $\alpha_b = 0.5$ , Fig. 18a), the same copolymer makes cylindrical (C) micelles only at low salt concentrations, and associates into spherical (S) micelles upon a further increase in  $\Phi_{\text{ion}}$ .

In addition to three canonical morphologies of aggregates (S, C, and L), more complex associations of block copolymer molecules could be found in certain regions of the diagram. In particular, a recent theoretical study [24] predicts the existence of branched cylinders in the vicinity of the S–C binodal line. The latter occupy a narrow corridor and coexist with cylindrical and spherical micelles. Branched structures and networks of aggregates formed by diblock copolymer with quenched PE block were also considered in [17].

## 12 Experiment Versus Theory

In this last section of the review, we compare the theoretical results with the available experimental data. Clearly, we can not discuss here all the relevant papers on self-assembly of ionic/hydrophobic block copolymers. A comprehensive discussion of experimental developments and trends in this field can be found elsewhere (see, e.g., [8, 9]). Instead, we focus here on selected experimental findings that are used to confront the predictions of theoretical models formulated above.

The assembly of amphiphilic ionic/hydrophobic block copolymers in aqueous media suggests that the effective (hydrophobic) attraction between the associating blocks is sufficiently strong to counterbalance repulsions between the PE blocks. That is, the corresponding cohesive free energies for the hydrophobic core-forming blocks are significantly larger than those involved in the assembly of non-ionic block copolymers in selective organic solvents. In order to assure the stability of micelles in wide ranges of temperature and salinity, polymers with high  $T_g$ , e.g., PS or poly(*tert*-butyl styrene) are often chosen for core-forming block [98–114]. The hydrophobic domains in these aggregates are found in a glassy (“frozen”) state and can hardly rearrange once micelles are formed. Moreover, assembly of the

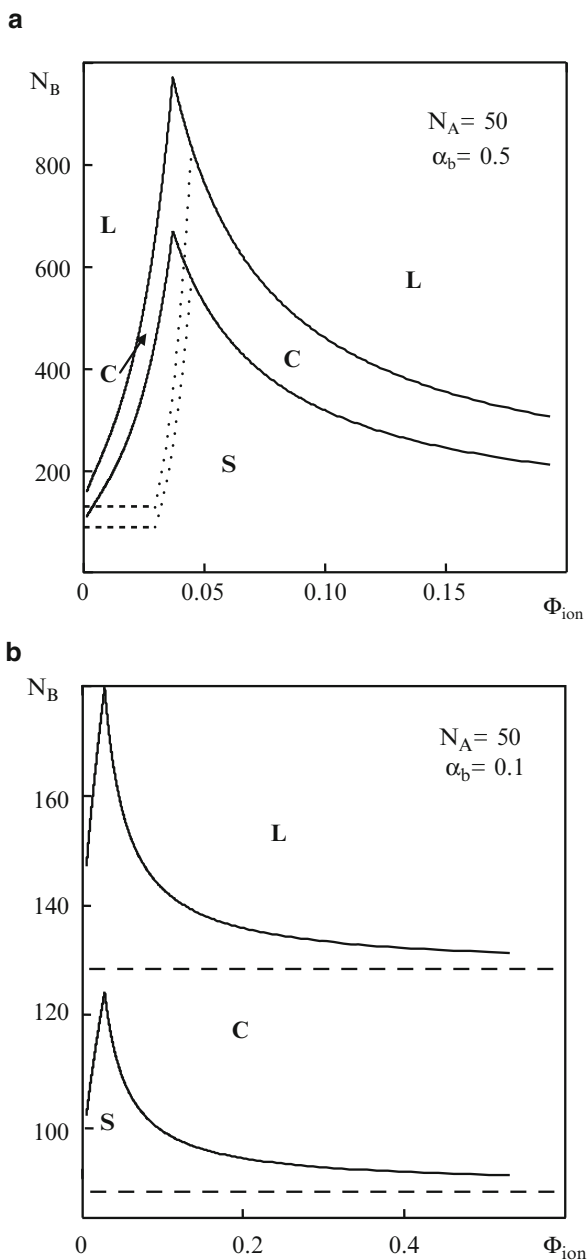


**Fig. 18** Diagram of states in  $N_B, \Phi_{ion}$  coordinates for diblock copolymer solution at different values of  $pH - pK_a$ , corresponding to  $\alpha_b = 0.5$  (a) and  $\alpha_b = 0.1$  (b). Other parameters are  $\gamma = 1$ ,  $\varphi = 1$ ,  $v_A = 0.4$ ,  $N_A = 50$ . Dashed and dotted lines correspond to asymptotic expressions for the binodal lines given by (142) (at  $\alpha_b = 0$ ) and (149)

ionic/hydrophobic block copolymers in water may lead to out-of-equilibrium frozen aggregates, even for copolymers with a core-forming block that exhibits relative low  $T_g$ , e.g., poly(*n*-butyl acrylate) [115–119]. The nonequilibrium nature of the aggregates with non-glassy cores is often explained by high activation energy barriers for exchange between copolymers included in the micelles and those existing in unimer state in the solution [120].

Depending on the intramolecular hydrophilic/hydrophobic balance, micelles with frozen cores can be obtained either by direct dissolution of the copolymers in water (at elevated temperature) or by dialysis of the molecular solution of the copolymer from common solvent (e.g., dioxane) to water. The “freezing” of the core (quenching of the aggregation state) occurs below a certain temperature or upon a decrease of the content of the common solvent in the mixture with water.

The aggregation number (and the size of core domain) in micelles with glassy core, is little affected by variations in environmental conditions. Moreover, the frozen micelles retain their integrity at arbitrary low concentration, i.e., exhibit no CMC. Since the aggregation number is fixed, variations in the ionic strength and/or in pH may lead to only conformational changes in the corona. Depending on the ratio between the lengths of the hydrophobic and PE blocks, the coronae of frozen micelles are similar to colloidal PE brushes or to multiple-arm PE stars.

Structural characterization of block copolymer aggregates by dynamic and static light scattering (DLS and SLS) in combination with small angle neutron scattering (SANS) at variable ionic strength and pH in the solution enables one to discriminate between frozen and dynamic (equilibrium) micelles. In particular, SANS provides direct information about the core size and shape because of relatively low scattering density of the corona.

The theory predicts that in the case of frozen starlike micelles with strongly dissociating PE corona, the hydrodynamic radius of the micelle (measured by DLS) is expected to decrease as  $R_{\text{corona}} \sim c_s^{-1/5}$  upon an increase in salt concentration  $c_s$  [10]. This theoretical prediction is in agreement with findings in [106] on poly(*tert*-butyl styrene)-*block*-poly(sodium styrene sulfonate) micelles, that proves the frozen nature of these aggregates. Starlike micelles with frozen PS core and pH-sensitive poly(acrylic acid) coronae were systematically studied in [112–114]. Conformational changes in the corona induced by variations in the ionic strength and pH in the solution were analyzed by SANS, and a good agreement with theoretical predictions [62, 64] concerning conformations of pH-sensitive PE stars was established.

Hence, it is still a challenging experimental task to produce dynamic, equilibrium micelles. The dynamic nature of micelles is inherently linked to the stimuli-responsive properties, i.e., an ability to change reversibly the aggregation number and morphology of the aggregate in response to specific variation in the environmental conditions. An ability of micelles to disintegration, triggered by external stimuli, is most valuable in certain applications, e.g., drug delivery and controlled release systems [121, 122].

Most experimental studies searching for dynamic micelles have focused on the proper choice of “soft” hydrophobic block to assure equilibrium, i.e., reversible association of the ionic/hydrophobic block copolymers. Copolymers with such soft

hydrophobic blocks as poly(ethylene) [123], poly(isobutylene) [124–127], or poly(diethyleneglycol ethylether acrylate) [128] have been extensively explored.

The solution behavior of poly(ethylene)-*block*-poly(styrene sulfonic acid) was studied by combining DLS, SLS, cryo-TEM, and SANS [123]. Here, the combination of a soft hydrophobic block (with  $T_g \approx -25^\circ\text{C}$ ) with a strongly dissociating PE block was chosen to analyze the effect of ionic strength on the block copolymer assembly in a wide range of salt concentrations (three orders of magnitude in  $c_s$ ). It was found that an increase in concentration of added salt leads to an increase in the aggregation number (and in core size) and in a simultaneous decrease in the hydrodynamic radius of the micelle as  $R_{\text{corona}} \sim c_s^{-x}$  with the apparent exponent  $x \approx 0.12$ . The latter value is close to the theoretical exponent  $1/11 \approx 0.09$  (89), which is expected for equilibrium micelles in which the aggregation number increases upon an increase in salt concentration (87). Note that the value of experimental exponent is noticeably smaller than the 0.2, predicted for frozen micelles (PE stars). This suggests that micelles of poly(ethylene)-*block*-poly(styrene sulfonic acid) copolymer in aqueous solution might be close to equilibrium.

Micellization of poly(isobutylene)-*block*-poly(methacrylic acid) copolymers with short hydrophobic and long PE blocks has been studied [124–127] by DLS, SLS, SANS, and pyrene titration experiments supported by cryo-TEM imaging. It was unambiguously demonstrated that at high pH, when the poly(methacrylic acid) blocks are fully ionized, the aggregation number increases whereas the hydrodynamic radius decreases as a function of salt concentration. Both dependencies can be approximated by power laws with exponents close to those predicted by theory (87), (89), which again points to the dynamic nature of these micelles.

Micellization of poly[2-(dimethylamino)ethyl methacrylate]-*block*-poly[2-(diethylamino)ethyl methacrylate] (DMAEMA/DEAEMA) gives rise to pH-responsive spherical micelles that are found in aqueous solution above a certain critical pH [129, 130]. Under acidic conditions, protonation of the amino groups transforms the block copolymers in PEs and keeps them as unimers in solution. Deprotonation of the DEAEMA block by addition of base makes this block hydrophobic and causes formation of micelles, with the corona formed by still-protonated (annealing) DMAEMA blocks. The electrostatic properties of the micellar corona were additionally tailored by using copolymer with the DMAEMA block selectively quaternized with benzyl chloride (Q-DMAEMA/DEAEMA), and by substituting the DMAEMA block by a PEO block. In the former case, one finds strongly charged (quenched) corona whereas in the latter case the hydrophilic micellar corona is electroneutral [130]. The data obtained from potentiometric titrations, DLS, SLS, and SANS allowed the probing of the dependence of aggregation number  $p$  as a function of the degree of chain ionization,  $\alpha \sim \alpha_b$ . The starlike DMAEMA/DEAEMA micelles demonstrated a power law decrease in aggregation number,  $p \sim \alpha_b^{-y}$  with apparent exponent  $y = 1.5$ , upon an increase in  $\alpha_b$  (a decrease in pH). The equilibrium theory predicts the value of exponent  $y = 12/11 \approx 1.1$  for starlike micelles in the salt-dominated regime, (87). The theoretical exponent is reasonably close to the experimental exponent, specified for DMAEMA/DEAEMA micelles at the boundary between osmotic and salt-dominated regimes [130]. At the same time, the rearrangements of these micelles

due to additions of salt ions after micellization were hindered, suggesting the lack of full equilibrium. “Softness” of the core-forming DEAEEMA block was also demonstrated by the salt-induced rearrangements in Q-DMAEMA/DEAEEMA micelles. Here, the degree of ionization of the coronal blocks,  $\alpha \sim 1$ , was not sensitive to variations in solution pH, but the forming micelles responded to additions of salt both before and after micellization.

We remark, however, that a soft hydrophobic block alone does not necessarily ensure the dynamic (equilibrium) nature of the forming aggregate. On the contrary, there are experimental indications that a combination of softness of the core-forming block with “intrinsic hydrophobicity” of the PE block [e.g., in the cases of poly(styrene sulfonic) or poly(methacrylic) acid] might be important. A tentative explanation assumes the influence of the coronal block on the core–corona interfacial energy. In addition, we also note that in experimental studies of dynamic micelles, mostly asymmetric or nearly symmetric block copolymers with longer PE block were investigated. These block copolymers form starlike aggregates in aqueous solutions. Currently, we are not aware of reliable experimental evidence of dynamic crew-cut micelles formed by copolymers with long hydrophobic core-forming block.

An alternative strategy for design of dynamic, stimuli-responsive PE micelles is to use block copolymers with thermosensitive associating blocks, e.g., poly(*N*-isopropylacrylamide) [131, 134, 135] poly(*N,N*-diethylacrylamide) [131–133], and poly(*N,N*-dimethylacrylamide) [134]. In this case, reversible micellization–dissociation can be triggered by temperature variations that affect the solubility of the core-forming blocks. For example, in [131] it was shown that poly(acrylic acid)-*block*-poly(*N*-isopropylacrylamide) copolymers can form micelles with poly(*N*-isopropylacrylamide) core and poly(acrylic acid) corona at pH 6 and  $T \geq 45^\circ\text{C}$ , whereas at pH 4 and room temperature “inverse” micelles are formed.

Moreover, in the vicinity of the LCST (or UCST) the insoluble core is soft enough to undergo structural transformations in response to variations in strength of ionic interactions in the corona. In [135], micellization of poly(*N*-isopropylacrylamide)-*block*-poly(DMAEMA) in aqueous solution was studied as a function of pH and temperature. Predicted by the theory [19], a pH-induced, jump-wise transition between spherical micelles with distinctively different aggregation numbers was observed by combination of DLS and AFM at temperatures  $T > \text{LCST}$  for the core-forming *N*-isopropylacrylamide block. To the best of our knowledge, to date this study is the only experimental evidence of abrupt structural transformations in spherical micelles with annealing PE corona.

Nonspherical aggregates (cylindrical micelles, vesicles, lamellae, etc.) were detected experimentally for a number of non-ionic block copolymers (see, e.g., [50, 136–139]) and copolymers with weakly dissociating PE block [102, 140]. Morphological transformations in non-ionic PI-*block*-PS micelles were triggered by variations in molecular weight of the PS block [50] or by variations in the solvent composition [137, 138]. The latter studies clearly indicate the possibility of stimuli-responsive transitions (sphere  $\rightarrow$  cylinder  $\rightarrow$  vesicle) for non-ionic block copolymer aggregates in mixed organic solvents. It was also demonstrated [58] that

mild swelling of PS core of the micelle in a single solvent *n*-heptane (a preferential solvent for PI block) leads to the decrease in  $T_g$  of the core-forming block down to  $\approx 28^\circ\text{C}$ , and allows for a close to equilibrium state of the aggregates at temperatures slightly elevated above  $T_g$ .

Experimental observations on stimuli-induced equilibrium morphological transitions in aggregates formed by amphiphilic ionic/hydrophobic block copolymers, are still lacking. Nanoaggregates of different morphologies (spherical starlike and crew-cut micelles, cylinders, vesicles and “complex” micelles) were obtained by Eisenberg et al [102, 140] via dialysis of the molecular solution of poly(acrylic acid)-*block*-PS copolymers from a common solvent (dioxane) into water at different pH. The aggregates (spherical or cylindrical micelles) were formed by copolymers with different ratios of the lengths of PE and hydrophobic blocks at a certain composition of the mixed solvent. Copolymer with shorter PS blocks formed spheres, and longer hydrophobic blocks gave rise to cylinders. However, below a certain content of dioxane, the PS core was kinetically frozen. Hence once formed, the aggregates could not change the morphology (aggregation state) upon variations in the ionic strength and pH, but rather responded by conformational changes in the corona.

**Acknowledgment** The support of the European Union within the Marie Curie Research and Training Network POLYAMPHI and of the Russian Foundation for Basic Research, grant 08-03-336 is gratefully acknowledged. OVB acknowledges the Alexander von Humboldt Foundation for support of his stay in the University of Bayreuth.

## References

1. Galaev I, Mattiasson B (ed) (2008) Smart polymers: applications in biotechnology and biomedicine, CRC, Boca Raton
2. Dai L (2003) Intelligent macromolecules for Smart devices: from material synthesis to device application. Springer, London
3. Minko S (2006) Responsive polymer materials: design and applications. Backwell, Oxford
4. Lazzari M, Liu G, Lecommandoux S (ed) (2006) Block copolymers in nanoscience. Wiley, Weinheim
5. Hamley IW (1998) The physics of block copolymers. Oxford University Press, New York
6. Riess G (2003) Micellization of block copolymers. Prog Polym Sci 28:1107–1170
7. Gohy JF (2005) Adv Polym Sci 190:65
8. Förster S, Abetz V, Müller AHE (2004) Adv Polym Sci 166:267
9. Cohen Stuart MA, Hof B, Voets IK, de Keizer A (2005) Curr Opin Coll Int Sci 10:30
10. Borisov OV, Zhulina EB, Leermakers FAM, Müller AHE, Ballauff M (2011) Adv Polym Sci DOI: 12\_2010\_104
11. Aseyev VO, Tenhu H, Winnik FM (2006) Adv Polym Sci 196:1
12. Dimitrov I, Trzebici B, Müller AHE, Dworak A, Tsvetanov CD (2007) Prog Polym Sci 32:1275
13. Marko JF, Rabin Y (1992) Macromolecules 25:1503
14. Wittmer J, Joanny J-F (1993) Macromolecules 26:2691
15. Shusharina NP, Nyrkova IA, Khokhlov AR (1996) Macromolecules 29:3167
16. Huang C, Olivera de la Cruz M, Delsanti M, Guenoun P (1997) Macromolecules 30:8019
17. Netz RR (1999) Europhys Lett 47:391
18. Borisov OV, Zhulina EB (2002) Macromolecules 35:4472

19. Zhulina EB, Borisov OV (2002) *Macromolecules* 35:9191
20. Borisov OV, Zhulina EB (2003) *Macromolecules* 36:10029
21. Borisov OV, Zhulina EB (2005) *Langmuir* 21:3229
22. Zhulina EB, Borisov OV (2005) *Macromolecules* 38:6726
23. Lauw Y, Leermakers FAM, Cohen Stuart MA, Borisov OV, Zhulina EB (2006) *Macromolecules* 39:3628
24. Viktorov AI, Plotnikov NV, Hong P-D (2010) *J Phys Chem B* 114:8846
25. Pincus PA (1991) *Macromolecules* 24:2912
26. Ross R, Pincus P (1992) *Macromolecules* 25:2177
27. Borisov OV, Birshtein TM, Zhulina EB (1991) *J Phys II (France)* 1:521
28. Borisov OV, Zhulina EB, Birshtein TM (1994) *Macromolecules* 27:4795
29. Zhulina EB, Borisov OV (1996) *Macromolecules* 29:2618
30. Zhulina EB, Borisov OV (1997) *J Chem Phys* 107:5952
31. Zhulina EB, Birshtein TM, Borisov OV (1995) *Macromolecules* 28:1491
32. Zhulina EB, Birshtein TM, Borisov OV (2006) *Eur Phys J E* 20:243
33. Ballauff M, Borisov OV (2006) *Curr Opin Colloid Interface Sci* 11:316
34. Tanford C (1973) *The hydrophobic effect: formation of micelles and biological membranes*. Wiley-Interscience, New York
35. Israelachvili JN (1985) *Intermolecular and surface forces*. Academic, London
36. Hill TL (1994) *Thermodynamics of small systems*. Dover, New York
37. Izzo D, Marques CM (1993) *Macromolecules* 26:7189
38. Konop AJ, Colby RH (1999) *Langmuir* 15:58
39. Halperin A, Tirrell M, Lodge T (1990) *Adv Polym Sci* 100:31
40. Borisov OV, Zhulina EB (2008) Responsive polymer brushes: a theoretical outlook. In: Galaev I, Mattiasson B (eds) *Smart polymers: applications in biotechnology and biomedicine*. CRC, Boca Raton, p 53
41. Grosberg AY, Khokhlov AR (1994) *Statistical physics of macromolecules*. AIS, New York
42. Polotsky AA, Daoud M, Borisov OV, Birshtein TM (2010) *Macromolecules* 43:1629
43. Flory P (1953) *Principles of polymer chemistry*. Cornell University Press, Ithaca
44. Ushakova AS, Govogun EN, Khokhlov AR (2006) *J Phys Condens Matter* 18:915
45. Zhulina YB, Birshtein TM (1985) *Polym Sci USSR* 27:570
46. Halperin A (1987) *Macromolecules* 20:2943
47. Halperin A (1989) *Europhys Lett* 8:351
48. Halperin A, Alexander S (1989) *Macromolecules* 22:2403
49. Birshtein TM, Zhulina EB (1989) *Polymer* 30:170
50. Zhulina EB, Adam M, Sheiko S, LaRue I, Rubinstein M (2005) *Macromolecules* 38:5330
51. Alexander S (1977) *J Phys (France)* 38:983
52. de Gennes PG (1980) *Macromolecules* 13:1069
53. Daoud M, Cotton JP (1982) *J Phys (France)* 43:531
54. Zhulina YB (1984) *Polym Sci USSR* 26:794
55. Birshtein TM, Zhulina EB (1984) *Polymer* 25:1453
56. Birshtein TM, Zhulina EB, Borisov OV (1986) *Polymer* 27:1079
57. de Gennes PG (1979) *Scaling concepts in polymer physics*. Cornell University Press, Ithaca
58. LaRue I, Adam M, Zhulina EB, Rubinstein M, Pitsikalis M, Hadjichristidis N, Hammouda B, Lin MY, Ivanov DA, Gearba RI, Anokhin DV, Sheiko SS (2008) *Macromolecules* 41:6555
59. Semenov AN (1985) *Sov Phys JETP* 61:733
60. Wang Z-G, Safran SA (1988) *J Chem Phys* 89:5323
61. Borisov OV (1996) *J Phys II (France)* 6:1
62. Borisov OV, Zhulina EB (1998) *Eur Phys J B* 4:205
63. Klein Wolterink J, Leermakers FAM, Fleer GJ, Koopal LK, Zhulina EB, Borisov OV (1999) *Macromolecules* 32:2365
64. Klein Wolterink J, van Male J, Cohen Stuart MA, Koopal LK, Zhulina EB, Borisov OV (2002) *Macromolecules* 35:9176
65. Noolandi J, Hong KM (1983) *Macromolecules* 16:1443
66. Leermakers FAM, Scheutjens JM (1988) *J Chem Phys* 89:3264



67. Leermakers FAM, Scheutjens JMHM (1989) *J Phys Chem* 93:7417
68. Leermakers FAM, Scheutjens JMHM (1988) *J Chem Phys* 89:6912
69. Leermakers FAM, Scheutjens JMHM (1990) *Biochim Biophys Acta* 1024:139
70. Leermakers FAM, Scheutjens JMHM (1990) *J Colloid Interface Sci* 136:231
71. Leermakers FAM, Lyklema J (1992) *Colloids Surf* 67:239
72. Cogan KA, Leermakers FAM, Gast AP (1992) *Langmuir* 8:429
73. Leermakers FAM, Wijmans CM, Fleer GJ (1995) *Macromolecules* 28:3434
74. Fleer GJ, Cohen Stuart MA, Scheutjens JMHM, Cosgrove T, Vincent B (1993) *Polymers at interfaces*. Chapman and Hall, London
75. Evers OA, Scheutjens JMHM, Fleer GJ (1990) *Macromolecules* 23:5221
76. Leermakers FAM, Rabinovich AL (2007) *Phys Rev E* 76:031904/1
77. Charlaganov MI, Borisov OV, Leermakers FAM (2008) *Macromolecules* 41:3668
78. Jódar-Reyes AB, Ortega-Vinuesa JL, Martín-Rodríguez A, Leermakers FAM (2003) *Langmuir* 19:878
79. Lauw Y, Leermakers FAM, Cohen Stuart MA (2003) *J Phys Chem* 107:10912
80. Oversteegen SM, Leermakers FAM (2000) *Phys Rev E* 62:8453
81. Jódar-Reyes AB, Leermakers FAM (2006) *J Phys Chem B* 110:6300
82. Li F, Marcelis ATM, Sudholter EJR, Cohen Stuart MA, Leermakers FAM (2009) *Soft Matter* 5:4173
83. Meijer LA, Leermakers FAM, Lyklema J (1994) *Recl Trav Chim Pays-Bas* 113:167
84. Claessens MMAE, van Oort BF, Leermakers FAM, Hoekstra FA, Cohen Stuart MA (2004) *Biophys J* 87:3882
85. Lauw Y, Leermakers FAM, Cohen Stuart MA (2006) *J Phys Chem B* 110:465
86. Lauw Y, Leermakers FAM, Cohen Stuart MA (2007) *J Phys Chem B* 111:8158
87. Leermakers FAM, van der Schoot PPAM, Scheutjens JMHM, Lyklema J (1990) In: Mittal KL (ed) *Surfactants in solution*, vol 7. Plenum, New York, pp 43–60
88. Leermakers FAM, Eriksson JC, Lyklema J (2005) Association colloids and their equilibrium modelling. In: Lyklema J (ed) *Fundamentals of interface and colloid science*, vol V: Soft colloids. Elsevier, Amsterdam, pp 4.1–4.121
89. Israëls R, Leermakers FAM, Fleer GJ, Zhulina EB (1994) *Macromolecules* 27:3249
90. Israëls R, Leermakers FAM, Fleer GJ (1994) *Macromolecules* 27:3087
91. Edwards SF (1966) *Proc Phys Soc* 88:265
92. Hall DG, Pethica BA (1967) In: Schick MJ (ed) *Nonionic surfactants*. Marcel Dekker, New York, pp 515–557
93. Voets IK, Leermakers FAM (2008) *Phys Rev E* 78:061801
94. Meijer LA, Leermakers FAM, Lyklema J (1999) *J Chem Phys* 110:6560
95. Kik RA, Leermakers FAM, Kleijn JM (2005) *Phys Chem Chem Phys* 7:1996
96. Kik RA, Leermakers FAM, Kleijn JM (2010) *Phys Rev E* 81:021915
97. Biesheuvel PM (2004) *J Colloid Interface Sci* 275:97
98. Kiserow D, Prochazka K, Ramireddy C, Tuzar Z, Munk P, Webber SE (1992) *Macromolecules* 25:461
99. Qin A, Tian M, Ramireddy C, Webber SE, Munk P (1994) *Macromolecules* 27:120
100. Matějříček P, Podhájecká K, Humpolíčková J, Uhlík F, Jelínek K, Limpouchová Z, Procházka K (2004) *Macromolecules* 37:10141
101. Khougaz K, Astafieva I, Eisenberg A (1995) *Macromolecules* 28:7135
102. Zang L, Eisenberg A (1995) *Science* 268:1728
103. Zang L, Barlow RJ, Eisenberg A (1995) *Macromolecules* 28:6055
104. Gao Z, Yarshney SK, Wong S, Eisenberg A (1994) *Macromolecules* 27:7923
105. Shen H, Eisenberg A (2000) *Macromolecules* 33:2561
106. Guenoun P, Davis HT, Tirrell M, Mays JW (1996) *Macromolecules* 29:3965
107. Guenoun P, Muller F, Delsanti M, Auvray L, Chen YJ, Mays JW, Tirrell M (1998) *Phys Rev Lett* 81:3872
108. Guenoun P, Delsanti M, Gaseau D, Auvray L, Cook DC, Mays JW, Tirrell M (1998) *Eur Phys J B* 1:77



109. Förster S, Hemsdorf N, Leube W, Schnablegger H, Regenbrecht M, Akari S, Lindner P, Böttcher C (1999) *J Phys Chem* 103:6657
110. Muller F, Delsanti M, Auvray L, Yang J, Chen YJ, Mays JW, Demé B, Tirrell M, Guenoun P (2000) *Eur Phys J E* 3:45
111. Muller F, Guenoun P, Delsanti M, Deme B, Auvray L, Yang J, Mays JW (2004) *Eur Phys J E* 15:465
112. Van der Maarel JRC, Groenewegen W, Egelhaaf SU, Lapp A (2000) *Langmuir* 16:7510
113. Groenewegen W, Egelhaaf SU, Lapp A, van der Maarel JRC (2000) *Macromolecules* 33:3283
114. Groenewegen W, Lapp A, Egelhaaf SU, van der Maarel JRC (2000) *Macromolecules* 33:4080
115. Müller AHE, Cai Y, Hartenstein M, Gradzielski M, Zhang M, Mori H, Pergushov DV (2004) *Polymer Prepr (Am Chem Soc, Div Polym Chem)* 45:267
116. Eghbali E, Colombani O, Drechsler M, Müller AHE, Hoffmann H (2006) *Langmuir* 22:4766
117. Schumacher M, Ruppel M, Burkhardt M, Drechsler M, Colombani O, Schweins R, Müller AHE (2007) *Polym Mater Sci Eng* 96:374
118. Colombani O, Ruppel M, Schubert F, Zettl H, Pergushov DV, Müller AHE (2007) *Macromolecules* 40:4338
119. Colombani O, Ruppel M, Burkhardt M, Drechsler M, Schumacher M, Schweins R, Müller AHE (2007) *Macromolecules* 40:4351
120. Won YY, Davis HT, Bates FS (2003) *Macromolecules* 36:953
121. Kataoka K, Harada A, Nagasaki Y (2001) *Adv Drug Deliv Rev* 47:113
122. Gillies ER, Fréchet MJ (2004) *Pure Appl Chem* 76:1295
123. Förster S, Hemsdorf N, Böttcher C, Lindner P (2002) *Macromolecules* 35:4096
124. Schuch H, Klingler J, Rossmannith P, Frechen T, Gerst N, Feldthusen J, Müller AHE (2000) *Macromolecules* 33:1734
125. Pergushov DV, Remizova EV, Gradzielski M, Lindner P, Feldthusen J, Zezin AB, Müller AHE (2004) *Polymer* 45:367
126. Burkhardt M, Martinez-Castro N, Tea S, Drechsler M, Babin I, Grishagin I, Schweins R, Pergushov DV, Gradzielski M, Zezin AB, Müller AHE (2007) *Langmuir* 23:12864
127. Burkhardt M, Ruppel M, Tea S, Drechsler M, Schweins R, Pergushov DV, Gradzielski M, Zezin AB, Müller AHE (2008) *Langmuir* 24:1769
128. Jacquin M, Muller P, Cottet H, Théodoly O (2010) *Langmuir* 26:18681
129. Lee AS, Gast AP, Bütün V, Armes SP (1999) *Macromolecules* 32:4302
130. Lee AS, Bütün V, Vamvakaki M, Armes SP, Pople JA, Gast AP (2002) *Macromolecules* 35:8540
131. Schilli CM, Zhang M, Müller AHE, Rizzardo E, Thang SH, Chong YK, Karlsson G (2004) *Macromolecules* 37:7861
132. André X, Zhang M, Müller AHE (2005) *Macromol Rapid Commun* 26:558
133. André X, Burkhardt M, Drechsler M, Lindner P, Gradzielski M, Müller AHE (2007) *Polym Mater Sci Eng* 96:560
134. Lokitz BS, York AW, Stempka JE, Treat ND, Li Y, Jarrett WL, McCormick CL (2007) *Macromolecules* 40:6473
135. Xu L, Zhu Z, Borisov OV, Zhulina EB, Sukhishvili SA (2009) *Phys Rev Lett* 103:N118301
136. Won YY, Bates FS (2006) In: Zana R, Kaler EW (eds) *Giant micelles: properties and applications*. CRC, Boca Raton
137. Lodge TP, Bang J, Li Z, Hillmayer MA, Talmon YR (2005) *Soc Chem Faraday Discuss* 128:1
138. Bang J, Jain S, Li Z, Lodge PT (2006) *Macromolecules* 39:1199
139. Larue I, Adam M, Sheiko S, Rubinstein M (2003) *Polym Mater Sci Eng* 88:236
140. Khougaz K, Zhang L, Moffitt M, Eisenberg A (1996) *Polymer Science* 38A:331

Self Organized Nanostructures of Amphiphilic Block  
Copolymers I

Müller, A.H.E.; Borisov, O. (Eds.)

2011, XIV, 254 p., Hardcover

ISBN: 978-3-642-22485-0